Doctoral Dissertation

Design of Thermal Conductive Polymer Nanocomposites Based on Nanoparticle Distribution Control

Zhang Xi

Supervisor: Assoc. Prof. Toshiaki Taniike

Graduate School of Advanced Science and Technology

Japan Advanced Institute of Science and Technology

Materials Science

September 2020

Design of Thermal Conductive Polymer Nanocomposites Based on Nanoparticle Distribution Control

Zhang Xi

1720418

Along with the miniaturization and lightweight design of electronic devices, greater demands are constantly raised on materials having high thermal conductivity and low density. Polymer nanocomposites are excellent candidates owing to the general characteristics of polymer materials such as good processability, light weight, high electrical resistivity, and low cost. However, the present polymer nanocomposites usually exhibit insufficient thermal conductivity unless impractical formulations are adopted, and key factors affecting the formation of thermal conductive networks are still unclear. In this thesis, I aimed to study the thermal conductivity of polyolefin/aluminum oxide (Al_2O_3) nanocomposites to clarify the key factors that affect the thermal conductivity. Polymer nanocomposites with continuous thermal conductive networks were designed based on controlling the selective distribution of Al_2O_3 nanoparticles. The influences of filler dispersion, filler migration and phase morphology evolution on the formation of thermal conductive networks were studied, and the relationship of filler distribution and thermal conductivity was investigated. The main research results are as follows:

In **Chapter 2**, I applied a reactor granule technology (RGT) to immiscible polypropylene (PP)/polyolefin elastomer (POE) blends to control the localization of nanoparticles at the interface of PP and POE. The RGT afforded uniform dispersion of in-situ generated Al_2O_3 nanoparticles in PP, and this guaranteed the migration of nanoparticles to the interface of a co-continuous structure when blended with POE. The selective localization of nanoparticles at the interface was never achieved when preformed Al_2O_3 nanoparticles were used, and this fact stresses the importance of uniform dispersion in controlling the migration of nanoparticles.

In **Chapter 3**, the relationship among the filler dispersion, phase morphology evolution and the distribution of fillers was revealed by studying the migration of nanoparticles during the annealing process. It was found that the uniform dispersion of nanoparticles decreased the phase domain size to facilitate the successful migration to the interface. Further, the formation of nanoparticle networks decelerated the phase coarsening during annealing. Contrary, the formation of agglomerates and clusters prevented the successful migration of nanoparticles and thus suppression of the phase coarsening became much less effective.

In **Chapter 4**, a continuous segregated structure was designed to improve the thermal conductivity of PP/Al_2O_3 nanocomposites. I achieved the thermal conductivity of 1.07 W/m K at an Al_2O_3 loading of 27.5 vol%. The same strategy was also used in combination with RGT to control the balance between the number and density of thermal conductive paths.

In conclusion, the filler dispersion, phase domain size, and filler distribution in nanocomposites have important cooperation to determine the thermal conductivity of nanocomposites (Fig. 1). RGT and other developed strategies are believed to be promising for designing practical thermal conductive polymer nanocomposites.

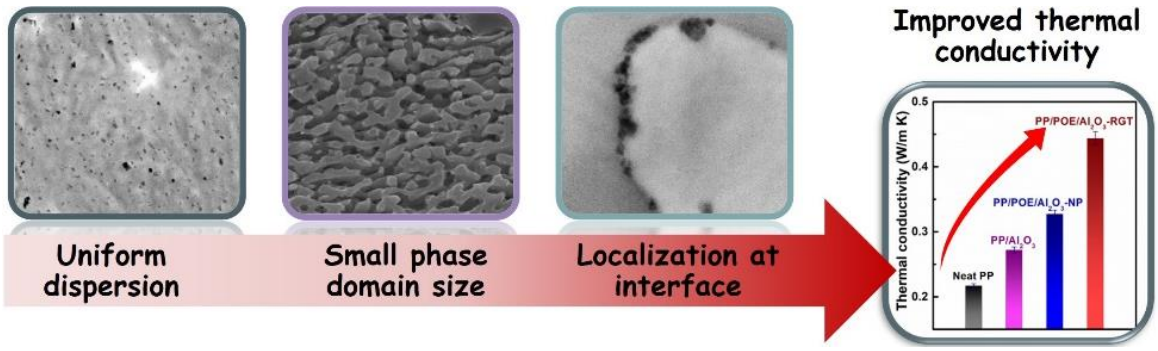

Fig. 1 Influence of filler dispersion, phase domain size and filler distribution on thermal conductivity.

Keywords: Nanocomposites; Thermal conductivity; Network; Immiscible blends; Selective distribution

Referee-in-chief: Associate Professor Toshiaki Taniike
Japan Advanced Institute of Science and Technology

Referees: Associate Professor Kazuaki Matsumura
Japan Advanced Institute of Science and Technology

Associate Professor Ken-ichi Shinohara
Japan Advanced Institute of Science and Technology

Associate Professor Kosuke Okeyoshi
Japan Advanced Institute of Science and Technology

Associate Professor Yusuke Hiejima
Kanazawa University

Preface

The present thesis is submitted for the Degree of Doctor of Philosophy at Japan Advanced Institute of Science and Technology, Japan. The thesis is consolidation of results of the research work on the topic “design of thermal conductive polymer nanocomposites based on nanoparticle distribution control” and implemented during October 2017–September 2020 under the supervision of Assoc. Prof. Toshiaki Taniike at Graduate School of Advanced Science and Technology, Japan Advanced Institute of Science and Technology.

Chapter 1 provides a general introduction of the research field, and accordingly the objective of this thesis. **Chapter 2** introduces selective localization of aluminum oxide (Al_2O_3) at interface and its effect on thermal conductivity in polypropylene (PP)/polyolefin elastomer (POE) blends. **Chapter 3** reports cooperative influences of nanoparticle localization and phase coarsening on thermal conductivity of PP/POE blends. **Chapter 4** reports design of continuous segregated PP/Al_2O_3 nanocomposites and impact of controlled Al_2O_3 distribution on thermal conductivity. Finally, **Chapter 5** describes the general conclusions of this thesis. The work is original and no part of this thesis has been plagiarized.

Zhang Xi

Graduate School of Advanced Science and Technology

Japan Advanced Institute of Science and Technology

June 2020

Acknowledgements

I would like to express my sincere gratitude to my supervisor, Assoc. Prof. Toshiaki Taniike, Graduate School of Advanced Science and Technology, Japan Advanced Institute of Science and Technology, who has offered me kind guidance and whose valuable suggestions, incisive comment, constructive criticism, and heartfelt encouragement have contributed greatly to the completion of this thesis. I am grateful to him for his tremendous assistance in developing the framework and revising the draft of this thesis several times. His patience, encouragement, and professional instructions helped me in all the time of research and writing of this thesis.

I would also take this opportunity to thank Prof. Tatsuo Kaneko and Prof. Noriyoshi Matsumi in JAIST for their guidance and encouragement for me. Without their kind support and help, the completion of the present thesis would not have been possible.

I would like to thank the nanocomposite research group of Taniike laboratory for stimulating discussions and constant help. I am also heartily grateful to all the members of Taniike laboratory for their valuable suggestions, cooperation and support.

I would also like to thank the members of my review committee, Assoc. Prof. Kazuaki Matsumura (JAIST), Assoc. Prof. Ken-ichi Shinohara (JAIST), Assoc. Prof.

Kosuke Okeyoshi (JAIST), and Assoc. Prof. Yusuke Hiejima (Kanazawa University), who have spent their valuable time to read the thesis, and provided their insightful comments and remarks to enhance the quality of this thesis from various perspectives.

I am also grateful for the scholarship of the Ministry of Education, Culture, Sports, Science and Technology, Japan during my doctoral course studying.

Last but not the least, my gratitude also extends to my family who has been assisting, supporting and caring for me all my life. Special thanks should go to my friends for their utmost care and moral support.

Zhang Xi

Graduate School of Advanced Science and Technology

Japan Advanced Institute of Science and Technology

May 2020

Table of contents

Chapter 1

General Introduction

Chapter 1

1.1 Thermal conductive polymer composites

Polymer materials have been widely applied in the fields of electric and electronic devices, energy, biology, medicine, and so on [1–8], because they possess many advantages such as light weight, good processability, low cost, and excellent chemical stability [9–12]. Among them, thermal conductive materials have attracted great attention in recent years owing to the rapidly developing integration, miniaturization and functionalization of electronics, as well as the emergence of new applications such as ultrahigh-voltage electric devices, three-dimensional chip stack architectures, light emitting diodes, flexible electronics, and so on [13–16]. In these applications, efficient thermal dissipation is very important for electronic devices to maintain desired performance, long lifetime and good reliability. For example, personal computers have developed from original big desktops to present compact tablets even with more functions and faster operation, while it inevitably results in the generation of a large amount of heat per volume. If such heat cannot be dissipated, the electronic devices would accelerate the aging and degradation. It was reported that the performance stability of these devices decreases 10% with the increase of temperature by 2 ^{o}C and the lifetime decreases to 1/6 if the temperature increases from 25 to 50 ^{o}C [17]. Likewise, solving the heat dissipation problem is critical to the electronic information technology, which provides a good opportunity for the design and development of thermal conductive materials.

Chapter 1

Thermal conductive polymer materials are generally divided into intrinsic thermal conductive polymers and thermal conductive polymer composites with a thermal conductive inclusion. Intrinsic thermal conductive polymers refer to polymers with high thermal conductivity by themselves. They are usually obtained by regulating the molecular structures during the synthesis and formation process. The thermal conductivity of these polymers is largely determined by the chain morphology. As shown in Fig. 1.1a, a semi-crystalline polymer contains crystalline domains with periodically aligned polymer chains and amorphous domains with randomly entangled polymer chains [18]. The transportation of phonons in the crystalline domain is much more effective than in the amorphous domain; when the former is dominant in a polymer, the vibration mode tends to be localized and the thermal conductivity is thus low. Therefore, enhancing the alignment of polymer chains is expected a promising way to improve the thermal conductivity. According to the molecular dynamic simulations, the thermal conductivity of a single extended polyethylene (PE) chains can be as high as 350 W/m K [19,20]. In literature, a thermal conductivity value of ~ 104 W/m K was achieved by ultra-drawing polyethylene into nanofibers with diameters of 50 ~ 500 nm and lengths up to tens of millimeters [21]. Even for polydimethylsiloxane, a polymer with a large barrier for heat flow, a single molecular chain still had a thermal conductivity of ~ 7 W/m K [22]. Virendra et al. developed an electro-polymerization using nanoscale

templates to improve the thermal conductivity of polythiophene nanofibers up to ~ 4.4 W/m K and it was more than 20 times than the bulk polymer. The enhancement was attributed to the significant polymer chain orientation [23]. Apart from the fibration to obtain highly aligned polymer chains, a locally ordered structure is also useful for thermal conduction. As shown in Fig. 1.2, Kim et al. utilized strong hydrogen bonding between short and rigid polymer A and long and flexible polymer B to realize the penetration of polymer A within the gyration radius of polymer B. Under the influence of polymer B and strong hydrogen bonding, polymer A tended to form an ordered structure, which greatly reduced the barrier of phonon transportation [24].

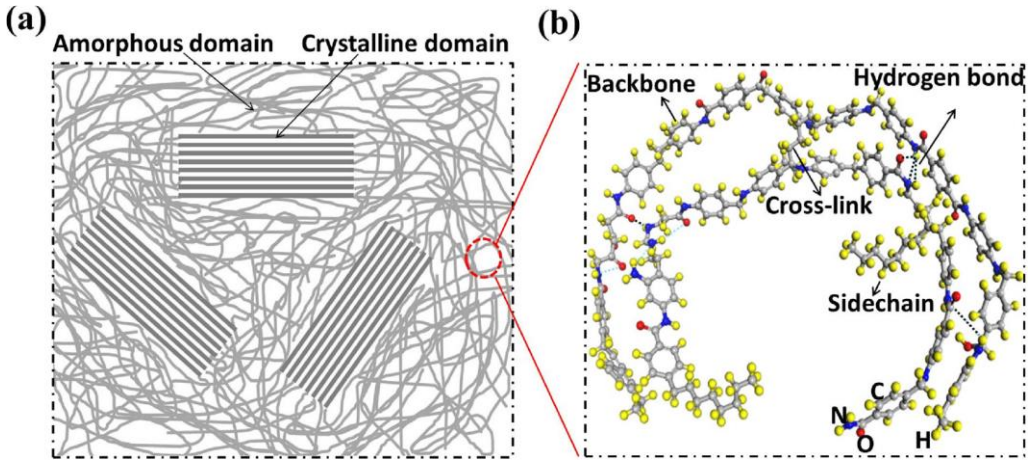

Fig. 1.1. Schematic illustration of a polymer: a) the morphology of a polymer consisting of crystalline and amorphous domains, and b) structure of a polymer chain. Reproduced from Ref. [18].

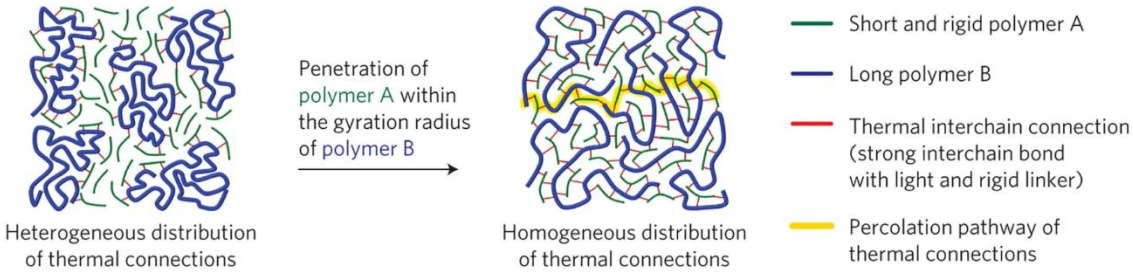

Fig. 1.2. Illustrations of heterogeneous (left) and homogeneous (right) distribution of thermal conductive interchain connections. Reproduced from Ref. [24].

As discussed above, some special polymers equipped with high thermal conductivity have been obtained, while the fabrication of such special polymers is often extremely complicated and expensive. Moreover, the form of the materials is generally a nano-sized solid, which severely limits the applications. Besides, the thermal conductivity of the polymers is largely influenced by other factors such as the chain alignment, chain defects, and interfacial vibration, which would greatly scatter the phonons [25]. Due to these reasons, the study of intrinsic thermal conductive polymers is still in the laboratory exploration stage.

Compared with intrinsic thermal conductive polymers, thermal conductive polymer composites are more attractive and promising candidates for heat dissipation due to the ease, feasibility, and flexibility of the processing. In fact, the thermal conductivity of practical polymers is low, which usually falls in the range of 0.2 ~ 0.50 W/m K [7,26–29], due to significant phonon scattering by defects and

grain boundaries in polymer matrices. By adding fillers with high thermal conductivity, the thermal conductivity of polymers can be greatly enhanced while maintaining the good processability of the original polymers. Many thermal conductive fillers can be used for the preparation of thermal conductive composites. Among them, thermal conductive fillers with electrical insulating properties including aluminium oxide (Al_2O_3), aluminum nitride (AlN), boron nitride (BN), magnesium oxide (MgO), zinc oxide (ZnO), silicon oxide (SiO_2), silicon carbide (SiC) have been widely used to fabricate insulating thermal conductive composites [30–37] to satisfy the requirement of high thermal conductivity and electrical insulation. Yao et al. improved the thermal conductivity of glass fiber-reinforced bismaleimide-triazine resin to 1.07 W/m K by adding 70 wt% Al_2O_3 nanoparticles [30]. Lee et al. obtained epoxy/AlN composites with the thermal conductivity of 3.39 W/m K, 15 times higher than the pure epoxy at the loading of 57 vol% [38]. As such, an extremely high filler loading, typically over 50 vol%, is usually required to achieve the desired thermal conductivity, which is detrimental for the weight, cost and processing. Accordingly, the current research focus in thermal conductive polymer materials is the improvement of the thermal conductivity using a reduced filler loading.

1.2 Applications of thermal conductive polymer composites

Thermal conductive material attracts great attention with the rapidly increasing cooling demand in emerging industries. Polymer composites are very promising for many practical applications due to their advantages, such as light weight, good processability, low cost, and the controllable electrical conduction and insulation. Here, four representative applications of thermal conductive polymer composites are described.

1.2.1 Electronic packaging

The rapid miniaturization and high degree of integration of electronic devices inevitably result in the generation of a large amount of heat in small space. This heat must be efficiently dissipated, otherwise the lifetime and performance of electronic devices will be influenced. The design of electronic packaging is thus very important for heat dissipation and elimination of hot spots in electronic devices. Inorganic thermal conductive materials with good electrical insulating, including metal oxides, nitride ceramics, and other non-metallic materials, were the main electronic packing materials at the early stage. However, they cannot satisfy the demand of the modern electronic packaging technology due to their high price and poor processability. Thermal conductive polymer materials have become a promising alternative and gradually replaced the traditional ceramic electronic

packing materials. The application of thermal conductive composites in electronic packaging are mainly focused on automotive electronic control units, single chip packages, and 3D chip packages [13].

1.2.2 LED packaging

Light emitting diode (LED) has higher energy efficiency and longer lifetime than traditional lighting, thus attracting attentions. However, even for high-efficiency LED devices, only 15 ~ 20 % of the input energy can be converted to light, and the remaining energy is transferred to heat. If this heat cannot be dissipated from LED devices, the lighting performance, lifetime and energy efficiency can be significantly influenced. Therefore, materials with good thermal conductivity for heat dissipation from the LED inside package to the outside are very important.

Conventionally, the thermal management system of LED devices contains a heat sink and thermal interface materials. The thermal conductivity of commonly used thermal interface materials, including phase-change materials, silicon-based grease and gels, is relatively low. Increasing the thermal conductivity of thermal interface materials or reducing the interfacial thermal resistance can improve the heat dissipation of LED devices. Hu et al. applied CNTs into silicone/metal composites, obtaining a thermal interface material with high thermal conductivity [39]. Aligning CNTs in the direction perpendicularly with the contact surface is regarded as a useful method to further enhance the thermal conductivity of thermal interface materials

[40–42].

A new direction to improve the heat dissipation efficiency is directly placing chips on the heat sink. Good electrical insulation of the heat sink is the prerequisite of this method. The commonly used method is filling polymer with thermal conductive ceramic materials. However, a very high filler loading is needed to reach a required thermal conductivity value higher than 10 W/m K. Such a high filler loading brings new problems such as high cost and poor processability. Therefore, achieving high thermal conductivity at a low filler loading becomes a current research target. Besides, the heat dissipation efficiency is also affected by the geometry of the heat sink [43,44].

1.2.3 Aerospace applications

High-performance engineering polymers or their composites are important components in the aerospace area. These materials offer advantages such as excellent mechanical properties, corrosion resistance, lightness, self-lubrication, and economy in fabrication and decoration processes. Generally, aerospace devices should endure hash environments such as high frequency, high pressure and high power factor, to maintain their stability and high performance. In this case, the good heat dissipation must be guaranteed. At present, thermal conductive composites filled with Al_2O_3 or AlN powder have been widely used to prepare highly thermal conductive composites for packaging and connecting materials in the aerospace area.

1.2.4 Batteries

Thermal management is also very important for batteries especially because that they are more powerful and applied in many devices. More heat can be generated than the dissipated heat when the charge/discharge rate is high or when the batteries are used at high temperature. If too much heat is concentrated in the batteries, the bursting could happen due to the internal pressure buildup. Due to this reason, materials with high thermal conductivity are needed to effectively dissipate the heat inside the batteries, for which thermal conductive composites have been used. For example, Maleki et al. found a hybrid graphite and carbon black filled PVDF composite is a good alternative for the traditional negative electrode in Li-icon cells, due to the high thermal conductivity [45]. Khan et al. fabricated graphene nanoflakes embedded polyacrylonitrile and polymethyl methacrylate nanofiber separators by electrospinning [46]. The thermal conductivity became as high as 8.5 W/m K by the addition of 8 wt% of graphene.

1.3 Mechanisms and models of thermal conductive composites

1.3.1 Thermal conductive mechanisms

Heat transfer concerns about the generation, use, conversion, and change of heat and is usually realized in the means of thermal conduction, thermal radiation, and thermal conversion. According to the thermal dynamic theory, it associates with the

movement, vibration, and rotation of molecules, atoms and electrons [10,47,48]. A mater shows different thermal conductivity at different states, while no matter in what states, the thermal conduction transfers the vibrational energy to the neighboring one and is resulted from the collision and without any motion of mater (Fig. 1.3) [11,49,50].

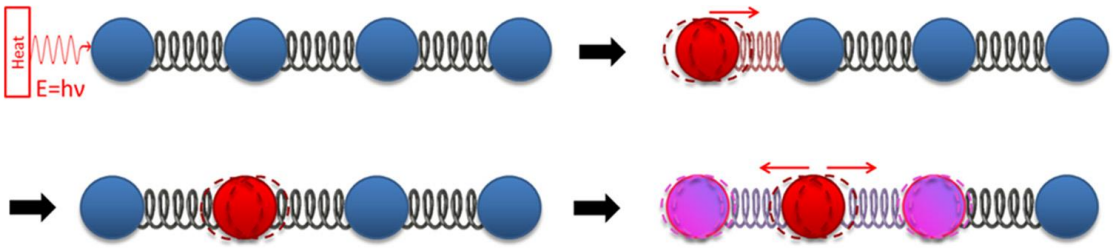

Fig. 1.3. Heat conduction caused by collision. Reproduced from Ref. [11].

The thermal conduction carrier in a solid mainly includes electrons, photons and phonons. For most polymers, the primary thermal conductivity is dominated by phonons [51]. In the crystalline domains, the thermal conduction comes from the vibration of highly ordered crystalline lattice. When heat is applied, it firstly arrives at the closest surface atom and then flows to the adjacent atom. Such vibration of atoms will be transmitted in a similar way as the propagation of waves through the whole crystal [11]. The quantization of the collective lattice vibration energy is called a phonon [52]. In the amorphous domains, the thermal conduction is based on the independent or non-correlated vibration among the neighboring atoms, where

heat cannot flow as waves, but will diffuse much more slowly. When heat reaches the atoms, it causes disordered vibration and rotation of other atoms around them and then heat is scattered to the adjacent chains [53]. The crystallinity for most polymers is low and the crystals are usually not perfect, thus the thermal conductivity of polymers is limited. Furthermore, inherent defects in polymers including impurities, voids, entanglements, and chain ends can cause considerable phonon scattering, resulting in low thermal conductivity.

The thermal conductive percolation theory and thermal conductive path theory are the main thermal conductive mechanisms of thermal conductive composites. In fact, the percolation theory has been widely used to explain the electrical conductive behavior of electrical conductive composites consisting of electrical insulating polymer matrices and electrical conductive fillers. With the increase of filler loading, materials transfer from insulator to conductor and the electrical conductivity dramatically jumps up over a critical loading, termed the percolation threshold [54–58]. For thermal conductive composites, the percolation theory works only for the system filled with specific fillers such as carbon nanotubes and graphite [59,60]. Many problems appeared when using the percolation theory to explain the thermal conductive behavior. Unlike the sudden increase of electric conductivity at the percolation threshold, the increase of thermal conductivity is much slower. In further increasing the thermal conductive fillers over the percolation threshold, the thermal

conductivity tends to increase linearly rather than keeping a constant value [61]. These problems limit the application of the percolation theory in the field of thermal conductive composites.

Compared with the percolation theory, the thermal conductive path theory is more versatile and widely applied by scholars to explain the thermal conductive behavior of composites. As shown in Fig. 1.4a, individual particles of a thermal conductive filler are isolated in a polymer matrix at a low filler loading. In this case, the polymer matrix constitutes a continuous phase and the filler the dispersed phase, in which filler particles are surrounded by the matrix without any contact or overlap between particles, forming a structure similar to the "sea-island" structure. Therefore, the thermal conductivity of composites under this condition is mainly determined by the thermal conductivity of the polymer matrix. The addition of the filler causes a minor impact on the thermal conductivity. With the increase of the filler loading, the concentration of filler particles in the polymer matrix increases, and some filler clusters are formed (Fig. 1.4b,c). The formed filler clusters contact and overlap with each other and local thermal conductive paths can be thus constructed. When the loading is further increased, thermal conductive paths can gradually connect with each other, and finally develop to a thermal conductive network throughout the whole material (Fig. 1.4d). Under this condition, both of the polymer matrix and filler are continuous and the interpenetrating thermal conductive network

significantly improves the thermal conductivity of composites [62].

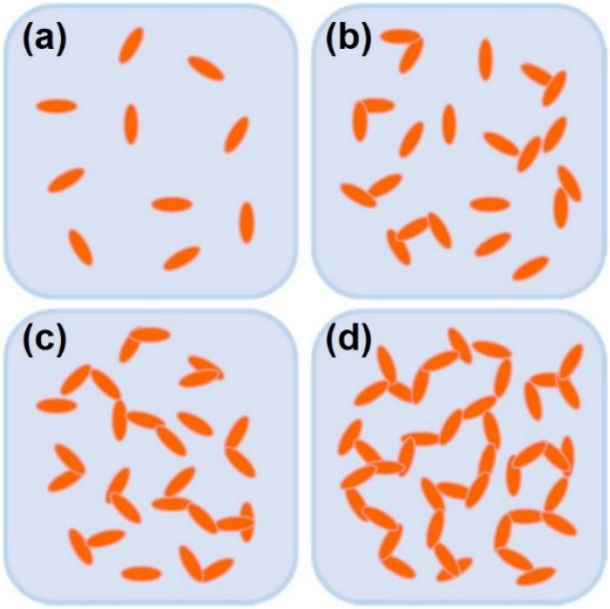

Fig. 1.4. Thermal conductive composite with different filler loadings. a) fillers are isolated in matrix at extremely low loading, b) some fillers contact with each other when more fillers are added, c) local thermal conductive paths are formed with the further increase of fillers, and d) continuous thermal conductive paths are formed at a high filler loading. Reproduced from Ref. [10].

1.3.2 Thermal conductive models and equations

The thermal conductivity of fillers and polymer matrices, and the interfacial thermal resistance greatly affect thermal conductivity of polymer composites, and it also has a close relationship of the microstructure of polymers as well as the loading,

shape, surface performance, dispersion, and distribution of thermal conductive fillers [63]. Therefore, estimating the thermal conductivity of composites by suitable models and equations is very crucial. Based on the thermal conductive path theory, many models and equations were proposed to predict the thermal conductivity of composites [51,64–67].

Parallel and series models

Series and parallel models (Fig. 1.5) are two simple and basic models developed to predict the thermal conductivity of polymer composites. The parallel model assumes that the temperature gradient is uniform in composites and the total heat flux is the weight sum of the heat flux in the filler and polymer parts. The series model assumes that the heat flux is uniform in composites and the temperature gradient is the weight sum of the temperature gradient in the filler and polymer parts [13].

According to the parallel model, a polymer matrix and a thermal conductive filler contribute to the overall thermal conductivity independently in proportional to their volume fractions,

$$\lambda=(1-V_f)\lambda_p+V_f\lambda_f \quad (1\text{-}1).$$

Here, λ, λ_p and λ_f are the thermal conductivity of the composite, polymer matrix and filler, respectively. V_f represents the volume fraction of the filler. This model

maximizes the contribution of the filler because it is based on the assumption that the filler particles are perfectly contacted in fully percolated networks. At present, the parallel model has been applied for composites filled with continuous fibers in the direction parallel to the fibers and to estimate the upper bound of the thermal conductivity of composites.

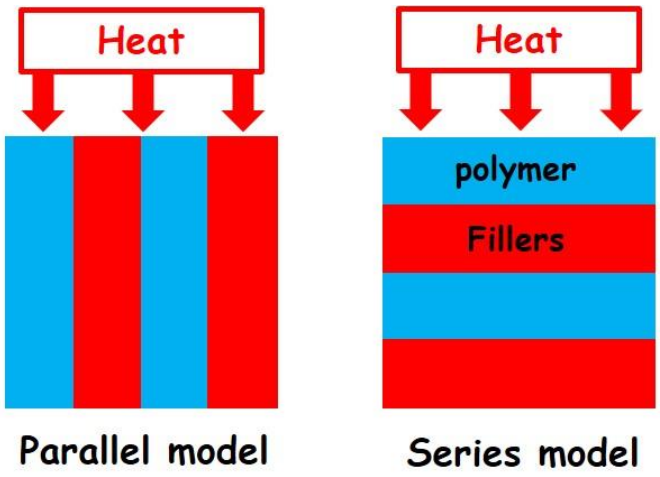

Fig. 1.5. Series and parallel models for thermal conductive composites. Reproduced from Ref. [13]

Compared with the parallel model, the series model assumes that fillers are isolated with each other and no contact between filler particles is present, and thus the model gives the lower boundary. Within this model, the thermal conductivity of composites can be predicted by Eq. (1-2). When thermal conductive filler particles are uniformly distributed in a polymer matrix and no thermal conductive networks

are formed in composites, the series model shows high accuracy.

$$\lambda=\frac{\lambda_p\lambda_f}{\lambda_f(1-V_f)+\lambda_p V_f} \quad (1\text{-}2).$$

It is known that the thermal conductivity of composites usually falls in the region between the parallel and series models. Even so, the series model is generally closer to the experimental value, thus resulting to the development of many other thermal conductive models based on the series model.

Hashin-Shtrikman model

The Hashin-Shikman model was developed to predict the thermal conductivity of macroscopically homogeneous and isotropic composites [68]. When the thermal conductivity of the polymer matrix is lower than that of the filler, the thermal conductivity of composites can be estimated by the Hashin-Shtrikman low boundary (λ^{HS-}) as,

$$\lambda^{HS-}=\lambda_p\frac{2\lambda_p+\lambda_f-2V_f(\lambda_p-\lambda_f)}{2\lambda_p+\lambda_f+V_f(\lambda_p-\lambda_f)} \quad (1\text{-}3).$$

If the polymer matrix processes higher thermal conductivity and surrounds filler particles with lower thermal conductivity, the Hashin-Shtrikman upper boundary (λ^{HS+}) can be used to predict the thermal conductivity of composites,

$$\lambda^{HS+}=\lambda_f\frac{2\lambda_f+\lambda_p-2V_p(\lambda_f-\lambda_p)}{2\lambda_f+\lambda_p+V_p(\lambda_f-\lambda_p)} \quad (1\text{-}4).$$

Using the Hashin-Shtrikman low and upper boundaries, the interconnectivity of the thermal conductive part in composites ($X_{interconnected}$) can be evaluated based on,

$$X_{interconnected}=\frac{\lambda_{measured}-\lambda^{HS-}}{\lambda^{HS+}-\lambda^{HS-}} \quad (1\text{-}5),$$

which can be used to evaluate the network formation to the ideally interconnected network [69]. The closer to 1 the $X_{interconnected}$ is, the better the interconnection of the thermal conductive paths is. The Hashin-Shikman bounds always fall within the parallel-series bounds, regardless of the volume fraction and the thermal conductivity of polymers and fillers, thus they are the best possible boundaries for homogeneous, isotropic binary systems [63,70–73]. However, the Hashin-Shtrikman model assumes a spherical approximation for thermal conductive fillers, and it is not suitable for fillers with high aspect ratio and/or microgeometry/morphology.

Bruggeman model

Even though many models have been proved successful to predict the thermal conductivity of composites, they are basically based on the assumption that the thermal conductive fillers are isolated in the polymer matrix. Therefore, these models are not valid for composites with a high filler loading, where some fillers are likely to contact with each other and possibly results in the formation of thermal conductive paths [74]. For such composites, a theoretical model proposed by Bruggeman [75] and modified by Landauer [76] (Eq. 1-6) is more suitable for predicting the thermal conductivity,

$$1-V_f=\frac{\lambda_f-\lambda_c}{\lambda_f-\lambda_p}\left(\frac{\lambda_p}{\lambda_c}\right)^{1/3} \quad (1\text{-}6).$$

This model is based on the differential effective medium (DEM) theory, which assumes the composite can be built up incrementally by introducing infinitesimal changes to a material that already exists. This model uses the mean field approach to capture the interconnection among the fillers that are randomly distributed in the polymer matrix and no limitation is present for the filler concentration [77]. Due to this reason, the Bruggeman model is applicable for the prediction of highly filled composites where filler clusters are formed.

Hatta model

The Hatta model is usually applied to predict the thermal conductivity of composites filled with thermal conductive fillers of a platelet shape.

$$\lambda=\left[1+\frac{V_f}{S(1-V_f)+\lambda_p/(\lambda_f-\lambda_p)}\right]\lambda_p \quad (1\text{-}7).$$

Here, S is related to the measurement direction: S = πd/4t in the plane direction and 1-πd/4t in the thickness direction, where d and t are the diameter and thickness of the plates, respectively. This model incorporate the effect of the filler orientation, shape as well as anisotropy in the particle shape, proven to be sufficiently accurate for composites with platelet-shaped fillers, such as graphene and boron nitride [78–81].

Agari model

The Agari model is another suitable theoretical model for polymer composites at a high filler loading by introducing the vertical and parallel conduction mechanism [82–84]. Unlike other models assuming the shape of fillers (usually spherical), Agari model does not define any shape factors of fillers. In addition, the Agari model takes the filler dispersion state into consideration by introducing two factors C_1 and C_2 as,

$$\log \lambda = V_f C_2 \log \lambda_f + (1-V_f) \log(C_1 \lambda_p) \quad (1\text{-}8),$$

where C_1 is a factor relating to the polymer structure, such as crystallinity and crystal size, and C_2 is a factor relating to the ease of forming thermal conductive paths. The closer to 1 C_2 is, the easier for the fillers to form thermal conductive paths. According to the Agari model, the thermal conductivity of composites can vary with the change of filler dispersion state, even if they are consisted with the same components. In other words, based on fitting the experimental data into the Agari model, the dispersion states of fillers in composites can be obtained [85,86].

Apart from the above-mentioned models, other theoretical models such as Hamilton-Crosser model [87], Zhou model [65], Cheng-Vachon model [88], Russell model [89], Baschirow-Selenew model [90], Nielsen-Lewis model [91], and Spinger-Tasi model [92] have also been developed to predict the thermal conductivity of polymer composites. They can reasonably fit the experimental data for specific systems. In general, the thermal conductive models can give an estimate

for the thermal conductivity of composites and avoid obviously unnecessary experiments. On the other hand, the models are generally based on some ideal assumptions such as isolated fillers with spherical shapes, perfectly aligned fibers or plates, which are different from the real case. Therefore, more accurate analysis is required and the models need to be further modified [13].

1.4 Main research directions for high thermal conductivity

As discussed in 1.1, preparing thermal conductive polymer composites by adding highly thermal conductive fillers is more feasible than controlling the polymer morphology at an atomic/molecular level. At present, a high filler loading is usually needed to achieve high thermal conductivity, while it compromises other important properties such as mechanical and optical properties. Based on these considerations, improving the thermal conductivity of composites at a low filler loading is a major challenge of the field. The research efforts in this direction is described below, which are subdivided into interface engineering, filler orientation, hybrid fillers, and formation of filler networks as different strategies.

1.4.1 Interfacial engineering

In practice, the enhancement of thermal conductivity in composites is usually unsatisfied because of the high interfacial resistance originated from strong interfacial phonon scattering [93–97]. The aggregation states of polymer matrices

and thermal conductive fillers are different, causing inharmonic phonon vibration and interfacial phonon scattering. In addition, defects and voids resulted from poor filler dispersion and interfacial incompatibility between the polymer matrix and fillers hinder the thermal conductivity enhancement. Therefore, engineering the interface between matrices and fillers becomes a trend to fabricate highly thermal conductive composites.

The surface treatment and functionalization of thermal conductive fillers by covalent and non-covalent bonding have been widely applied to enhance the coupling of polymer matrices and fillers. Commonly used covalent modifiers include silane coupling agents, surfactants, grafted polymer chains and etc. [98–101]. According to molecular dynamics simulations, the interfacial thermal resistance of graphene–polymer can be reduced by grafting polymer chains to graphene [102–104]. The improvement of thermal conductivity by surface treatment and functionalization were also proven by many experiments. In our previous research, it was found that a silane coupling agent, (2-phenylethyl)trimethoxysilane, can tailor the interfacial interaction between PP and Al_2O_3 nanoparticles, leading to the enhancement of thermal conductivity of 0.74 W/m K at 20 wt% compared to 0.41 W/m K for the unmodified nanocomposite at the same loading [105]. Wattanakul et al. improved the thermal conductivity of BN filled epoxy composites from 1.5 W/m K for untreated BN to 2.69 W/m K by admicellar treatment to

enhance the interfacial adhesion [106]. Ding et al. synthesized polyamide-6 (PA6)/graphene (GO) composites by in-situ ring-opening polymerization reaction, in which PA6 chains were covalently grafted onto GO sheets through the "grafting to" strategy. The good interfacial adhesion between PA6 and GO improved the thermal conductivity from 0.196 W/m K for neat PA6 to 0.416 W/m K of PA6/GO composite at a GO loading of 10 wt% [107]. Yu et al. treated Al_2O_3 nanoparticles with a silane coupling agent and then grafted hyperbranched aromatic polyamide from the modified surface. The resultant Al_2O_3 nanoparticles were uniformly distributed in an epoxy matrix and the interfacial interaction was improved, leading to enhanced thermal conductivity [108].

Even though the above and other research efforts demonstrated that covalent functionalization of fillers could improve the thermal conductivity of composites, many other results reported that it leads to minor improvement or even could reduce the thermal conductivity of composites. This is because the covalent functionalization may deteriorate the surface structure of fillers, resulting in the loss of the instinct thermal conductivity of fillers [109–111]. In this light, non-covalent functionalization is an alternative approach to enhance the polymer-filler interfacial interaction without reducing the instinct thermal conductivity of fillers. Teng et al. functionalized graphene nanosheets (GNSs) by π–π stacking of pyrene having a functional segmented polymer chain in the molecular structure, which resulted in

the significant enhancement of thermal conductivity to 1.91 W/m K,, which was 20% higher than GNS/epoxy and 267% higher than carbon nanotube (CNT)/epoxy [112]. Zhang et al. enhanced the interfacial interaction of CNTs and poly(vinylidene fluoride) (PVDF) by treating CNTs using polyvinylpyrrolidone, resulting in the improvement of thermal conductivity to 0.63 W/m K at the CNT loading of 10 wt%, which was 34% higher than untreated CNT filled PVDF [113]. Wu et al. found that non-covalent functionalization of BN by polydopamine not only improved the thermal conductivity of nanocomposites, but also resulted in outstanding mechanical properties and dimensional stability [114].

The functionalization of thermal conductive fillers can improve the interfacial performance of polymer and fillers. However, the introduced organic modifier is an isolation layer of heat and overmuch modification can reduce the thermal conductivity. In contrast, inorganic coating can not only enhance the interfacial interaction between polymer and fillers, but also further improve the thermal conductivity by employing thermal conductive layer [115]. Besides, thermal conductive materials need to be electrically insulating for many applications. However, many thermal conductive fillers such as metal particles and carbon materials have good electrical conductivity. By coating the surface of electrically conductive fillers with insulating inorganic materials, electrical insulating polymer composites with high thermal conductivity can be obtained. Cui et al. successfully

prepared core-shell structured MWCNT@SiO_2 with a uniform SiO_2 coating on the surface of MWCNTs, and added them into an epoxy matrix [93]. They found the less stiff SiO_2 intermediate shell introduced on the surface of MWCNTs not only reduced the modulus mismatch between the soft epoxy matrix and the stiff MWCNTs, but also enhanced the interaction, resulting in the increase of thermal conductivity by 67% at a low filler loading of 1 wt%. Similar enhancement of thermal conductivity was reported by Chen et al. using a sol-gel method to synthesized SiO_2-coated silver nanowires [116], and by Choi et al. using a polyvinylpyrrolidone (PVP)-assisted sol-gel reaction to prepare SiO_2-coated graphite [117]. Al_2O_3 nanoparticles were also used to form the core-shell structure. Sun et al. utilized supercritical carbon dioxide ($scCO_2$) to form Al_2O_3 nanoparticle-coated graphene nanoplatelets (GNPs) and then used them to prepare epoxy-based composites [118]. The obtained composites exhibited a high thermal conductivity of 1.49 W/m K at a filler loading of 12 wt%. Al_2O_3-coated aluminum (Al) nanoparticles were also proposed to obtain electrical insulating materials with high thermal conductivity by Badi et al. [119].

1.4.2 Filler orientation

One dimensional (1D) and two dimensional (2D) fillers such as fibers, CNTs, nanowires, palate-like BN, graphene sheets and graphite flakes usually have anisotropic thermal conductivity [13]. The axial or in-plane thermal conductivity of

these fillers is generally higher than that of the other direction. For example, the in-plane thermal conductivity of BN is ~ 600 W/m K, much higher than ~ 30 W/m K in the out-of-plane direction [120]. For composites filled with 1D or 2D thermal conductive fillers, a perfect orientation of fillers in their longitudinal axes can result in great thermal conductivity enhancement in the direction parallel to the orientation direction. The orientation of fillers is also advantageous for the formation of thermal conductive networks; thus, this strategy is very powerful for improving the thermal conductivity of composites at a low filler loading.

Research efforts on the filler orientation include those related to the in-plane orientation and through-plane orientation. For the former, 1D or 2D fillers preferentially align in the in-plane direction of the thermal conductive composite films and form thermal conductive networks in the in-plane direction. In this case, the thermal conductivity of the composites in the in-plane direction is much higher than that in through-plane direction. Zeng et al. prepared BN nanotube (BNNT)/cellulose nanofiber nanocomposites by vacuum filtration (Fig. 1.6 a,b) [121]. They found that BNNTs were uniformly dispersed in the cellulose nanofiber matrix because of the strong interaction of fillers and the matrix. Due to the gravity and vacuum filtration, BNNTs presented an obviously orientated distribution (Fig. 1.6 c,d). The obtained composites had a thermal conductivity value of 21.39 W/m K in the in-plane direction and 4.71W/m K in the out-of-plane direction at a BNNTs

loading of 25 wt%. Kumar et al. utilized a simple solution casting method to fabricate high self-aligned large-area reduced graphene oxide (rLGO)/poly (vinylidene fluoride-co-hexafluoropropylene) (PVDF-HFP) composite films [122]. The obtained film revealed ultrahigh in-plane thermal conductivity of ~ 19.5 W/m K at a filler loading of 27.2 wt%. Apart from these methods, other polymer processing approaches such as two-roll milling [123], melt extrusion [124,125], injection molding [126–128], and spinning [129] can be used to prepare in-plane thermal conductive composites.

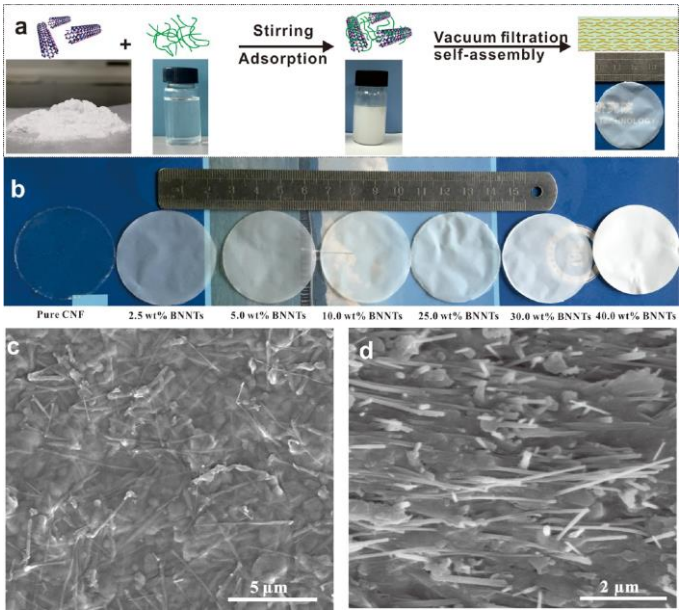

Fig. 1.6. a) Schematic illustration of the fabrication of the CNF/BNNT nanocomposites. b) Optical images of CNF/BNNT nanocomposites with different BNNT loadings. c) Surface SEM and d) cross-section morphology of CNF/BNNT nanocomposites with 25 wt % of BNNTs. Reproduced from Ref. [121].

Compared with the in-plane thermal conductivity, increasing the out-of-plane thermal conductivity of composites are more important for practical electronic applications. Unfortunately, it is still a challenge and relatively little research was reported. In recent years, with the technical development of aligning fillers by external fields, such as magnetic and electric fields, and the proposal of an ice-templated assembly strategy, the research of increasing the out-of-plane thermal conductivity of composites has made some progress. Yuan et al. modified the surface of hexagonal BN (hBN) with superparamagnetic iron oxide nanoparticles, then aligned fillers by an external magnetic field (Fig. 1.7) [130]. The resultant composites revealed 44.5 % higher out-of-plane thermal conductivity than unaligned composites at a filler loading of 9.14 vol%. Alignment of thermal conductive fillers by magnetic fields for the thermal conductivity enhancement of composites have also been reported by other researchers [131–135].

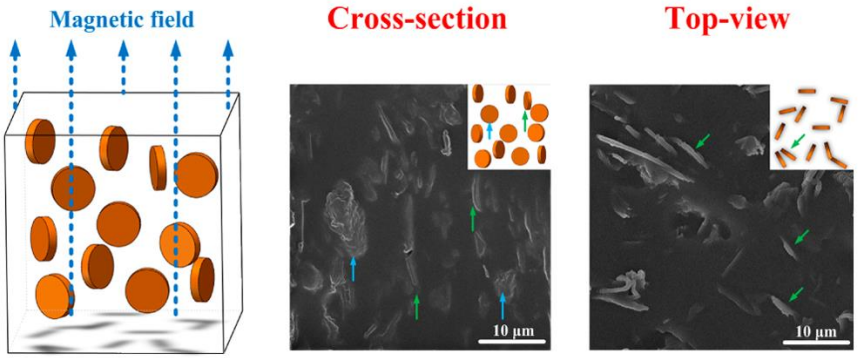

Fig. 1.7. Illustration and SEM micrographs of epoxy/hBN composites. Reproduced from Ref. [130].

An electric field is also used to align thermal conductive fillers for enhancing the out-of-plane thermal conductivity. Cho et al. used a high DC electric field to form linear assemble hBN nanosheets (Fig. 1.8a) [136]. The oriented structure (Fig. 1.8b) resulted in effective thermal conduction in the out-of-plane direction. Fujihara et al. further advanced this strategy to assemble hBN nanosheets into a filament-like structure with denser population and extended length in a polymer matrix by microscopic molds [137]. The thermal diffusivity increased from 8.67×10^{-8} m^2/s for random distribution to 9.04×10^{-8} m^2/s for the composites with oriented distribution.

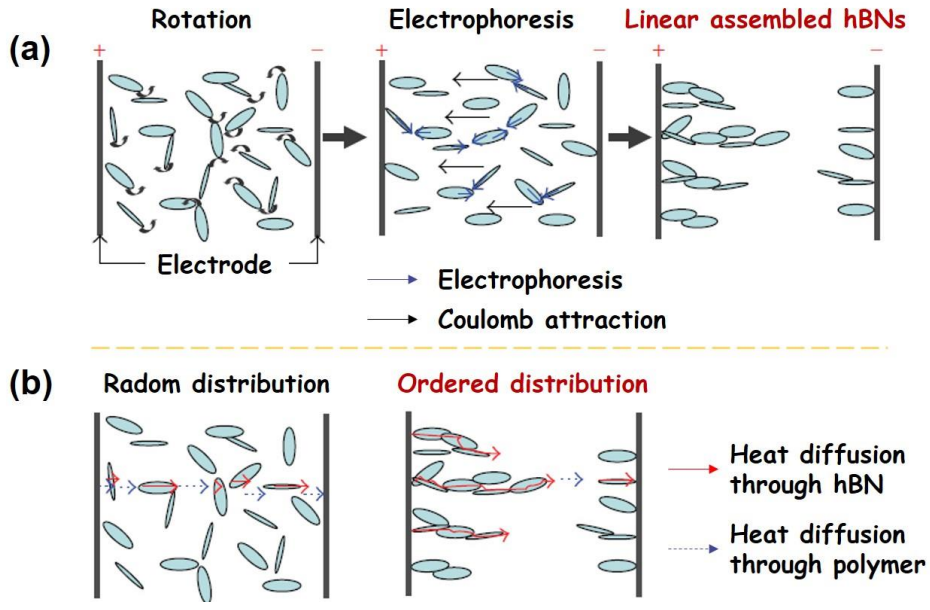

Fig. 1.8. Schematic illustration of a) formation of linear assembled hBN under a DC electric field, and b) heat diffusion in composites with different hBN distribution. Reproduced from Ref. [136].

In recent years, an ice-templated assembly strategy was proposed to orient thermal conductive fillers along the ice-growth direction. Zeng et al. reported the fabrication of a 3D boron nitride nanosheet network by an ice-templated strategy and then infiltration (Fig. 1.9) [138]. The resulting composites exhibited a high out-of-plane thermal conductivity of 2.85 W/m K at the filler loading of 9.29 vol%. This strategy is very effective to design the thermal conductive network structure for high out-of-plane thermal conductivity by controlling the crystalline state of ice in the scaffold during the freezing process, thus it has attracted great attention [139–146]. Even though efficient thermal conductive networks can be generated by the ice-templated assembly strategy, the obtained composites are usually limited to epoxy-based composites due to the preformed network structure.

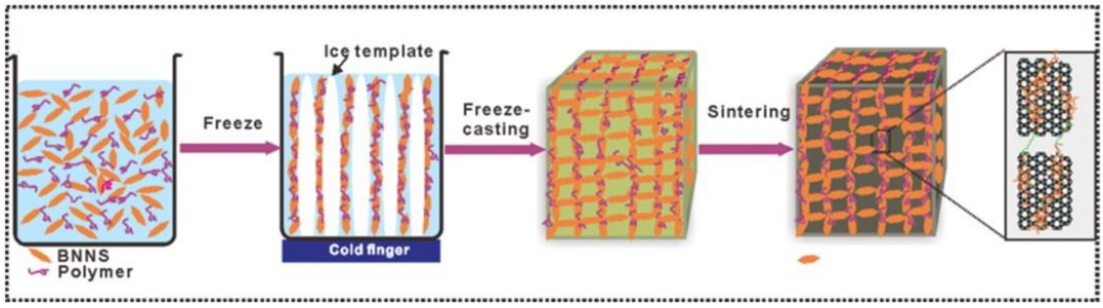

Fig. 1.9. Schematic diagram of the preparation of 3D-BNNS aerogels. Reproduced from Ref. [138].

1.4.3 Hybrid fillers

Thermal conductive networks formed by a single kind of fillers usually remain some undesired voids or defects. The addition of another kind of fillers can fill these voids to further improve the thermal conductivity of composites. The combination of two or more fillers with different sizes or shapes often shows a synergistic effect and can greatly enhance the thermal conductivity by improving filler dispersion, forming bridges between fillers and maximizing the filler packing density. Besides, the utilization of hybrid fillers can significantly reduce the filler loading, thus it can reduce the difficulty of processing. Due to these advantages, hybrid fillers have been widely used to improve the thermal conductivity of composites [24].

For thermal conductive composites, an inevitable problem is the existence of voids between fillers and/or between the polymer matrix and fillers, especially at a high filler loading. They would break the local thermal conductive networks and significantly scatter phonons at the interface, hindering the enhancement of thermal conductivity. At the same time, it is very difficult to fill these voids by adding fillers with the same size due to the space limitation. Therefore, adding fillers with the same shape but different sizes shows advantages for optimizing the packing density of fillers. As shown in Fig. 1.10, Choi et al. hybridized aluminum nitride (AlN) particles and Al_2O_3 particles with different sizes [147]. Two types of composites were prepared: one filled with large-sized AlN (10 μm) and small-sized Al_2O_3

nanoparticles (0.5 μm), and the other filled with large-sized Al_2O_3 (10 μm) and small-sized AlN (0.1 μm) particles. High thermal conductivity values of 3.402 W/m K and 2. 842 W/m K were achieved for these two types of composites at a total filler loading of 58.4 vol%. The enhancement of thermal conductivity by the hybridization of fillers with different sizes was reported in Al_2O_3 and BN composites [148,149].

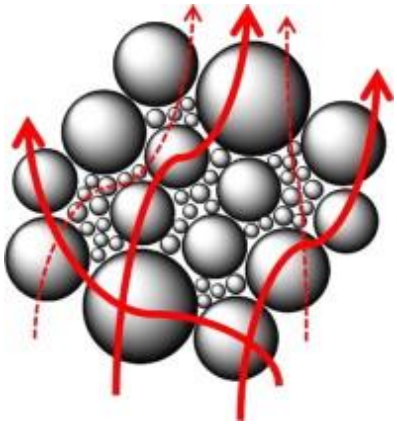

Fig. 1.10 Schematic illustration for the synergistic effect of hybrid fillers with different sizes. Reproduce from Ref. [147].

Hybridization of fillers with different shapes can also improve the thermal conductivity of composites by creating bridges between fillers. To be specific, the combination of 0D, 2D and 3D fillers are usually used to form thermal conductive networks as shown in Fig. 1.11. Generally, fillers with a high aspect ratio can serve as bridges between other fillers in the hybrid system, thus increasing the thermal

conductive paths. For example, Cao et al. reported an obvious synergistic effect between SiC (0D) and MWCNTs (1D) in PVDF/polystyrene (PS) blends, where the thermal conductivity of composites was increased from 0.98 W/m K at a SiC loading of 11.4 vol% to 1.85 W/m K by adding 2.9 vol% MWCNTs [24]. Such improvement of thermal conductivity was attributed to the bridging effect of MWCNTs among SiC nanoparticles. The similar synergistic effect of hybrid fillers was also reported using 1D and 2D fillers such as CNT and GNP [150], and CNT and BN [151–156], as well as the hybridization of 0D and 2D fillers such as Al_2O_3 and graphene [148], and Al_2O_3 and BN [157].

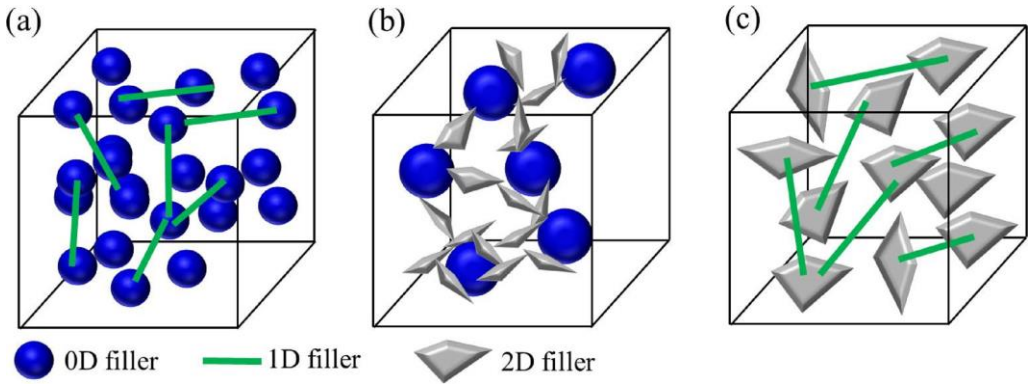

Fig. 1.11 Schematic illustration for the synergistic effect of hybrid fillers with different shapes. Reproduce from Ref. [18].

1.4.4 Formation of filler networks

Forming continuous filler networks is very critical to improve the thermal

conductivity of composites. When thermal conductive fillers are uniformly distributed in the polymer matrix, the thermal conductivity cannot be effectively improved due to the high interfacial thermal resistance, and as a consequence, as 60 ~ 70 vol% filler loading is needed to form a continuous filler network [13]. However, such a high filler loading leads to the difficulty in processing and high cost. Many approaches have been proposed to construct continuous network at a low filler loading.

A self-assembly approach has been used to construct continuous thermal conductive networks. The thermal conductive networks can be self-constructed by sintering fillers at low temperatures during the polymer curing. Nanoparticles are usually employed in this approach as they tend to sinter at lower temperatures than microparticles [158,159]. Pashayi et al. designed a three-step method, consisting of self-assembly by i) diffusion-controlled aggregation of polyvinylpyrrolidone (PVP) coated nanoparticles, ii) removal of PVP coating from the surface, and iii) sintering of silver nanoparticles in networked structures (Fig. 1.12), to construct dendritic networks of silver in a epoxy resin [160]. By careful self-assembly control and multistep condition design, a high thermal conductive value of 12.05 W/K m at a silver concentration of 10 vol% was achieved, which is up to 300% greater than the state-of-art composites at the similar silver loading.

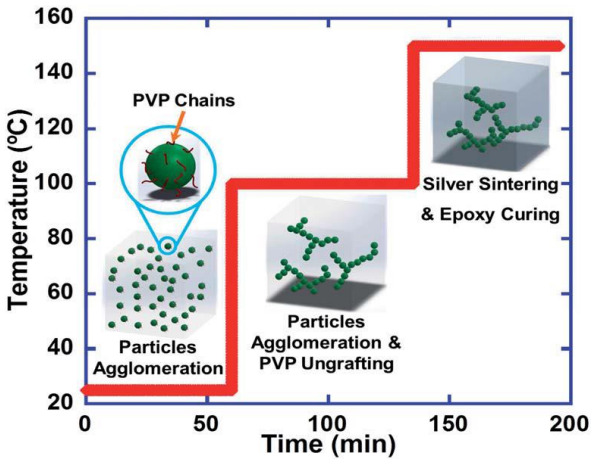

Fig. 1.12. Three-step formation of tree-shape thermal conductive networks. Reproduce from Ref. [160].

In recent years, self-supported 3D interconnected filler networks, such as 3D carbon foams (Fig. 1.13) and graphite foams have been used to reduce the high interfacial thermal resistance [161–163]. Due to the rigidity of these foams, they can maintain stable continuous networks for phonon transport. Besides, the 3D foams have high porosity and large pore sizes, which allow the introduction of polymer matrix to prepare composites [164,165]. For example, Li et al. incorporated polyamide-6 (PA6) into a graphene foam. The obtained composites exhibited the thermal conductivity of 0.847 W/m K at the graphene loading of only 2 wt% [166]. The enhancement of thermal conductivity of composites by 3D interconnected filler networks can be also found in other reports [161,167–169]. However, 3D foams face many challenges such as complex fabrication, high cost, as well as the limitation of the matrix into thermoset polymers like epoxy.

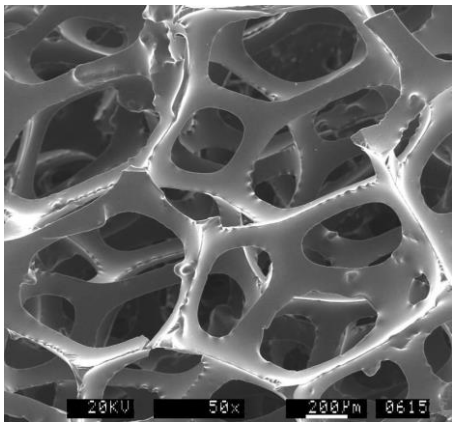

Fig. 1.13 SEM micrograph of a carbon foam. Reproduce from Ref. [163].

Recently, a segregated structure has been widely applied for reducing the percolation threshold in electrical materials by constructing local electrical conductive networks [119,170]. A segregated structure means a segregated filler dispersion state where the polymer particles are surrounded by fillers. This structure is usually constructed by mechanically mixing fillers and polymer particles, followed by compression molding of the mixture. When thermal conductive fillers are used to fabricate such a structure, the fillers can contact with each other at a low filler loading. The traditional preparation process of a segregated structure is shown in Fig. 1.14 [171]. First, fillers and polymer particles are mixed in a solvent or physically mixed to enhance the absorption of fillers on the surface of polymer particles. The obtained mixture is compression-molded at a temperature around the melting point of the polymer. Hu et al. [171] fabricated Polypropylene (PP)/AlN composites with a segregated structure by grinding PP particles and AlN powder,

and subsequent compression molding. The resulting composites showed more than 20% higher thermal conductivity than that of composites prepared by solution mixing and melt mixing. Other research also indicated the improvement of thermal conductivity by the segregated structure [172,173]. A potential concern of this strategy is imperfection of networks, e.g. physical blending may lead to non-uniform coating of polymer particles by fillers, random packing of particles may remain voids even after the hot-pressing, and so on.

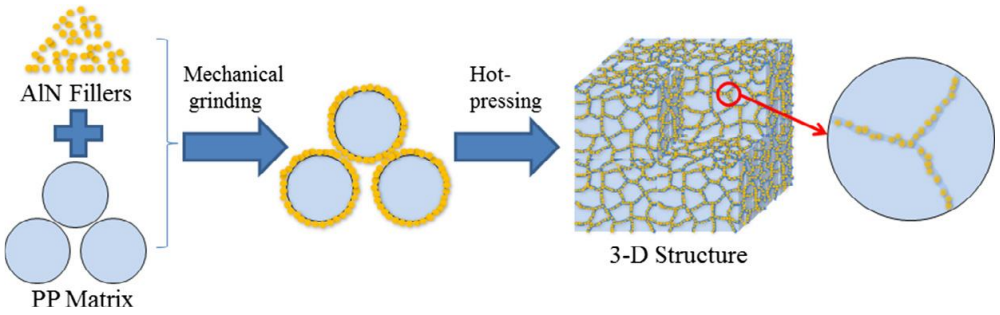

Fig. 1.14. Schematic illustration for the preparation of PP/AlN composites with a segregated structure Reproduce from Ref. [171].

Distribution of fillers in the matrix is a critical factor that determine the formation of thermal conductive networks. Increasing the local concentration of thermal conductive fillers can effectively help the formation of continuous thermal conductive networks, realizing high thermal conductivity at a low loading. The co-

continuous structure in immiscible two-phase polymer blends has been used to enhance the electrical conductivity of polymer composites [174–177]. In this structure, both two phases are continuous and fillers are selectively distributed in one phase (Fig. 1.15) due to the different affinity of the fillers to two phases, which greatly increase the local concentration of fillers in the one phase at a low filler loading. Only recently, this approach has been applied for thermal conductive materials. Cao et al. prepared SiC-filled PS/PVDF blends with a co-continuous structure [25]. They realized the selective distribution of SiC in the PVDF phase by controlling the melting sequence, resulting in the thermal conductivity value of 1.88 W/m K at a filler loading of 23.1 vol%. They further applied this structure for hybrid fillers (CNT and SiC), and obtained the thermal conductivity of 1.85 W/m K with 2.9 vol% CNT and 11.4 vol% SiC [24]. Huang et al. prepared a masterbatch of poly(lactic acid) (PLA)/graphene by solution mixing [178]. Then the masterbatch was solution-mixed with poly(ε-caprolactone) (PCL), during which fillers were driven to the interface of a continuous structure of PLA/PCL blends. Due to the selective localization of fillers at the interface, the thermal conductivity of composites reached 1.28 W/m K at the filler loading of 0.53 vol%. Compared to the above strategies, the utilization of the co-continuous structure to control the selective distribution of thermal conductive fillers is promising to be applied in many systems due to the easy processability and low cost. However, relatively little

research has been conducted at present, and many important questions for controlling the filler distribution are still open and need to be studied in detail.

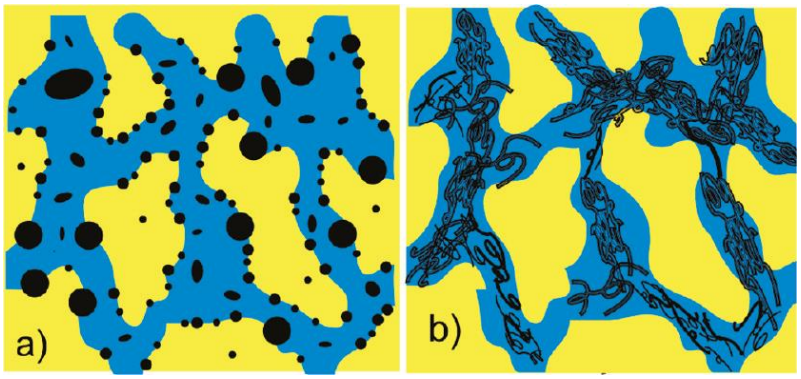

Fig. 1.15. Schematic illustrations for the selective distribution of a) low- and b) high-aspect ratio fillers [179].

From the above literature review, it can be known that many strategies have been proposed to improve the thermal conductivity of polymer composites. However, most of these strategies need complicated, i.e. impractical processes otherwise the use of prohibitively expensive fillers (remember one of the most important advantages of polymers is its cheapness). Besides, a majority of approaches are only suitable for a specific polymer matrix, such as epoxy resins. These disadvantages significantly limit the potential applications of thermal conductive polymer composites. Therefore, studying the key factors that affect the thermal conductivity, and based on which to optimize the existed strategies for new methods that are more versatile and cheaper is very important.

1.4.5 Polyolefin-based composites and reactor granule technology

Polyolefins are considered as one of the most commonly used thermoplastics due to their good environmental compatibility and excellent mechanical properties. However, it is extremely challenging to fabricate performant polyolefin-based nanocomposites, including thermal conductive ones, due to the chemical inertness of polyolefin against inorganic fillers, compared to other polar polymers. Especially for nano-sized fillers, in most of the cases, they cannot disperse in the polyolefin matrix, resulting in the formation of large and compact filler agglomerates. In such a case, it is extremely difficult for fillers to effectively form thermal conductive network. In addition, the existence of these agglomerates inevitably causes significant reduction in other properties such as mechanical properties and transparency [180]. Therefore, it is very important to develop strategies to avoid the formation of filler agglomerates in polyolefin matrices.

The olefin polymerization based on standard heterogeneous catalysts necessarily produces spherical polymer granule with a 3D porous architecture, within which monomers can diffuse and get polymerized to continue the growth [181]. In another words, the porous polymer particles can itself become a polymerization reactor. This technology is called the reactor granule technology (RGT).

For heterogeneous olefin polymerization, the particle growth usually follows the

"multi-grain" model [182] as shown in Fig. 1.16. According to this model, the catalyst is comprised of multi-grained particles. During the polymerization, the initial catalyst support becomes fragments and dispersed with the growth of polymer. Monomers polymerize on active centers of these catalyst fragments, forming a polymer shell and causing the catalyst grain to further expand progressively [183]. Thus, obtained polymer granule with a porous architecture is called reactor granule. Generally, the obtained reactor granule is immediately melt-mixed into pellets for easy shipping, and the porous structure is not normally utilized except reactor alloying for high-impact PP [184].

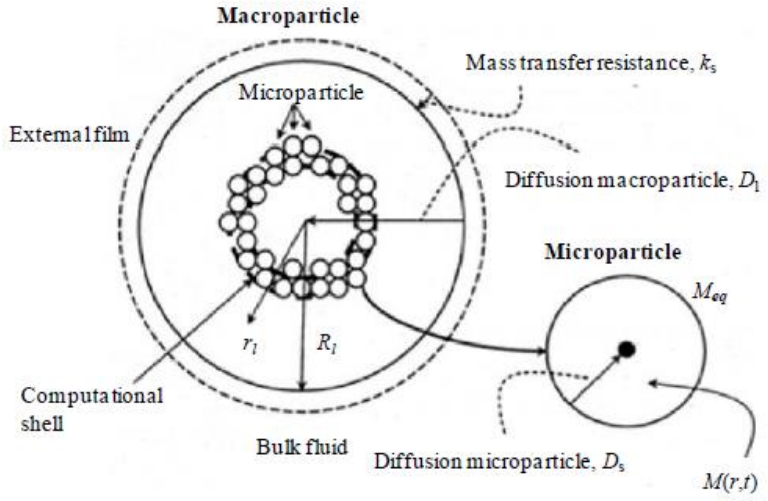

Fig. 1.16. Schematic representation of the "multi-grain" model. Reproduced from Ref. [185].

Our research group has successfully applied the pore confinement concept to in-

situ fabricate polyolefin nanocomposites, which involves the impregnation of a molecular precursor of fillers and subsequently conversion into nanoparticles using melt-mixing (Fig. 1.17). Many nanoparticles, including titanium dioxide (TiO_2), Al_2O_3, magnesium hydroxide ($Mg(OH)_2$) gold (Au) and silver (Ag), have been synthesized in the pores of polyolefin based on RGT [186–188]. Due to the pore confinement (Fig. 1.17a,b), extremely uniform dispersion (Fig. 17c) was achieved. It was found that the uniform dispersion of Al_2O_3 nanoparticles attributed to a higher thermal conductivity at a lower loading in the absence or presence of a compatibilizer (maleic anhydride grafted PP) (Fig. 17d) [186]. For further improvement, the group also melt-mixed impregnated reactor granule with pristine reactor granule to create the distribution of the dispersion [105]. These results indicate the potential of RGT in filler distribution control for polyolefin composites with high thermal conductivity (Fig. 1.19).

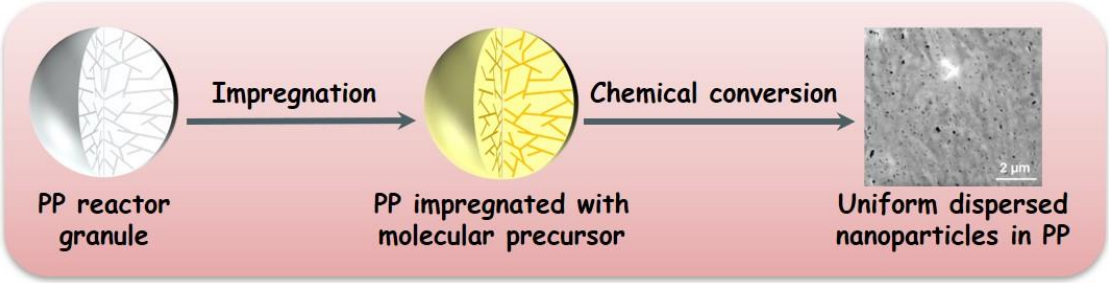

Fig. 1.17 Schematic illustrations for the reactor granule technology.

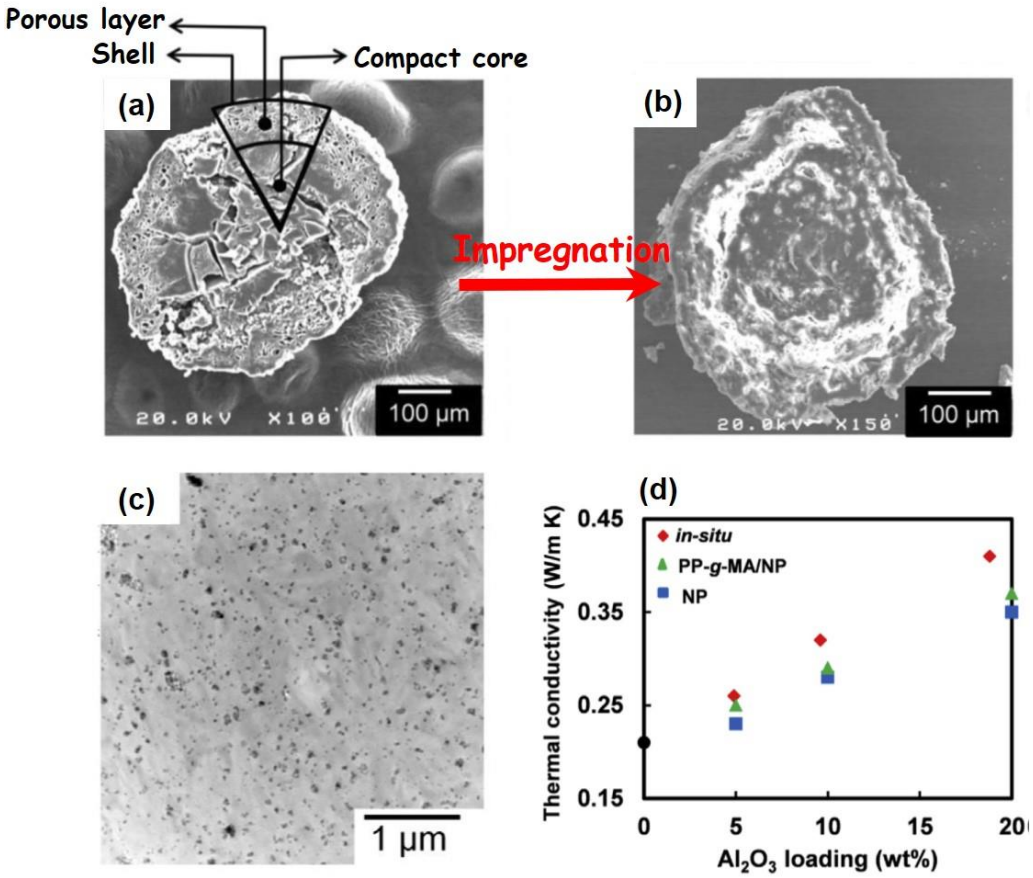

Fig. 1.18. Cross-sectional SEM micrographs of neat PP reactor granule and b) impregnated with Al(O*i*Pr)$_3$. c) TEM micrograph of the PP/Al_2O_3 nanocomposite prepared by RGT at the Al_2O_3 loading of 20 wt%. d) Thermal conductivity of three types of PP/Al_2O_3 nanocomposites. Reproduced from Ref. [186].

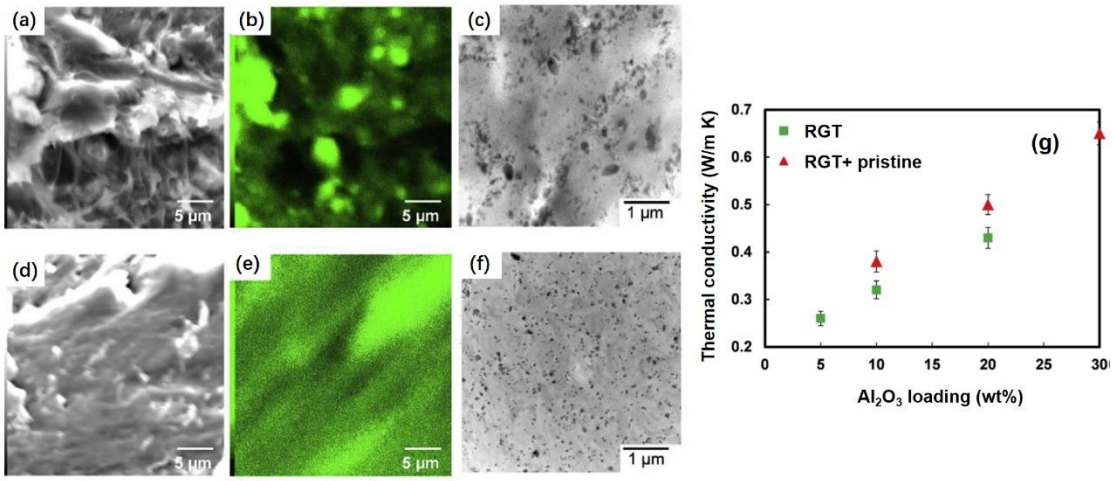

Fig. 1.19. Distribution of Al_2O_3 nanoparticles in PP for samples prepared by melt-mixing impregnated reactor granule with pristine reactor granule a,b,c) and standard RGT d,e,f). g) Thermal conductivity of two types of PP/Al_2O_3 nanocomposites. Reproduced from Ref. [105].

1.5 Aim of thesis

The rapid development of electronic integration technology results in the greatly increased packing density and remarkably reduced volume of electronic devices and logic circuits. This necessarily accompanies a large amount of heat generated and accumulated in a limited space. Efficient dissipation and elimination of this heat become a key issue to guarantee the reliable operation of relevant devices. Under such circumstances, thermal conductive composites have emerged as attractive materials in many fields, such as micro-electronic devices, LED, aerospace,

batteries, and etc. These materials offer advantages such as light weight, good processability, low cost, excellent chemical stability, and electrical insulation, thus attracting great attention in recent years. To obtain polymer composites with desired thermal conductivity, many strategies have been proposed. However, these methods generally aim at improving the thermal conductivity of specified systems, and usually require complex processing as well as very expensive thermal conductive fillers, which greatly increase the fabrication cost and significantly limit the application of obtained materials. In this light, it is very important to study the thermal conductive composites based on more commonly used polymer matrices and thermal conductive fillers. Therefore, this thesis focuses on polyolefin as the matrix, because it is one of the most commonly used thermoplastics with balanced properties and price. Spherical Al_2O_3 nanoparticles were used as the thermal conductive fillers. Even though, the thermal conductivity of Al_2O_3 is only moderate (~ 30 W/m K), it has advantages of abundance, electrical insulation and low cost [108,189]. Besides, the incorporation of spherical particles guarantees isotropic heat release in the resultant composite materials [190].

In this thesis, I aim to study the thermal conductivity of polyolefin composites filled with Al_2O_3 nanoparticles, and to clarify the key factors that affect the thermal conductivity. For this, I designed polymer nanocomposites with continuous thermal conductive networks by controlling the selective localization of nanoparticles. The

influence of filler dispersion, filler migration and phase morphology evolution on the formation of thermal conductive networks was studied, and the relationship of filler distribution and thermal conductivity was investigated. My research is mainly comprised of the following three chapters:

In Chapter 2, the reactor granule technology (RGT) was applied to immiscible polypropylene (PP)/polyolefin elastomer (POE) blends to effectively control the localization of nanoparticles at the interface. This study aims to reveal the importance of filler dispersion for controlling the distribution and realize the selective localization at the interface.

In Chapter 3, PP/POE/Al_2O_3 composites were annealed with different durations and the filler migration and phase morphology evolution were studied by electron microscopy. The relationship among nanoparticle migration, phase morphology evolution, and the thermal conductivity were investigated in detail.

In Chapter 4, a continuous segregated structure was designed to improve the thermal conductivity of PP-based nanocomposites. This proposal was based on the selective distribution of Al_2O_3 nanoparticles in the POE phase and the compression of a porous scaffold by eating POE of PP/POE blends with a co-continuous structure. The formation of this structure achieved great improvement of thermal conductivity.

References

[1] Damen L, Hassoun J, Mastragostino M, Scrosati B. Solid-state, rechargeable Li/$LiFePO_4$ polymer battery for electric vehicle application. J. Power Sources 2010; 195(19): 6902–4.

[2] Ishiguro Y, Inagi S, Fuchigami T. Site-controlled application of electric potential on a conducting polymer “canvas”. J. Am. Chem. Soc. 2012; 134(9): 4034–6.

[3] Wu C, Chiu DT. Highly fluorescent semiconducting polymer dots for biology and medicine. Angew. Chem. Int. Ed. 2013; 52(11): 3086–109.

[4] Nguyen MK, Alsberg E. Bioactive factor delivery strategies from engineered polymer hydrogels for therapeutic medicine. Prog. Polym. Sci. 2014; 39(7): 1235–65.

[5] Maitz MF. Applications of synthetic polymers in clinical medicine. Biosurf. Biotri. 2015; 1(3): 161–76.

[6] Nyholm L, Nystrom G, Mihranyan A, Stromme M. Toward flexible polymer and paper-based energy storage devices. Adv. Mater. 2011; 23(33): 3751–69.

[7] Zhang Y, Zhang C, Feng Y, Zhang T, Chen Q, Chi Q, et al. Excellent energy storage performance and thermal property of polymer-based composite induced by multifunctional one-dimensional nanofibers oriented in-plane direction. Nano. Energy 2019; 56: 138–50.

[8] Zhang X, Zheng X, Ren D, Liu Z, Yang W, Yang M. Unusual positive temperature coefficient effect of polyolefin/carbon fiber conductive composites. Mater. Lett. 2016; 164: 587–90.

[9] Deng H, Lin L, Ji M, Zhang S, Yang M, Fu Q. Progress on the morphological control of conductive network in conductive polymer composites and the use as electroactive multifunctional materials. Prog. Polym. Sci. 2014; 39(4): 627–55.

[10] Yang X, Liang C, Ma T, Guo Y, Kong J, Gu J, et al. A review on thermally conductive polymeric composites: classification, measurement, model and equations, mechanism and fabrication methods. Adv. Compos. Hybr. Mater. 2018; 1(2): 207–230.

[11] Burger N, Laachachi A, Ferriol M, Lutz M, Toniazzo V, Ruch D. Review of thermal conductivity in composites: mechanisms, parameters and theory. Prog. Polym. Sci. 2016; 61: 1–28.

[12] Vadivelu M, Kumar CR, Joshi GM. Polymer composites for thermal management: a review. Compos. Interfaces 2016; 23(9): 847–72.

[13] Chen H, Ginzburg VV, Yang J, Yang Y, Liu W, Huang Y, et al. Thermal conductivity of polymer-based composites: Fundamentals and applications. Prog. Polym. Sci. 2016; 59: 41–85.

[14] Moore AL, Shi L. Emerging challenges and materials for thermal management

of electronics. Mater. Today 2014; 17(4): 163–74.

[15] Zhang L, Deng H, Fu Q. Recent progress on thermal conductive and electrical insulating polymer composites. Compos. Commun . 2018; 8: 74–82.

[16] Jiang H, Yi Z, Cheng P, Kong C, Li M, Wang X, et al. Modified thermal resistance networks model for transverse thermal conductivity of unidirectional fiber composite. Compos Commun. 2017; 6: 52–8.

[17] Chen J, Huang X, Zhu Y, Jiang P. Cellulose nanofiber supported 3D interconnected BN nanosheets for epoxy nanocomposites with ultrahigh thermal management capability. Adv. Funct. Mater. 2017; 27(5): 1604754.

[18] Huang C, Qian X, Yang R. Thermal conductivity of polymers and polymer nanocomposites. Mater. Sci. Eng. R-Reports. 2018; 132: 1–22.

[19] Wang Z, Carter JA, Lagutchev A, Koh YK, Seong N-H, Cahill DG, et al. Ultrafast flash thermal conductance of molecular chains. Science 2007; 317(5839): 787–90.

[20] Wang RY, Segalman RA, Majumdar A. Room temperature thermal conductance of alkanedithiol self-assembled monolayers. Appl. Phys. Lett. 2006; 89(17): 173113.

[21] Shen S, Henry A, Tong J, Zheng R, Chen G. Polyethylene nanofibres with very high thermal conductivities. Nat. Nanotechnol. 2010; 5(4): 251.

[22] Luo T, Esfarjani K, Shiomi J, Henry A, Chen G. Molecular dynamics

simulation of thermal energy transport in polydimethylsiloxane. J. Appl. Phys. 2011; 109(7): 074321.

[23] Singh V, Bougher TL, Weathers A, Cai Y, Bi K, Pettes MT, et al. High thermal conductivity of chain-oriented amorphous polythiophene. Nat. Nanotechnol. 2014; 9(5): 384.

[24] Kim G H, Lee D, Shanker A, et al. High thermal conductivity in amorphous polymer blends by engineered interchain interactions[J]. Nat. Mater. 2015, 14(3): 295–300.

[25] Cao JP, Zhao X, Zhao J, Zha JW, Hu GH, Dang ZM. Improved thermal conductivity and flame retardancy in polystyrene/poly (vinylidene fluoride) blends by controlling selective localization and surface modification of SiC nanoparticles. ACS Appl. Mater. Inter. 2013; 5(15): 6915–24.

[26] Huang X, Jiang P, Tanaka T. A review of dielectric polymer composites with high thermal conductivity. IEEE Electr. Insul. M. 2011; 27(4): 8–16.

[27] Huang X, Zhi C, Jiang P, Golberg D, Bando Y, Tanaka T. Polyhedral oligosilsesquioxane-modified boron nitride nanotube based epoxy nanocomposites: an ideal dielectric material with high thermal conductivity. Adv. Funct. Mater. 2013; 23(14): 1824–31.

[28] Shahil KM, Balandin AA. Graphene–multilayer graphene nanocomposites as highly efficient thermal interface materials. Nano Lett. 2012; 12(2): 861–7.

[29] Yang J, Yu P, Tang LS, Bao RY, Liu ZY, Yang MB, et al. Hierarchically interconnected porous scaffolds for phase change materials with improved thermal conductivity and efficient solar-to-electric energy conversion. Nanoscale. 2017; 9(45): 17704–9.

[30] Yao Y, Zeng X, Guo K, Sun R, Xu J-b. The effect of interfacial state on the thermal conductivity of functionalized Al2O3 filled glass fibers reinforced polymer composites. Compos. Part A-Appl. S. 2015; 69: 49–55.

[31] Dang TML, Kim C Y, Zhang Y, Yang J F, Masaki T, Yoon D H. Enhanced thermal conductivity of polymer composites via hybrid fillers of anisotropic aluminum nitride whiskers and isotropic spheres. Compos. Part B-Eng. 2017; 114: 237–46.

[32] Guerra V, Wan C, McNally T. Thermal conductivity of 2D nano-structured boron nitride (BN) and its composites with polymers. Prog. Mater. Sci. 2019; 100: 170–86.

[33] Wereszczak AA, Morrissey TG, Volante CN, Farris PJ, Groele RJ, Wiles RH, et al. Thermally conductive MgO-filled epoxy molding compounds. IEEE Comp. Pack. Man. 2013; 3(12): 1994–2005.

[34] Mu Q, Feng S, Diao G. Thermal conductivity of silicone rubber filled with ZnO. Polym. Compos. 2007; 28(2): 125–30.

[35] Machrafi H, Lebon G, Iorio CS. Effect of volume-fraction dependent

agglomeration of nanoparticles on the thermal conductivity of nanocomposites: Applications to epoxy resins, filled by SiO2, AlN and MgO nanoparticles. Compos. Sci. Technol. 2016; 130: 78–87.

[36] Yao Y, Zhu X, Zeng X, Sun R, Xu JB, Wong CP. Vertically aligned and interconnected SiC nanowire networks leading to significantly enhanced thermal conductivity of polymer composites. ACS. Appl. Mater. Inter. 2018; 10(11): 9669–78.

[37] Agrawal A, Satapathy A. Effect of Al_2O_3 addition on thermo-electrical properties of polymer composites: An experimental investigation. Polym. Compos. 2015; 36(1): 102–12.

[38] Lee ES, Lee SM, Shanefield DJ, Cannon WR. Enhanced thermal conductivity of polymer matrix composite via high solids loading of aluminum nitride in epoxy resin. J. Am. Ceram. Soc. 2008; 91(4): 1169–74.

[39] Hu X, Jiang L, Goodson KE. Thermal conductance enhancement of particle-filled thermal interface materials using carbon nanotube inclusions. IEEE 2004; 63–9.

[40] Cao A, Dickrell PL, Sawyer WG, Ghasemi-Nejhad MN, Ajayan PM. Super-compressible foamlike carbon nanotube films. Science 2005; 310(5752): 1307–10.

[41] Shaikh S, Li L, Lafdi K, Huie J. Thermal conductivity of an aligned carbon

nanotube array. Carbon 2007; 45(13): 2608–13.

[42] Cola BA, Xu J, Cheng C, Xu X, Fisher TS, Hu H. Photoacoustic characterization of carbon nanotube array thermal interfaces. J. Appl. Phys. 2007; 101(5): 054313.

[43] Naik S, Probert S, Wood C. Natural-convection characteristics of a horizontally-based vertical rectangular fin-array in the presence of a shroud. Appl. Energ. 1987; 28(4): 295–319.

[44] Costa VA, Lopes AM. Improved radial heat sink for led lamp cooling. Appl. Therm. Eng. 2014; 70(1): 131–8.

[45] Maleki H, Selman JR, Dinwiddie R, Wang H. High thermal conductivity negative electrode material for lithium-ion batteries. J. Power Sources 2001; 94(1): 26–35.

[46] Khan WS, Asmatulu R, Rodriguez V, Ceylan M. Enhancing thermal and ionic conductivities of electrospun PAN and PMMA nanofibers by graphene nanoflake additions for battery-separator applications. Int. J. Energ. Res. 2014; 38(15): 2044–51.

[47] Zhou Y, Liu F, Wang H. Novel organic–inorganic composites with high thermal conductivity for electronic packaging applications: A key issue review. Polym. Compos. 2017; 38(4): 803–13.

[48] Lee JH, Lee SH, Choi C, Jang S, Choi S. A review of thermal conductivity

data, mechanisms and models for nanofluids. Int. J. Micro-nano Scale Trans . 2011; 1(4): 17593093.

[49] Lu S, McGaughey AJ. Thermal conductance of superlattice junctions. AIP Adv. 2015; 5(5): 053205.

[50] Berber S, Kwon YK, Tomanek D. Unusually high thermal conductivity of carbon nanotubes. Phys Rev Lett. 2000; 84(20): 4613.

[51] Han Z, Fina A. Thermal conductivity of carbon nanotubes and their polymer nanocomposites: A review. Prog. Polym. Sci. 2011; 36(7): 914–44.

[52] Wingert MC, Zheng J, Kwon S, Chen R. Thermal transport in amorphous materials: a review. Semicond. Sci. Technol. 2016; 31(11): 113003.

[53] Slack GA. The thermal conductivity of nonmetallic crystals. Solid State Phys: Elsevier 1979; 34: 1–71.

[54] Bhattacharya M. Polymer nanocomposites-a comparison between carbon nanotubes, graphene, and clay as nanofillers. Materials 2016; 9(4): 262.

[55] Zhang X, Zheng S, Zheng X, Liu Z, Yang W, Yang M. Distinct positive temperature coefficient effect of polymer–carbon fiber composites evaluated in terms of polymer absorption on fiber surface. Phys. Chem. Chem. Phys. 2016; 18(11): 8081–7.

[56] Gao J, Wang H, Huang X, Hu M, Xue H, Li RK. Electrically conductive polymer nanofiber composite with an ultralow percolation threshold for

chemical vapour sensing. Compos. Sci. Technol. 2018; 161: 135–42.

[57] Zheng D, Tang G, Zhang HB, Yu ZZ, Yavari F, Koratkar N, et al. In situ thermal reduction of graphene oxide for high electrical conductivity and low percolation threshold in polyamide 6 nanocomposites. Compos. Sci. Technol. 2012; 72(2): 284–9.

[58] Last B, Thouless D. Percolation theory and electrical conductivity. Phys. Rev. Lett. 1971; 27(25): 1719.

[59] Oya T, Nomura T, Tsubota M, Okinaka N, Akiyama T. Thermal conductivity enhancement of erythritol as PCM by using graphite and nickel particles. Appl. Therm. Eng. 2013; 61(2): 825–8.

[60] Kwon SY, Kwon IM, Kim Y-G, Lee S, Seo Y-S. A large increase in the thermal conductivity of carbon nanotube/polymer composites produced by percolation phenomena. Carbon 2013; 55: 285–90.

[61] Yang X, Tang L, Guo Y, Liang C, Zhang Q, Kou K, et al. Improvement of thermal conductivities for PPS dielectric nanocomposites via incorporating NH_2-POSS functionalized nBN fillers. Compos. Part A-Appl S. 2017; 101: 237–42.

[62] Gu J, Li N, Tian L, Lv Z, Zhang Q. High thermal conductivity graphite nanoplatelet/UHMWPE nanocomposites. RSC Adv. 2015; 5(46): 36334–9.

[63] Carson JK, Lovatt SJ, Tanner DJ, Cleland AC. Thermal conductivity bounds

for isotropic, porous materials. Int J. Heat Mass Transfer. 2005; 48(11): 2150–8.

[64] Bigg D. Thermal conductivity of heterophase polymer compositions. Thermal and electrical conductivity of polymer materials: Springer 1995; 119: 1–30.

[65] Zhou H, Zhang S, Yang M. The effect of heat-transfer passages on the effective thermal conductivity of high filler loading composite materials. Compos. Sci. Technol. 2007; 67(6): 1035–40.

[66] Zeng J, Fu R, Agathopoulos S, Zhang S, Song X, He H. Numerical simulation of thermal conductivity of particle filled epoxy composites. J. Electr. Pack. 2009; 131(4): 041006.

[67] Wang J, Carson JK, North MF, Cleland DJ. A new structural model of effective thermal conductivity for heterogeneous materials with co-continuous phases. Int. J. Heat Mass Transfer. 2008; 51(9-10): 2389–97.

[68] Hashin Z, Shtrikman S. A variational approach to the theory of the effective magnetic permeability of multiphase materials. J. Appl. Phys. 1962; 33(10): 3125–31.

[69] Schilling F, Partzsch G. Quantifying partial melt fraction in the crust beneath the central Andes and the Tibetan Plateau. Phys. Chem. Earth PT A. 2001; 26(4-5): 239–46.

[70] Feng C, Ni H, Chen J, Yang W. Facile method to fabricate highly thermally

conductive graphite/PP composite with network structures. ACS Appl. Mater. Inter . 2016; 8(30): 19732–8.

[71] Weidenfeller B, Höfer M, Schilling F. Thermal and electrical properties of magnetite filled polymers. Compos. Part A-Appl. S.. 2002; 33(8): 1041–53.

[72] Weidenfeller B, Hofer M, Schilling FR. Thermal conductivity, thermal diffusivity, and specific heat capacity of particle filled polypropylene. Compos. Part A-Appl. S. 2004; 35(4): 423–9.

[73] Kim YK, Chung JY, Lee JG, Baek YK, Shin PW. Synergistic effect of spherical Al2O3 particles and BN nanoplates on the thermal transport properties of polymer composites. Compos. Part A-Appl. S. 2017; 98: 184–91.

[74] Tavman I. Thermal and mechanical properties of aluminum powder-filled high-density polyethylene composites. J. Appl. Polym. Sci. 1996; 62(12): 2161–7.

[75] Bruggeman VD. Berechnung verschiedener physikalischer Konstanten von heterogenen Substanzen. I. Dielektrizitatskonstanten und Leitfahigkeiten der Mischkorper aus isotropen Substanzen. Annalen der physik. 1935; 416(7): 636–64.

[76] Landauer R. The electrical resistance of binary metallic mixtures. J. Appl. Phys. 1952; 23(7): 779–84.

[77] Pietrak K, Wiśniewski TS. A review of models for effective thermal

conductivity of composite materials. J. Power Technol. 2014; 95(1): 14–24.

[78] Tarani E, Terzopoulou Z, Bikiaris D, Kyratsi T, Chrissafis K, Vourlias G. Thermal conductivity and degradation behavior of HDPE/graphene nanocomposites. J. Therm. Anal. Calorim. 2017; 129(3): 1715–26.

[79] Hatta H, Taya M, Kulacki F, Harder J. Thermal diffusivities of composites with various types of filler. J. Compos. Mater. 1992; 26(5): 612–25.

[80] Hatta H, Takei T, Taya M. Effects of dispersed microvoids on thermal expansion behavior of composite materials. Mater. Sci. Eng. A. 2000; 285(1-2): 99–110.

[81] AlyHassan MS, Hatta H, Wakayama S, Watanabe M, Miyagawa K. Comparison of 2D and 3D carbon/carbon composites with respect to damage and fracture resistance. Carbon 2003; 41(5): 1069–78.

[82] Agari Y, Ueda A, Nagai S. Thermal conductivity of a polymer composite. J. Appl. Polym. Sci. 1993; 49(9): 1625–34.

[83] Agari Y, Uno T. Estimation on thermal conductivities of filled polymers. J. Appl. Polym. Sci. 1986; 32(7): 5705–12.

[84] Agari Y, Ueda A, Nagai S. Thermal conductivities of composites in several types of dispersion systems. J. Appl. Polym. Sci. 1991; 42(6): 1665–9.

[85] Zhou W, Qi S, An Q, Zhao H, Liu N. Thermal conductivity of boron nitride reinforced polyethylene composites. Mater. Res. Bull. 2007; 42(10): 1863–73.

[86] Gu J, Lv Z, Wu Y, Guo Y, Tian L, Qiu H, et al. Dielectric thermally conductive boron nitride/polyimide composites with outstanding thermal stabilities via in-situ polymerization-electrospinning-hot press method. Compos. Part A-Appl. S.. 2017; 94: 209–16.

[87] Hamilton RL, Crosser O. Thermal conductivity of heterogeneous two-component systems. Industr. Eng. Chem. Fundamen. 1962; 1(3): 187–91.

[88] Cheng SC, Vachon R. The prediction of the thermal conductivity of two and three phase solid heterogeneous mixtures. Int. J. Heat Mass Transfer. 1969; 12(3): 249–64.

[89] Russell H. Principles of heat flow in porous insulators. J. Am. Ceram. Soc. 1935; 18(1-12): 1–5.

[90] Leung SN, Khan MO, Chan E, Naguib H, Dawson F, Adinkrah V, et al. Analytical modeling and characterization of heat transfer in thermally conductive polymer composites filled with spherical particulates. Compos. Part B-Eng. 2013; 45(1): 43–9.

[91] Lewis TB, Nielsen LE. Dynamic mechanical properties of particulate-filled composites. J. Appl. Polym. Sci. 1970; 14(6): 1449–71.

[92] Tavman I, Akinci H. Transverse thermal conductivity of fiber reinforced polymer composites. Int. Commun. Heat Mass Transfer. 2000; 27(2): 253–61.

[93] Cui W, Du F, Zhao J, Zhang W, Yang Y, Xie X, et al. Improving thermal

conductivity while retaining high electrical resistivity of epoxy composites by incorporating silica-coated multi-walled carbon nanotubes. Carbon 2011; 49(2): 495–500.

[94] Azizi K, Hirvonen P, Fan Z, Harju A, Elder KR, Ala-Nissila T, et al. Kapitza thermal resistance across individual grain boundaries in graphene. Carbon 2017; 125: 384–90.

[95] Shenogin S, Xue L, Ozisik R, Keblinski P, Cahill DG. Role of thermal boundary resistance on the heat flow in carbon-nanotube composites. J. Appl. Phys. 2004; 95(12): 8136–44.

[96] Yang S-Y, Ma C-CM, Teng C-C, Huang Y-W, Liao S-H, Huang Y-L, et al. Effect of functionalized carbon nanotubes on the thermal conductivity of epoxy composites. Carbon 2010; 48(3): 592–603.

[97] Huxtable ST, Cahill DG, Shenogin S, Xue L, Ozisik R, Barone P, et al. Interfacial heat flow in carbon nanotube suspensions. Nat. Mater. 2003; 2(11): 731–4.

[98] Hu Y, Shen J, Li N, Ma H, Shi M, Yan B, et al. Comparison of the thermal properties between composites reinforced by raw and amino-functionalized carbon materials. Compos. Sci. Technol. 2010; 70(15): 2176–82.

[99] Zhao J, Du F, Cui W, Zhu P, Zhou X, Xie X. Effect of silica coating thickness on the thermal conductivity of polyurethane/SiO2 coated multiwalled carbon

nanotube composites. Compos. Part A-Appl. S. 2014; 58: 1–6.

[100] Zhou Y, Wang L, Zhang H, Bai Y, Niu Y, Wang H. Enhanced high thermal conductivity and low permittivity of polyimide based composites by core-shell Ag@SiO2 nanoparticle fillers. Appl. Phys. Lett. 2012; 101(1): 012903.

[101] Yang J, Yang Y, Waltermire SW, Wu X, Zhang H, Gutu T, et al. Enhanced and switchable nanoscale thermal conduction due to van der Waals interfaces. Nat. Nanotechnol. 2012; 7(2): 91–5.

[102] Wang M, Hu N, Zhou L, Yan C. Enhanced interfacial thermal transport across graphene–polymer interfaces by grafting polymer chains. Carbon. 2015;85:414-21.

[103] Wang Y, Zhan H, Xiang Y, Yang C, Wang CM, Zhang Y. Effect of covalent functionalization on thermal transport across graphene–polymer interfaces. J. Phys. Chem. C 2015; 119(22): 12731–8.

[104] Shen X, Wang Z, Wu Y, Liu X, Kim J-K. Effect of functionalization on thermal conductivities of graphene/epoxy composites. Carbon 2016; 108: 412–22.

[105] Maira B, Takeuchi K, Chammingkwan P, Terano M, Taniike T. Thermal conductivity of polypropylene/aluminum oxide nanocomposites prepared based on reactor granule technology. Compos. Sci. Technol. 2018; 165: 259–65.

[106] Wattanakul K, Manuspiya H, Yanumet N. Effective Surface Treatments for

Enhancing the Thermal Conductivity of BN-Filled Epoxy Composite. J. App.l Polym. Sci. 2011; 119(6): 3234–43.

[107] Ding P, Su SS, Song N, Tang SF, Liu YM, Shi LY. Highly thermal conductive composites with polyamide-6 covalently-grafted graphene by an in situ polymerization and thermal reduction process. Carbon 2014; 66: 576–84.

[108] Yu J, Huang X, Wang L, Peng P, Wu C, Wu X, et al. Preparation of hyperbranched aromatic polyamide grafted nanoparticles for thermal properties reinforcement of epoxy composites. Polym. Chem. 2011; 2(6): 1380–8.

[109] Huang X, Iizuka T, Jiang P, Ohki Y, Tanaka T. Role of interface on the thermal conductivity of highly filled dielectric epoxy/AlN composites. J. Phys. Chemistry C 2012; 116(25): 13629–39.

[110] Kuan HC, Ma CCM, Chang WP, Yuen SM, Wu HH, Lee TM. Synthesis, thermal, mechanical and rheological properties of multiwall carbon nanotube/waterborne polyurethane nanocomposite. Compos. Sci. Technol. 2005; 65(11-12): 1703–10.

[111] Hayden H, Gunko YK, Perova TS. Chemical modification of multi-walled carbon nanotubes using a tetrazine derivative. Chem. Phys. Lett. 2007; 435(1-3): 84–9.

[112] Teng CC, Ma CCM, Lu CH, Yang SY, Lee SH, Hsiao MC, et al. Thermal

conductivity and structure of non-covalent functionalized graphene/epoxy composites. Carbon 2011; 49(15): 5107–16.

[113] Zhang W, Xu X, Yang J, Huang T, Zhang N, Wang Y, et al. High thermal conductivity of poly (vinylidene fluoride)/carbon nanotubes nanocomposites achieved by adding polyvinylpyrrolidone. Compos. Sci. Technol. 2015; 106: 1–8.

[114] Wu H, Kessler MR. Multifunctional cyanate ester nanocomposites reinforced by hexagonal boron nitride after noncovalent biomimetic functionalization. ACS Appl. Mater. Inter. 2015; 7(10): 5915–26.

[115] Yu S, Park BI, Park C, Hong SM, Han TH, Koo CM. RTA-treated carbon fiber/copper core/shell hybrid for thermally conductive composites. ACS Appl. Mater. Inter. 2014; 6(10): 7498–503.

[116] Chen C, Tang Y, Ye YS, Xue Z, Xue Y, Xie X, et al. High-performance epoxy/silica coated silver nanowire composites as underfill material for electronic packaging. Compos. Sci. Technol. 2014; 105: 80–5.

[117] Choi S, Kim K, Nam J, Shim SE. Synthesis of silica-coated graphite by enolization of polyvinylpyrrolidone and its thermal and electrical conductivity in polymer composites. Carbon 2013; 60: 254–65.

[118] Sun R, Yao H, Zhang HB, Li Y, Mai YW, Yu ZZ. Decoration of defect-free graphene nanoplatelets with alumina for thermally conductive and electrically

insulating epoxy composites. Compos. Sci. Technol. 2016; 137: 16–23.

[119] Badi N, Mekala R. Heat-Sink Solution Through Artificial Nanodielectrics for LED Lighting Application. Proc 2012; 1–5.

[120] Lin Z, Liu Y, Raghavan S, Moon K-s, Sitaraman SK, Wong C-p. Magnetic alignment of hexagonal boron nitride platelets in polymer matrix: toward high performance anisotropic polymer composites for electronic encapsulation. ACS Appl. Mater. Inter. 2013; 5(15): 7633–40.

[121] Zeng X, Sun J, Yao Y, Sun R, Xu JB, Wong CP. A combination of boron nitride nanotubes and cellulose nanofibers for the preparation of a nanocomposite with high thermal conductivity. ACS Nano. 2017; 11(5): 5167–78.

[122] Kumar P, Yu S, Shahzad F, Hong SM, Kim Y-H, Koo CM. Ultrahigh electrically and thermally conductive self-aligned graphene/polymer composites using large-area reduced graphene oxides. Carbon 2016; 101: 120–8.

[123] Kuang Z, Chen Y, Lu Y, Liu L, Hu S, Wen S, et al. Fabrication of highly oriented hexagonal boron nitride nanosheet/elastomer nanocomposites with high thermal conductivity. Small 2015; 11(14): 1655–9.

[124] Zhang X, Zhang J, Xia L, Li C, Wang J, Xu F, et al. Simple and consecutive Melt extrusion method to fabricate thermally conductive composites with highly oriented boron nitrides. ACS Appl. Mater. Inter. 2017; 9(27): 22977–

84.

[125] Ghose S, Working DC, Connell JW, Smith Jr J, Watson KA, Delozier DM, et al. Thermal conductivity of ultemTM/carbon nanofiller blends. High Perform. Polym. 2006; 18(6): 961–77.

[126] Yoo Y, Lee HL, Ha SM, Jeon BK, Won JC, Lee SG. Effect of graphite and carbon fiber contents on the morphology and properties of thermally conductive composites based on polyamide 6. Polym. Int. 2014; 63(1): 151–7.

[127] Zhang S, Ke Y, Cao X, Ma Y, Wang F. Effect of Al2O3 fibers on the thermal conductivity and mechanical properties of high density polyethylene with the absence and presence of compatibilizer. J. Appl. Polym. Sci. 2012; 124(6): 4874–81.

[128] Feller J, Roth S, Bourmaud A. Conductive polymer composites: Electrical, thermal, and rheological study of injected isotactic poly (propylene)/long stainless-steel fibers for electromagnetic interferences shielding. J. Appl. Polym. Sci. 2006; 100(4): 3280–7.

[129] He D, Wang Y, Song S, Liu S, Deng Y. Significantly Enhanced Dielectric Performances and High Thermal Conductivity in Poly (vinylidene fluoride)-Based Composites Enabled by SiC@SiO2 Core-Shell Whiskers Alignment. ACS Appl. Mater. Inter. 2017; 9(51): 44839–46.

[130] Yuan C, Duan B, Li L, Xie B, Huang M, Luo X. Thermal conductivity of polymer-based composites with magnetic aligned hexagonal boron nitride platelets. ACS Appl. Mater. Inter. 2015; 7(23): 13000–6.

[131] Yan H, Tang Y, Long W, Li Y. Enhanced thermal conductivity in polymer composites with aligned graphene nanosheets. J. Mater. Sci. 2014; 49(15): 5256–64.

[132] Gaska K, Kmita G, Rybak A, Sekula R, Goc K, Kapusta C. Magnetic-aligned, magnetite-filled epoxy composites with enhanced thermal conductivity. J. Mater. Sci. 2015; 50(6): 2510–6.

[133] Choi E, Brooks J, Eaton D, Al-Haik M, Hussaini M, Garmestani H, et al. Enhancement of thermal and electrical properties of carbon nanotube polymer composites by magnetic field processing. J. Appl. Phys. 2003; 94(9): 6034–9.

[134] Yuan F, Jiao W, Yang F, Liu W, Xu Z, Wang R. Surface modification and magnetic alignment of hexagonal boron nitride nanosheets for highly thermally conductive composites. RSC Adv. 2017; 7(69): 43380–9.

[135] Sun X-R, Gong T, Pu J-H, Bao R-Y, Xie B-H, Yang M-B, et al. Effect of phase coarsening under melt annealing on the electrical performance of polymer composites with a double percolation structure. Phys. Chem. Chem. Phys. 2018; 20(1): 137–47.

[136] Cho H-B, Nakayama T, Suzuki T, Tanaka S, Jiang W, Suematsu H, et al. Linear

assembles of BN nanosheets, fabricated in polymer/BN nanosheet composite film. J. Nanomate. 2011; 2011: 237050.

[137] Fujihara T, Cho HB, Nakayama T, Suzuki T, Jiang W, Suematsu H, et al. Field-induced orientation of hexagonal boron nitride nanosheets using microscopic mold for thermal interface materials. J. Am. Ceram. Soc. 2012; 95(1): 369–73.

[138] Zeng X, Yao Y, Gong Z, Wang F, Sun R, Xu J, et al. Ice-templated assembly strategy to construct 3D boron nitride nanosheet networks in polymer composites for thermal conductivity improvement. Small 2015; 11(46): 6205–13.

[139] Yang J, Tang LS, Bao RY, Bai L, Liu ZY, Yang W, et al. An ice-templated assembly strategy to construct graphene oxide/boron nitride hybrid porous scaffolds in phase change materials with enhanced thermal conductivity and shape stability for light–thermal–electric energy conversion. J. Mater. Chem. A. 2016; 4(48): 18841–51.

[140] Lian G, Tuan CC, Li L, Jiao S, Wang Q, Moon KS, et al. Vertically aligned and interconnected graphene networks for high thermal conductivity of epoxy composites with ultralow loading. Chem. Mater. 2016;28(17):6096-104.

[141] Shen H, Cai C, Guo J, Qian Z, Zhao N, Xu J. Fabrication of oriented hBN scaffolds for thermal interface materials. RSC Adv. 2016; 6(20): 16489–94.

[142] Schiffres SN, Harish S, Maruyama S, Shiomi J, Malen JA. Tunable electrical

and thermal transport in ice-templated multilayer graphene nanocomposites through freezing rate control. ACS Nano 2013; 7(12): 11183–9.

[143] Hu J, Huang Y, Yao Y, Pan G, Sun J, Zeng X, et al. Polymer composite with improved thermal conductivity by constructing a hierarchically ordered three-dimensional interconnected network of BN. ACS Appl. Mater. Inter. 2017; 9(15): 13544–53.

[144] Bai H, Walsh F, Gludovatz B, Delattre B, Huang C, Chen Y, et al. Bioinspired hydroxyapatite/poly (methyl methacrylate) composite with a nacre-mimetic architecture by a bidirectional freezing method. Adv. Mater. 2016; 28(1): 50–6.

[145] Feng CP, Bai L, Shao Y, Bao RY, Liu ZY, Yang MB, et al. A facile route to fabricate highly anisotropic thermally conductive elastomeric POE/NG composites for thermal management. Adv. Mate. Inter. 2018; 5(2): 1700946.

[146] Chen J, Huang X, Sun B, Wang Y, Zhu Y, Jiang P. Vertically aligned and interconnected boron nitride nanosheets for advanced flexible nanocomposite thermal interface materials. ACS Appl. Mater. Inter. 2017; 9(36): 30909–17.

[147] Choi S, Kim J. Thermal conductivity of epoxy composites with a binary-particle system of aluminum oxide and aluminum nitride fillers. Compos. Part B-Eng. 2013; 51: 140–7.

[148] Yu W, Xie H, Yin L, Zhao J, Xia L, Chen L. Exceptionally high thermal

conductivity of thermal grease: synergistic effects of graphene and alumina. Int. J. Thermal. Sci. 2015; 91: 76–82.

[149] Yung K, Liem H. Enhanced thermal conductivity of boron nitride epoxy-matrix composite through multi-modal particle size mixing. J. Appl. Polym. Sci. 2007; 106(6): 3587–91.

[150] Yu A, Ramesh P, Sun X, Bekyarova E, Itkis ME, Haddon RC. Enhanced thermal conductivity in a hybrid graphite nanoplatelet–carbon nanotube filler for epoxy composites. Adv. Mater. 2008; 20(24): 4740–4.

[151] He G, Zhou X, Liu J, Zhang J, Pan L, Liu S. Synergetic enhancement of thermal conductivity for highly explosive-filled polymer composites through hybrid carbon nanomaterials. Polym. Compos. 2018; 39(S3): 1452–62.

[152] Zhao C, Xu S, Qin Y, Chen H, Zhao W, Sun F, et al. Thermally conductive cyanate ester nanocomposites filled with graphene nanosheets and multiwalled carbon nanotubes. Polym. Adv. Technol. 2014; 25(12): 1546–51.

[153] Pak SY, Kim HM, Kim SY, Youn JR. Synergistic improvement of thermal conductivity of thermoplastic composites with mixed boron nitride and multi-walled carbon nanotube fillers. Carbon 2012; 50(13): 4830–8.

[154] Xiao Y, Wang W, Lin T, Chen X, Zhang Y, Yang J, et al. Largely enhanced thermal conductivity and high dielectric constant of poly (vinylidene fluoride)/boron nitride composites achieved by adding a few carbon nanotubes.

J Phys. Chem. C. 2016; 120(12): 6344–55.

[155] Kim K, Kim J. BN-MWCNT/PPS core-shell structured composite for high thermal conductivity with electrical insulating via particle coating. Polymer 2016; 101: 168–75.

[156] Teng CC, Ma CCM, Chiou KC, Lee TM, Shih YF. Synergetic effect of hybrid boron nitride and multi-walled carbon nanotubes on the thermal conductivity of epoxy composites. Mater. Chem. Phys. 2011; 126(3): 722–8.

[157] Li Z, Ju D, Han L, Dong L. Formation of more efficient thermally conductive pathways due to the synergistic effect of boron nitride and alumina in poly (3-hydroxylbutyrate). Thermochim. Acta. 2017; 652: 9–16.

[158] Hu A, Guo J, Alarifi H, Patane G, Zhou Y, Compagnini G, et al. Low temperature sintering of Ag nanoparticles for flexible electronics packaging. Appl. Phys. Lett. 2010; 97(15): 153117.

[159] Pashayi K, Fard HR, Lai F, Iruvanti S, Plawsky J, Borca-Tasciuc T. High thermal conductivity epoxy-silver composites based on self-constructed nanostructured metallic networks. J. Appl. Phys. 2012; 111(10): 104310.

[160] Pashayi K, Fard HR, Lai F, Iruvanti S, Plawsky J, Borca-Tasciuc T. Self-constructed tree-shape high thermal conductivity nanosilver networks in epoxy. Nanoscale. 2014; 6(8): 4292–6.

[161] Pettes MT, Ji H, Ruoff RS, Shi L. Thermal transport in three-dimensional foam

architectures of few-layer graphene and ultrathin graphite. Nano Lett. 2012; 12(6): 2959–64.

[162] Li M, Sun Y, Xiao H, Hu X, Yue Y. High temperature dependence of thermal transport in graphene foam. Nanotechnology 2015; 26(10): 105703.

[163] Klett J, Hardy R, Romine E, Walls C, Burchell T. High-thermal-conductivity, mesophase-pitch-derived carbon foams: effect of precursor on structure and properties. Carbon 2000; 38(7): 953–73.

[164] Kholmanov I, Kim J, Ou E, Ruoff RS, Shi L. Continuous carbon nanotube–ultrathin graphite hybrid foams for increased thermal conductivity and suppressed subcooling in composite phase change materials. ACS Nano 2015; 9(12): 11699–707.

[165] Li YC, Chen GH. HDPE/expanded graphite nanocomposites prepared via masterbatch process. Polym. Eng. Sci. 2007; 47(6): 882–8.

[166] Li X, Shao L, Song N, Shi L, Ding P. Enhanced thermal-conductive and anti-dripping properties of polyamide composites by 3D graphene structures at low filler content. Compos. Part A-Appl. S. 2016; 88: 305–14.

[167] Zhou S, Chen Y, Zou H, Liang M. Thermally conductive composites obtained by flake graphite filling immiscible polyamide 6/polycarbonate blends. Thermochim. Acta. 2013; 566: 84–91.

[168] Ji H, Sellan DP, Pettes MT, Kong X, Ji J, Shi L, et al. Enhanced thermal

conductivity of phase change materials with ultrathin-graphite foams for thermal energy storage. Energ. Environ. Sci. 2014; 7(3): 1185–92.

[169] Yin J, Li X, Zhou J, Guo W. Ultralight three-dimensional boron nitride foam with ultralow permittivity and superelasticity. Nano Lett. 2013; 13(7): 3232–6.

[170] Li M, Gao C, Hu H, Zhao Z. Electrical conductivity of thermally reduced graphene oxide/polymer composites with a segregated structure. Carbon 2013; 65: 371–3.

[171] Hu M, Feng J, Ng KM. Thermally conductive PP/AlN composites with a 3-D segregated structure. Compos. Sci. Technol. 2015; 110: 26–34.

[172] Jiang Y, Liu Y, Min P, Sui G. BN@PPS core-shell structure particles and their 3D segregated architecture composites with high thermal conductivities. Compos. Sci. Technol. 2017; 144: 63–9.

[173] Wu K, Lei C, Huang R, Yang W, Chai S, Geng C, et al. Design and preparation of a unique segregated double network with excellent thermal conductive property. ACS Appl. Mater. Inter. 2017; 9(8): 7637–47.

[174] Wu K, Xue Y, Yang W, Chai S, Chen F, Fu Q. Largely enhanced thermal and electrical conductivity via constructing double percolated filler network in polypropylene/expanded graphite-Multi-wall carbon nanotubes ternary composites. Compos. Sci. Technol. 2016; 130: 28–35.

[175] Huang J, Mao C, Zhu Y, Jiang W, Yang X. Control of carbon nanotubes at the interface of a co-continuous immiscible polymer blend to fabricate conductive composites with ultralow percolation thresholds. Carbon 2014; 73: 267–74.

[176] Nasti G, Gentile G, Cerruti P, Carfagna C, Ambrogi V. Double percolation of multiwalled carbon nanotubes in polystyrene/polylactic acid blends. Polymer 2016; 99: 193–203.

[177] Chen J, Cui X, Sui K, Zhu Y, Jiang W. Balance the electrical properties and mechanical properties of carbon black filled immiscible polymer blends with a double percolation structure. Compos. Sci. Technol. 2017; 140: 99–105.

[178] Huang J, Zhu Y, Xu L, Chen J, Jiang W, Nie X. Massive enhancement in the thermal conductivity of polymer composites by trapping graphene at the interface of a polymer blend. Compos. Sci. Technol. 2016; 129: 160–5.

[179] Goldel A, Marmur A, Kasaliwal GR, Pötschke P, Heinrich G. Shape-dependent localization of carbon nanotubes and carbon black in an immiscible polymer blend during melt mixing. Macromolecules 2011; 44(15): 6094–102.

[180] Ton-That MT, Perrin-Sarazin F, Cole K, Bureau M, Denault J. Polyolefin nanocomposites: formulation and development. Polym. Eng. Sci. 2004; 44(7): 1212–9.

[181] Galli P. The reactor granule technology: a revolutionary approach to polymer blends and alloys. Macromolecular Symposia: Wiley Online Library; 1994;

78(1): 269–84.

[182] Hock CW. How Ticl3 Catalysts Control the Texture of As-Polymerized Polypropylene. J. Polym. Sci. Part A Polym. Chem. 1966; 4(12): 3055–64.

[183] Chen Y, Chen Y, Chen W, Yang D. Morphology of high impact polypropylene particles. Polymer 2006; 47(19): 6808–13.

[184] Galli P. The reactor granule technology: The ultimate expansion of polypropylene properties? J. Macromol. Sci. Part A 1999; 36: 1561–86.

[185] Hutchinson R, Chen C, Ray W. Polymerization of olefins through heterogeneous catalysis X: Modeling of particle growth and morphology. J. Appl. Polym. Sci. 1992; 44(8): 1389–414.

[186] Maira B, Chammingkwan P, Terano M, Taniike T. Reactor granule technology for fabrication of functionally advantageous polypropylene nanocomposites with oxide nanoparticles. Compos. Sci. Technol. 2017; 144: 151–9.

[187] Qiagedeer A, Maira B, Strauss R, Zhao Y, Chammingkwan P, Mizutani G, et al. Preparation and characterization of polypropylene/noble metal nanocomposites based on reactor granule technology. Polymer 2017; 127: 251–8.

[188] Maira B, Chammingkwan P, Terano M, Taniike T. New reactor granule technology for highly filled nanocomposites: effective flame retardation of polypropylene/magnesium hydroxide nanocomposites. Macromol. Mater. Eng.

2015; 300(7): 679–83.

[189] Chen CH, Jian JY, Yen FS. Preparation and characterization of epoxy/γ-aluminum oxide nanocomposites. Compos. Part A-Appl. S. 2009; 40(4): 463–8.

[190] Fukuyama Y, Senda M, Kawai T, Kuroda S-i, Toyonaga M, Taniike T, et al. The effect of the addition of polypropylene-grafted SiO2 nanoparticle on the thermal conductivity of isotactic polypropylene. J. Therm. Anal. Calorim. 2014; 117(3): 1397–405.

Chapter 2

Selective Localization of Aluminum Oxide at Interface and Its Effect on Thermal Conductivity in Polypropylene/ Polyolefin Elastomer Blends

Chapter 2

Abstract

A reactor granule technology (RGT) was applied to immiscible polypropylene (PP)/polyolefin elastomer (POE) blends to effectively control the localization of nanoparticles at the interface. The RGT afforded uniform dispersion of in-situ generated aluminum oxide (Al_2O_3) nanoparticles in PP, and this guaranteed the migration of nanoparticles to the interface of a co-continuous structure when blended with POE. The selective localization of nanoparticles at the interface was confirmed by transmission electron microscope (TEM), scanning electron microscope (SEM), elemental mapping (EDX), and thermal gravimetric analysis (TGA). Such localization was never achieved when preformed Al_2O_3 nanoparticles were used, and this fact stresses the importance of uniform dispersion in controlling the migration of nanoparticles. The migration was also affected by the viscosity of POE: POE having higher viscosity resulted in a smaller domain size, and thereby more nanoparticles could migrate to the interface without agglomeration. The impacts of the selective localization at the interface and the phase domain size on the thermal conductivity of the resultant nanocomposites were studied and discussed.

Keywords: Thermal conductivity; Nanocomposite; Polypropylene; Immiscible blends; Interface

Chapter 2

2.1. Introduction

Along with the miniaturization and lightweight design of electronic device components, greater demands are constantly raised on materials having high thermal conductivity and low density [1–4]. Polymeric materials are excellent candidates owing to their general characteristics such as good processability, light weight, low water absorption, corrosion resistance, high electrical resistivity, and most importantly, low cost [5–12]. However, a majority of these polymeric materials possess poor thermal conductivity, which is usually restricted in the range of 0.10–0.25 W/m K [13]. As a consequence, electrically insulating nanoparticles with high thermal conductivity such as boron nitride (BN) [14], aluminum nitride (AlN) [15], silicon carbide (SiC) [16], and aluminum oxide (Al_2O_3) [17] are incorporated into polymers for applications that require both high thermal conductivity and electrical insulating properties.

Among these thermal conductive fillers, spherical Al_2O_3 particles have been widely used due the abundance [18–20]. The incorporation of spherical particles guarantees isotropic heat release in the resultant composite materials [21], but at the same time, necessitates a relatively high filler loading to construct a well-developed thermal conductive network [22,23]. A tradeoff between the thermal conductivity improvement and problems arising from a high loading such as complex processing, high density and severe particle agglomeration must be dealt with in the materials

design. Our research group has disclosed a novel reactor granule technology (RGT) to achieve uniform dispersion of nanoparticles in polyolefin-based nanocomposites and such uniform dispersion can be also realized even at an elevated loading. It is based on the impregnation and confinement of metal alkoxides in the pores of polymer reactor granule and subsequent chemical conversion of precursors into nanoparticles during a melt-mixing process [24–26]. In the past research, the group fabricated PP/Al_2O_3 nanocomposites based on this technology. Owing to the extremely uniform dispersion of Al_2O_3 nanoparticles, the improvement of thermal conductivity was achieved at a much lower loading compared with samples prepared by melt-mixing preformed Al_2O_3 nanoparticles in the absence or presence of a compatibilizer (maleic anhydride grafted PP) [24]. For further improvement, the group also melt-mixed impregnated reactor granule with pristine reactor granule to create the distribution of the dispersion. In detail, Al_2O_3-rich and polymer-rich domains were created at around 10 μm scale, in which the filler-rich domains offered a thermal conductive pathway and thus the thermal conductivity was improved to some extent [27]. These results encouraged me to further improve the thermal conductivity by tuning the selective distribution of nanoparticles.

An effective strategy to control the distribution of nanoparticles is the employment of immiscible polymer blends with a co-continuous structure. This strategy has been widely applied in designing electrically conductive polymer

composites to improve the electrical conductivity by the selective localization of nanoparticles in one phase [28–35], or, best of all, at the interface [36–38]. Many methods have been reported to achieve the selective localization of carbon black (CB) nanoparticles at the interface. For example, Gubbels et al. reported that compression molding of dry mixed polyethylene (PE), polystyrene (PS), and CB powder resulted in the localization of CB nanoparticles at the interface of PE and PS domains [39]. They also reported in the same paper that by first distributing CB nanoparticles in the less favored phase, the nanoparticles were thermodynamically driven to the interface at proper processing conditions [39]. Al-Saleh et al. proposed another strategy to utilize a compatibilizer for the selective localization of CB nanoparticles at the interface, where a styrene-butadiene-styrene (SBS) tri-block copolymer as a compatibilizer preferentially distributed at the interface of PP and PS domains, and CB nanoparticles were carried to the interface through the attractive interaction with SBS [36].

Recently, this co-continuous structure has also been exploited to design thermal conductive materials. For example, Li et al. introduced BN into poly(3-hydroxylbutyrate)/poly(ethylene oxide) blends with a co-continuous structure. A network of BN was formed in the poly(3-hydroxylbutyrate) phase [40]. Cao et al. achieved high thermal conductivity by controlling the distribution of multi-walled carbon nanotubes and SiC nanoparticles in the poly(vinylidene fluoride) (PVDF)

phase in PVDF/PS blends [41]. Cao et al. reported the selective localization of BN in the polyethylene rubber phase of polyethylene rubber/ethylene propylene diene rubber blends, which yielded high thermal conductivity [42]. All these recent studies revealed the utilization of a co-continuous structure as an effective means for the formation of a thermal conductive network at a reduced filler loading. However, the localization has been attained in one phase, not at the interface, still requiring a relatively high loading (e.g. 10 vol%) [43]. Moreover, the above-mentioned strategies for CB nanoparticles are not directly applicable to Al_2O_3 nanoparticles because of the extremely high surface tension of Al_2O_3 (114 mJ/m^2 vs. 55 mJ/m^2 for CB) [44,45]. They are inherently not dispersible in hydrophobic polymer matrices and tend to form agglomerates especially at a high loading [19]. In this light, thermodynamically driving Al_2O_3 nanoparticles to the interface is very challenging because the agglomeration tendency strongly hinders the migration of individual nanoparticles to the interface.

In this chapter, a novel strategy was proposed based on the RGT and immiscible polymer blends with a co-continuous structure for the first time. The RGT can prevent the agglomeration of in-situ generated Al_2O_3 nanoparticles and achieve uniform dispersion, which helps the nanoparticles migrate to the interface of immiscible polymer blends. Reactor granule of polypropylene (PP) was preliminarily impregnated with aluminum alkoxide and then melt-mixed with four

kinds of POE (used as an assistant phase) with different viscosity. The impacts of dispersion and phase domain size on the migration of nanoparticles were studied.

2.2. Experimental section

2.2.1. Materials

PP reactor granule (M_w = 2.6 × 10^5, M_w/M_n = 5.7, *mmmm* = 98 mol%) was synthesized by propylene polymerization using a $Mg(OEt)_2$-based Ziegler-Natta catalyst. The median size (D_{50}) and pore volume of the granule were determined as 637 μm and 0.56 mL/g based on laser scattering in ethanol (HORIBA partica, LA-950V2) and mercury porosimetry (Shimazu, Autopore IV 9505), respectively. Aluminium isopropoxide ($Al(OiPr)_3$) was supplied by Sigma-Aldrich and used as a precursor. *n*-Octdecyl-3-(3',5'-di-*t*-butyl-4'-hydroxyphenyl)-propionate (AO-50) and bis(1,2,2,6,6-pentamethyl-4-piperidyl) sebacate (LA-77) were donated by ADEKA. They were used as an anti-oxidant stabilizer and a catalyst for the sol-gel reaction, respectively [46]. Four kinds of POE having different viscosity and octene contents (termed POE1–4) were employed in this study. Table 2.1 summarizes their physical parameters, which are supplied by Dow Chemical Co. POE1 and POE2 have similarly high viscosities compared with those of POE3 and POE4, while POE1 and POE4 have octene contents nearly two times greater than the other

two. Such selection was based on the consideration that different viscosity and octene contents can affect the phase domain size and thereby influence the final localization of Al_2O_3 nanoparticles. Besides, the octene content has an impact on the specific heat capacity (Table 2.1) and this can also influence the thermal conductivity of obtained nanocomposites. Preformed Al_2O_3 nanoparticles having the average diameter of 15 nm (Alu, Nippon Aerosil) were used to prepare reference samples.

Table 2.1. Physical parameters of POE.

	POE1	POE2	POE3	POE4
MI (g/10 min)[a]	1	1	30	30
Mooney viscosity (MU)[b]	23	18	<5	<5
Octene content (wt%)	38	20	22	40
Density (g/cm^3)	0.870	0.902	0.902	0.870
Specific heat capacity (J/g K)[c]	2.81±0.01	2.33±0.01	2.51±0.02	2.83±0.03

[a] Measured at 2.16 kg and 190 °C based on ASTM D1238.

[b] ML 1+4 at 121 °C acquired based on ASTM D1646.

[c] Measured by DSC.

2.2.2. Sample preparation

PP/POE/Al_2O_3 nanocomposites were obtained based on the following procedure. First, 10 g of PP reactor granule was impregnated with 20 mL of a toluene solution of Al(O*i*Pr)$_3$ at 50 ºC under nitrogen for 12 h. The amount of the Al(O*i*Pr)$_3$ precursor was determined so as to obtain the Al_2O_3 loading of 20 wt% (= 5.5 vol%) in resultant PP/Al_2O_3 samples under the assumption of full conversion of the metal alkoxide to the oxide. After the impregnation and solvent removal in vacuo, the impregnated granule was subjected to 50 ºC and 100% relative humidity for 24 h to promote the hydrolysis and solidification of Al(O*i*Pr)$_3$ in the pores of PP [24]. Subsequently, it was melt-mixed with POE at 190 ºC and 100 rpm for 10 min. The weight ratio of PP and POE was kept at 1/1 wt/wt to ascertain the formation of a co-continuous structure (Fig. 2.1), and this resulted in the final Al_2O_3 loading of 11.1 wt% (corresponding to 2.8 vol%). The product was finally hot-pressed into films at 190 ºC and 10 MPa for 5 min, followed by quenching at 0 °C for 5 min. The prepared samples were denoted as PP/POE*x*/Al_2O_3-RGT, where *x* represents the type of POE employed (*x* = 1–4).

The following reference samples were also prepared.

i) PP/Al_2O_3-RGT-*y*: Impregnated PP granule was melt-mixed and hot-pressed in the absence of POE, where *y* represents the volume fraction of Al_2O_3 in the nanocomposites (*y* = 2.5 or 5.5 vol%).

ii) PP/POE*x*: Pristine PP was melt-mixed with POE at 1/1 wt/wt, where *x* represents the type of POE.

iii) PP/POE*x*/Al_2O_3-NP: Preformed Al_2O_3 nanoparticles were directly melt-mixed with pristine PP, followed by blending with POE at the PP/POE weight ratio of 1/1 wt/wt. The final Al_2O_3 loading was fixed at 2.8 vol%.

The conditions for the impregnation, melt mixing and hot pressing were totally the same as those employed for the preparation of PP/POE/Al_2O_3-RGT samples.

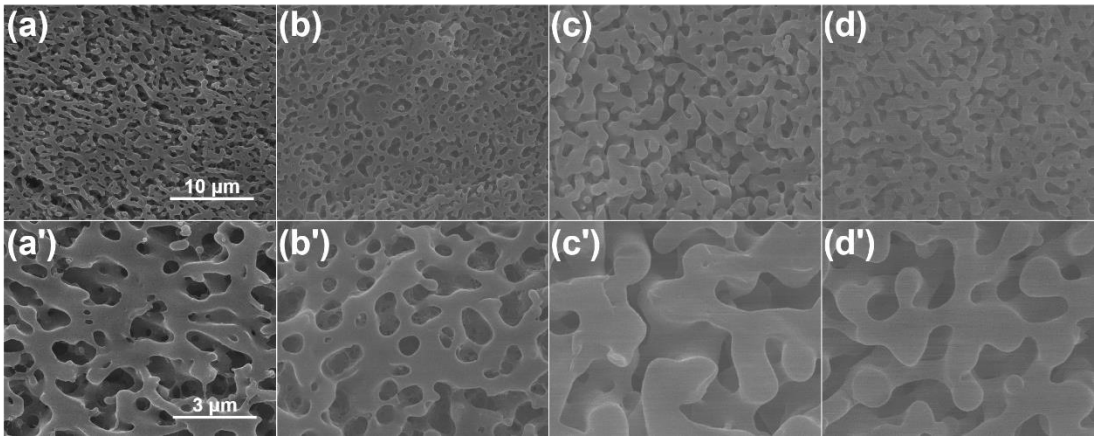

Fig. 2.1. SEM micrographs of etched surfaces of PP/POE blends with different kinds of POE. a,a') POE1, b,b') POE2, c,c') POE3, d,d') POE4. Note that the scale bar is applied to the individual entire row. The formation of a co-continuous structure was confirmed by selectively extracting the POE phase with heptane prior to the SEM measurements.

2.2.3. Characterization

The progress of the reaction and the formation of Al_2O_3 were qualitatively confirmed by recording attenuated total reflection infrared spectra (ATR-IR) (FT-IR, 100, Perkin Elmer) with a resolution of 4 cm^{-1} and 24 scans. The actual Al_2O_3 contents of prepared samples were measured by thermal gravimetric analysis (TGA, Thermo plus evo, Rigaku). A sample was heated from 25 ºC to 600 ºC in air at a heating rate of 10 ºC/min. The residual inorganic content at 600 ºC was regarded as the Al_2O_3 content. In order to investigate the localization of Al_2O_3 nanoparticles in a specific phase, PP/POE/Al_2O_3-RGT samples were etched by heptane to remove POE at 80 ºC for 24 h. After rinsing with heptane, ethanol, and deionized water, the samples were subjected to the same TGA measurement. The dispersion and distribution of Al_2O_3 nanoparticles in the matrix was monitored by a transmission electron microscope (TEM, Hitachi H-7100) operated at an acceleration voltage of 100 kV. TEM specimens with the thickness of 100 nm were prepared by an ultramicrotome (Reichent Ultracut FCS, Reica) equipped with a diamond knife (Diatome). A scanning electron microscope (SEM, Hitachi S-4100) with an acceleration voltage of 20 kV was used to observe the phase morphology of the PP/POE blends. The samples were cryo-fractured in liquid nitrogen and then etched according to the above-mentioned method. The samples were coated with platinum and palladium prior to the measurement. Elemental mapping was also performed

using an energy dispersive X-ray analyzer (EDX, Hitachi TM 3030Plus). The thermal diffusivity (α) of samples was measured by a temperature wave analyzer (ai-Phase mobile 1u/2, Hitachi High-Tech Science) [47]. A film sample was sandwiched between the heater and the sensor plates, and the distance between the two plates was adjusted to create a firm contact with both surfaces of the sample. The applied voltage was set to 1.4 V and the phase delay in the temperature wave was measured at eight frequency values within a range of 0.2–2 Hz. The thermal conductivity (λ) was derived from

$$\lambda = \alpha C_p \rho \quad (2\text{-}1),$$

where C_p is the specific heat capacity and ρ is the density of a sample. The specific heat capacity at room temperature was determined using a differential scanning calorimeter (DSC, Mettler Toledo DSC-822). The temperature was swept in the range of 0–50 ºC at 10 ºC/min under nitrogen flow of 200 mL/min. The density was measured by an electronic density meter (SANSYO DME-220).

2.3. Results and discussion

2.3.1. Formation and dispersion of Al_2O_3 nanoparticles

ATR-IR spectra was acquired for a PP/Al_2O_3 nanocomposite film to investigate the chemical conversion of the precursor (Fig. 2.2a). Compared to the spectrum of neat PP, the PP/Al_2O_3-RGT sample shows a new broad band

at around 500 cm^{-1}, which corresponds to the Al-O-Al vibration of in-situ formed Al_2O_3 [48]. TGA was employed to verify the actual Al_2O_3 content (Fig. 2-2b). Based on the residual weight at 600 °C, the actual Al_2O_3 loading was derived as 20.1 wt%, which was consistent with the theoretical loading (i.e. no evaporation or leaching loss of the precursor).

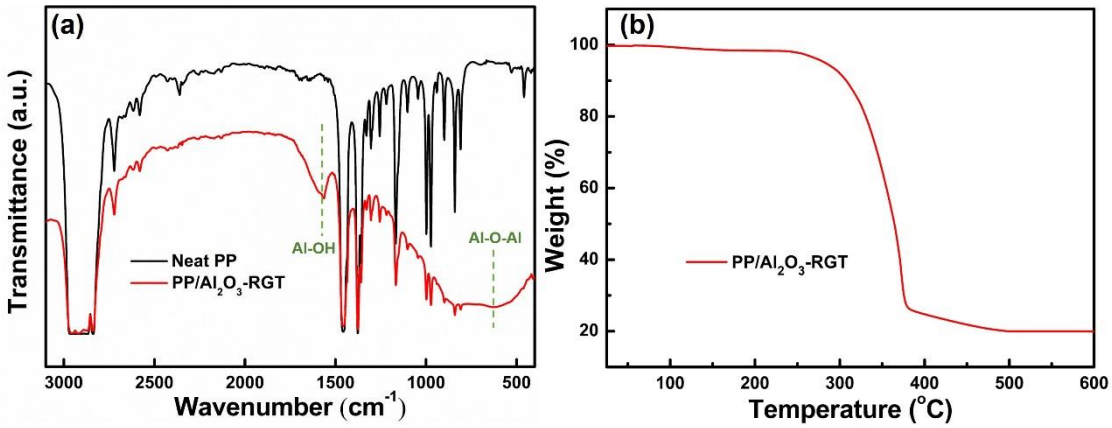

Fig. 2.2. a) ATR-IR spectra and b) TGA result for a PP/Al_2O_3-RGT nanocomposite having the theoretical Al_2O_3 loading of 20 wt%.

The RGT was adopted to realize the uniform dispersion of nanoparticles in the PP matrix. TEM was employed to confirm this expectation. As shown in Fig. 2.3a,b, Al_2O_3 nanoparticles were uniformly dispersed in the matrix and agglomerates were hardly observed. To further study the dispersion of nanoparticles, a particle size distribution profile was acquired by analyzing TEM images over 150 particles using ImageJ software. The result is shown

in the inset of Fig. 2.3b. It can be seen that the size of Al_2O_3 nanoparticles mostly fell in the range of 60–100 nm (the median size (D_{50}) = 74.8 nm). Thus, it was confirmed that the RGT generated uniformly dispersed Al_2O_3 nanoparticles in the PP matrix, and this was achieved at a relatively high loading (20 wt%) without adding any dispersant [24].

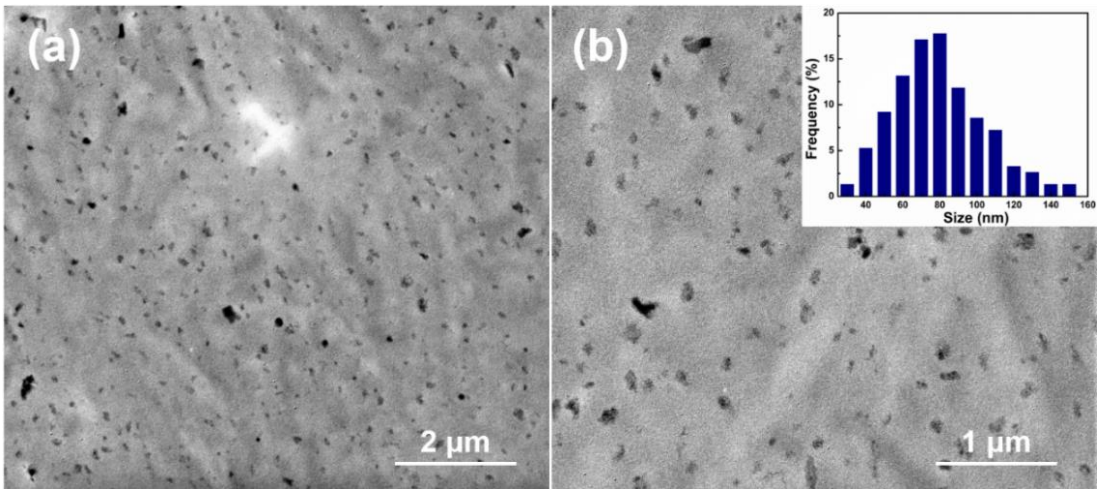

Fig. 2.3. TEM micrographs of PP/Al_2O_3-RGT (20 wt%). The inset shows the particle size distribution of Al_2O_3.

2.3.2. Selective localization of Al_2O_3 nanoparticles in PP/POE blends

To explore the distribution of Al_2O_3 nanoparticles after blending POE, TEM images of the ternary materials were acquired. From Fig. 2.4, the existence of two different phases was clearly observed for all the nanocomposites, while the distribution of Al_2O_3 nanoparticles depended on the viscosity of employed POE.

When POE1 and POE2 having higher viscosity were employed, many Al_2O_3 nanoparticles can be found at the interface between the PP and POE phases (Fig. 2.4a,b). As was confirmed in **2.3.1**, Al_2O_3 nanoparticles were uniformly dispersed in the PP matrix, so that the localization of Al_2O_3 nanoparticles indicated migration of these nanoparticles during the melt processing in the presence of POE. Contrary, the utilization of POE3 and POE4 with lower viscosity caused the confinement of most of Al_2O_3 nanoparticles in one phase, where particle agglomeration became more evident than the localization at the interface (Fig. 2.4c,d). The different localization behaviours of Al_2O_3 nanoparticles suggested that the viscosity of POE significantly affected the migration process, and the reason for it will be discussed later.

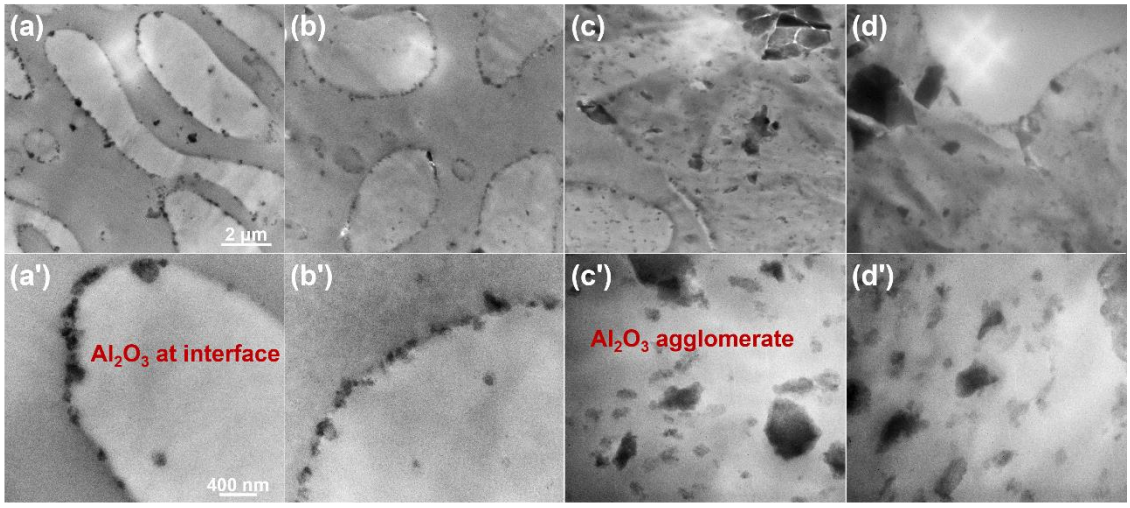

Fig. 2.4. TEM micrographs of PP/POE/Al_2O_3-RGT nanocomposites with different kinds of POE. a,a') POE1, b,b') POE2, c,c') POE3, d,d') POE4. Note that the scale bar is applied to the individual entire row.

An important role of the viscosity of POE was also confirmed by elemental mapping results for cross-sectioned samples (Fig. 2.5). The distribution of blue and dark regions figures out Al-rich and Al-poor domains, respectively. In the case of POE1 and POE2 (higher viscosity), Al was found concentratedly distributed in specific areas (Fig. 2.5a,b). In contrast, big blue spots were found for POE3 and POE4 (Fig. 2.5c,d), corresponding to the agglomerated Al_2O_3 nanoparticles.

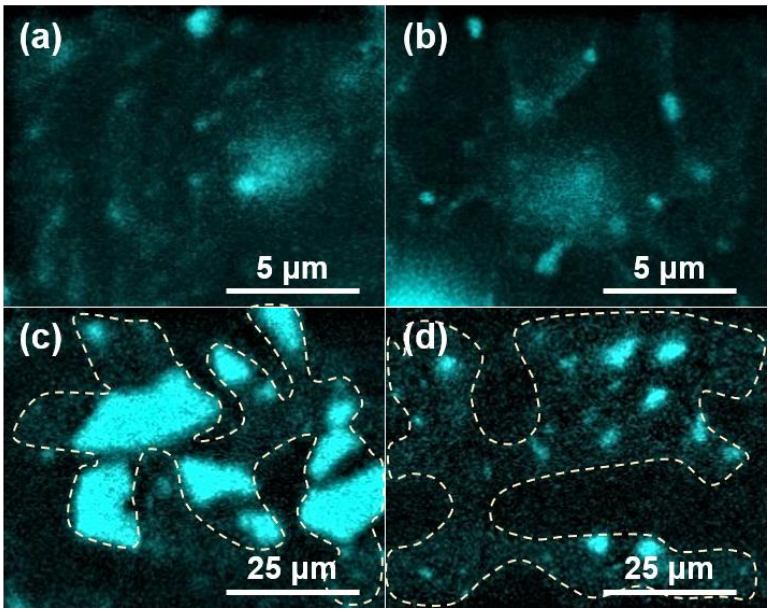

Fig. 2.5. EDX elemental mapping for Al in PP/POE/Al_2O_3-RGT nanocomposites with different kinds of POE. a) POE1, b) POE2, c) POE3, d) POE4. The dotted lines figure out Al-rich domains.

In order to identify the phase in which Al_2O_3 nanoparticles preferred to be distributed in, samples were etched with heptane to selectively extract the

POE phase. Then, TGA was used to determine the Al_2O_3 content in the remaining PP phase or at the interface (Fig. 2.6). Before etching the POE phase, the Al_2O_3 content was in the range of 10.2–10.6 wt% (Fig. 2.7), similar to the predicted value (11.1 wt%). After the selective extraction of the POE phase, the Al_2O_3 content was found to be around 20 wt% irrespective of the POE type, and the value was identical to that before adding POE. This fact indicates that most of Al_2O_3 nanoparticles were selectively localized in the PP phase and/or at the interface. Note that the Al_2O_3 nanoparticles were not dispersible in heptane and therefore, the nanoparticles must remain unextracted even though they were localized at the interface.

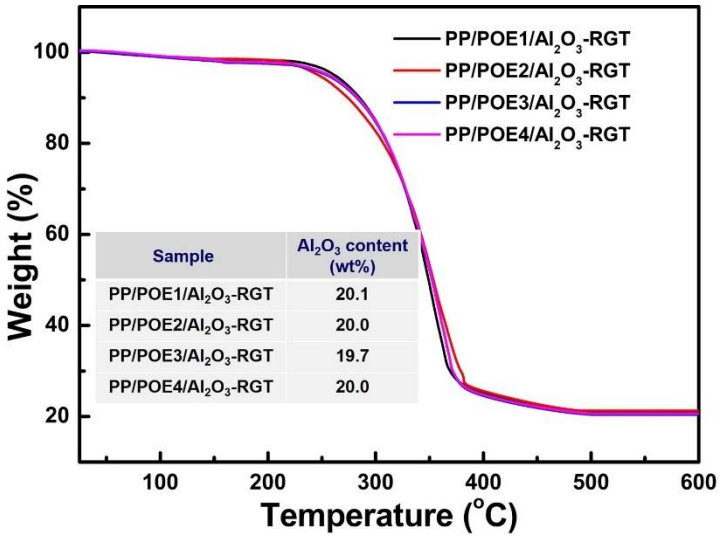

Fig. 2.6. TGA curves for PP/POE/Al_2O_3-RGT nanocomposites after selective extraction of the POE phase. The inset summarizes the Al_2O_3 content derived from the residual weight at 600 °C.

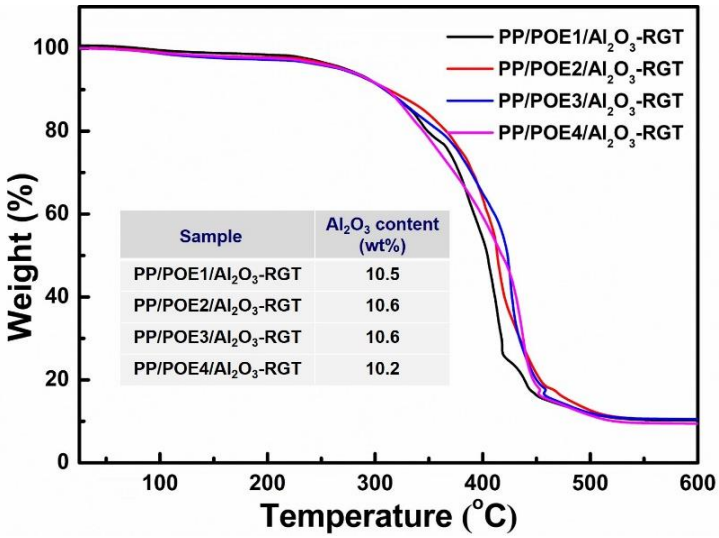

Fig. 2.7. TGA curves for PP/POE/Al_2O_3-RGT nanocomposites. The inset summarizes the Al_2O_3 content derived from the residual weight at 600 °C. The Al_2O_3 content was found to be consistent with the predicted value for all the samples (11.1 wt%).

Cross-sectional SEM images of the etched samples were also acquired (Fig. 2.8). A layer of Al_2O_3 nanoparticles could be observed at the etched surface of the PP phase in PP/POE1/Al_2O_3-RGT (Fig. 2.8a). This corresponds to the localization of Al_2O_3 nanoparticles at the interface, where the distance between nanoparticles was greatly shortened and many nanoparticles were apparently contacted with each other to form a network. The nanoparticle localization at the interface was similar in PP/POE2/Al_2O_3 (Fig. 2.8b). In consistent, agglomeration was observed in PP/POE3,4/Al_2O_3-RGT (marked in dotted circles in Fig. 2.8c,d), and relatively fewer nanoparticles were found

at the interface. On the basis of these TEM, EDX and TGA results, it was concluded that most of Al_2O_3 nanoparticles were localized at the interface for POE1 and POE2 (higher viscosity), while for POE3 and POE4 (lower viscosity), Al_2O_3 tended to be distributed in the PP phase. The localization at the interface was similarly observed from 0.6 vol% to 4.7 vol% in PP/POE1/Al_2O_3-RGT nanocomposites (Fig. 2.9).

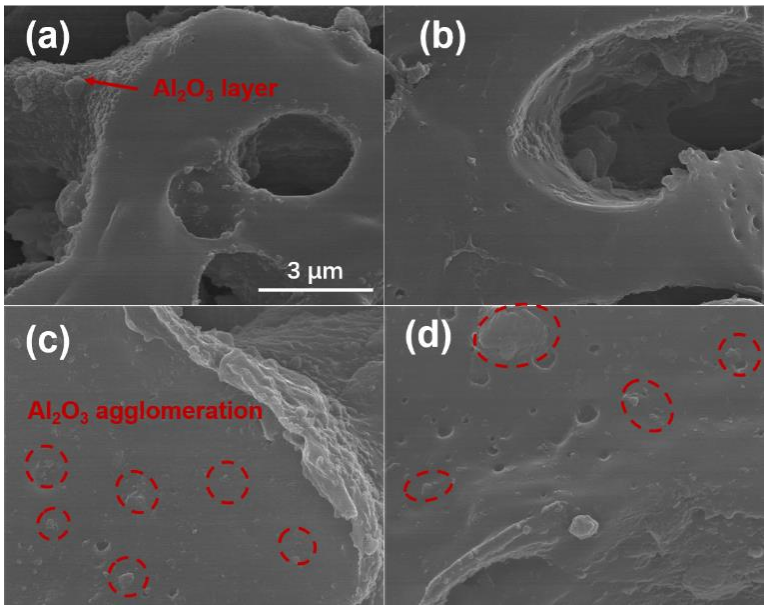

Fig. 2.8. SEM micrographs of PP/POE/Al_2O_3-RGT nanocomposites with different kinds of POE after selective extraction of the POE phase. a) POE1, b) POE2, c) POE3, d) POE4. Note that the scale bar is applied to all the samples.

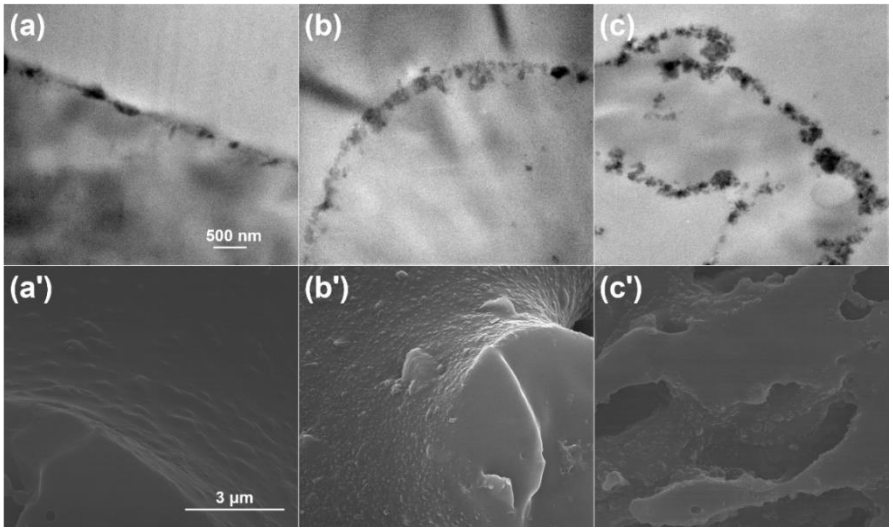

Fig. 2.9. TEM (upper) and SEM (lower) micrographs of PP/POE1/Al_2O_3-RGT nanocomposites with different Al_2O_3 loadings. a,a') 0.6 vol%, b,b') 1.3 vol%, c,c') 4.7 vol%. Note that the scale bar is applied to the individual entire row.

To clarify the reason why the localization of Al_2O_3 nanoparticles was dominated by the viscosity of POE, the phase morphology was observed by SEM and the results are summarized in Fig. 2.10a–d. The POE phase was preliminarily etched by heptane to give a clear observation. A co-continuous structure was formed in all the samples regardless of the difference in the viscosity and chemical composition of POE. The phase size for PP/POE1/Al_2O_3-RGT and PP/POE2/Al_2O_3-RGT was determined to be 1.8 μm and 2.6 μm, respectively, which were much smaller than 9.9 μm and 8.6 μm for POE3 and POE4 (Fig. 2.10e). In general, a large interfacial area in polymer blends leads to large interfacial free energy. The phase morphology

that is created under an external shear is not stable and it tends to translate to the state with lower interfacial free energy. A direct consequence of this is the coalescence of phases, leading to the increase of the phase size. In the PP/POE3,4 blends, the mobility of polymer chains was much greater so that the POE phase could coalesce and form larger phase morphologies.

According to all the above observations, the morphology of PP/POE/Al_2O_3-RGT nanocomposites is schematically illustrated in Fig. 2.11. When the phase size was large (PP/POE3,4/Al_2O_3-RGT), Al_2O_3 nanoparticles had to migrate farther for arriving at the interface, i.e. they had more chances to encounter with each other and form agglomerates. The agglomeration in turn hindered the further migration of nanoparticles. Thus, fewer Al_2O_3 nanoparticles could finally arrive at the interface. On the other hand, when the phase size was small (POE1 and POE2), many nanoparticles could migrate to the interface and get stabilized before encountering with each other in the PP phase. The selective localization of nanoparticles at the interface increased their concentration at these areas so that many particles could directly contact with each other to form thermal conductive networks. Besides, a smaller phase size could form more evenly distributed networks in the nanocomposites, and this must be profitable for avoiding the creation of a heterogeneous temperature profile upon heat releasing.

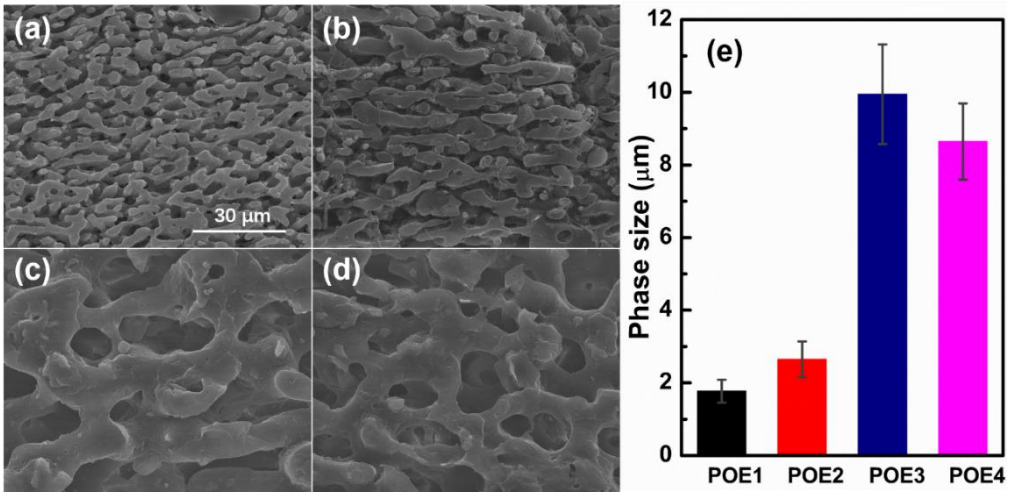

Fig. 2.10. Phase morphology of PP/POE/Al_2O_3-RGT nanocomposites with different kinds of POE after selective extraction of the POE phase. a) POE1, b) POE2, c) POE3, d) POE4. Note that the scale bar is applied to all the samples. e) Measured phase size.

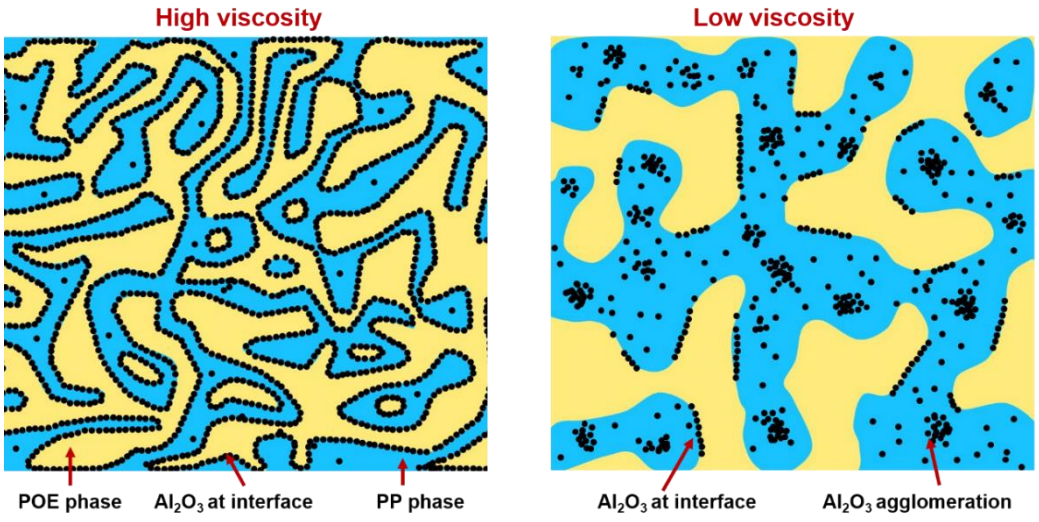

Fig. 2.11. Schematic illustration of the morphology of PP/POE/Al_2O_3-RGT nanocomposites. The blue domains represent the PP phase, the yellow domains the POE phase, and the black circles Al_2O_3 nanoparticles.

Here, the role of the polymer viscosity in achieving the localization of Al_2O_3 nanoparticles is discussed from a theoretical viewpoint. It is considered that the localization of nanoparticles is determined by the competition between the speeds of nanoparticle migration and phase coarsening, *e.g.* the successful localization of nanoparticles at the interface can be realized only when the nanoparticle migration is faster than the phase coarsening. The self-diffusion of nanoparticles in a phase that they are initially dispersed in is expressed by the Stokes-Einstein equation for the Brownian motion,

$$D_0 = \frac{k_B T}{6\pi\eta_1 r} \quad (2\text{-}2),$$

where D_0 corresponds to the diffusion coefficient of a spherical nanoparticle of radius r in a fluid with viscosity η_1 (in this study, PP) at temperature T, and k_B is the Boltzmann constant. The time (t_D) for the nanoparticle to migrate a distance r equal to its radius can be given as Eq. (2-3) [49],

$$t_D = \frac{r^2}{6D_0} = \frac{\pi\eta_1 r^3}{k_B T} \quad (2\text{-}3).$$

The rate of phase coarsening (k) in an immiscible blend follows the equation proposed by Veenstra et al. [50],

$$k = \frac{dR}{dt} = c\frac{\sigma}{\eta_b} \quad (2\text{-}4),$$

where dR/dt describes the rate of the enlargement of the average thickness (R) along the time, and σ and η_b are the interfacial tension and the viscosity of the polymer blend respectively. The dimensionless constant c is found to be 0.07 [48]. Thus, the

time (t_C) required for the phase domain size to grow a thickness of r can be obtained as Eq. (2-5).

$$t_C = \frac{r\eta_b}{c\sigma} \quad (2\text{-}5).$$

The successful localization of nanoparticles at the interface is expected only when the nanoparticle migration is faster than the phase coarsening, namely $t_D < t_C$. Hence the following relation should be satisfied,

$$\frac{\pi\eta_1 r^2}{k_B T} < \frac{\eta_b}{c\sigma} \quad (2\text{-}6).$$

According to Utracki et al. [51] the viscosity of a polymer blend consisting of polymer 1 and polymer 2 at 50/50 vol%/vol% is expressed by

$$\eta_b = \sqrt{\eta_1 \eta_2} \quad (2\text{-}7),$$

where η_1 and η_2 are the viscosity of polymer 1 and polymer 2 at temperature T. By substituting Inequality (2-7) into Eq. (2-6), the relationship is re-written as,

$$\sqrt{\frac{\eta_2}{\eta_1}} > \frac{c\pi\sigma r^2}{k_B T} \quad (2\text{-}8),$$

where the left side of the inequality corresponds to the square root of the viscosity ratio of the two polymers. Inequality (2-8) dictates that a higher viscosity of polymer 2 (POE) is more advantageous for the successful localization of nanoparticles at the interface, in agreement with our experimental observation. Meanwhile, a smaller interfacial tension and smaller particle size are other important factors to achieve the localization. The nanoparticle localization is also affected by the temperature dependence of the viscosity ratio (exponential) and $1/T$ of the right side. For

example, when prepared at 190 °C, the successful localization was confirmed for POE1 (and POE2). But, this is not the case when prepared at 230 °C (Fig. 2.12) because the viscosity ratio drops more sharply than 1/*T*.

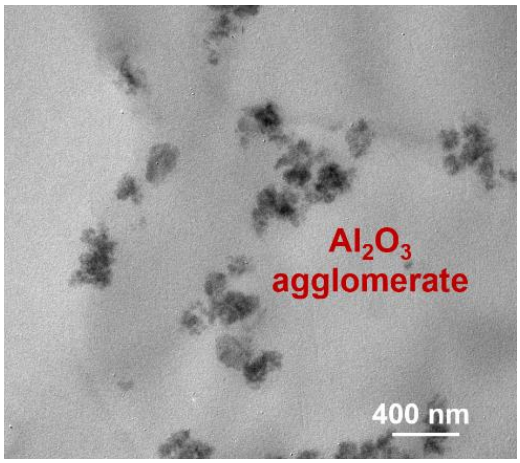

Fig. 2.12. TEM micrograph of PP/POE1/Al_2O_3-RGT nanocomposite prepared at 230 °C.

The preformed Al_2O_3 nanoparticles were also used to prepare PP/POE/Al_2O_3-NP nanocomposites as reference. From Fig. 2.13, poor dispersion of the nanoparticles was evident in all the samples. Such phenomenon is quite common for polyolefin-based nanocomposites because the surface energy of nanoparticles is significantly higher than that of the polymer matrix [52]. More importantly, the Al_2O_3 nanoparticles were dominantly localized in the PP phase, while only a minor fraction reached the interface, almost regardless of the viscosity of POE. This result suggested the

initially uniform dispersion as another key factor to realize the localization of the nanoparticles at the interface. When the nanoparticles are not uniformly dispersed in the PP phase, the migration itself or successful migration is greatly suppressed irrespective of the phase size. In this light, the RGT is regarded as an effective methodology for controlling the distribution of nanoparticles based on their uniform dispersion.

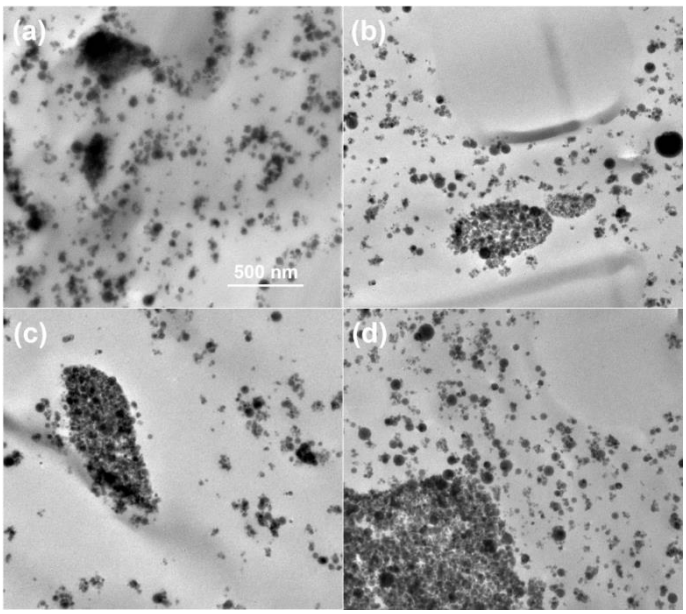

Fig. 2.13. TEM micrographs of PP/POE/Al_2O_3-NP nanocomposites with different kinds of POE. a) POE1, b) POE2, c) POE3, d): POE4. Note that the scale bar is applied to all the samples.

2.3.3. Thermal conductivity

Fig. 2.14 compares the thermal conductivity of various samples prepared in this chapter, that include neat PP, PP/POE blends, and PP/Al_2O_3-RGT, PP/POE/Al_2O_3-RGT and PP/POE/Al_2O_3-NP nanocomposites. The thermal conductivity of neat PP was 0.21 W/m K. It increased to 0.27 and 0.30 W/m K when 2.5 and 5.5 vol% of Al_2O_3 nanoparticles were uniformly dispersed in the PP matrix, respectively (PP/Al_2O_3-RGT, see Fig. 2.3). In the case of uniform dispersion, thermal transport happens from one particle to the closest particle by crossing the organic pathway with poor thermal conductivity [53]. Accordingly, the uniform dispersion is more efficient than agglomeration [24,54–57], but not suitable to form a thermal conductive network with direct contact among nanoparticles for omitting high interfacial thermal resistance of the organic pathway [58,59].

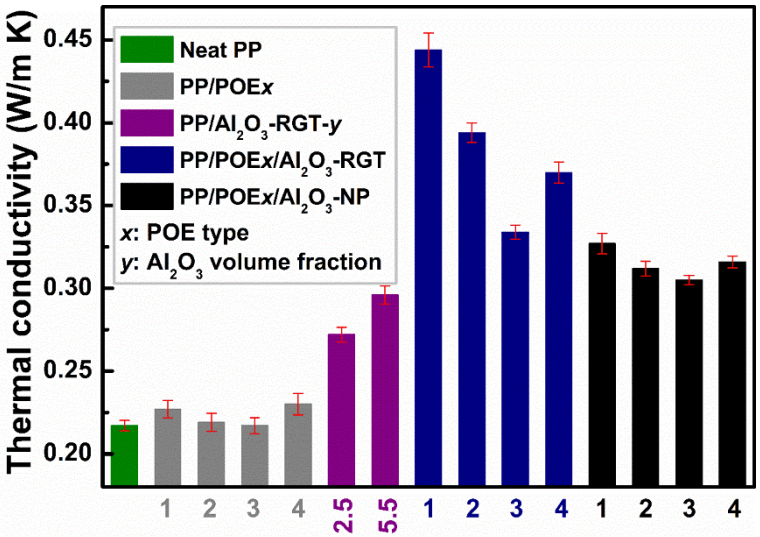

Fig. 2.14. Thermal conductivity of various samples prepared in this chapter. The values and error bars represent the average and standard deviation of ten independent measurements per sample, respectively. Different series of samples were classified by colors, where the numbers in the x-axis correspond to the POE type except for PP/Al_2O_3-RGT, where the volume percentage of Al_2O_3 is written (2.5 and 5.5 vol%). Note that the volume percentage of Al_2O_3 was kept at 2.8 vol% for all the PP/POE/Al_2O_3 samples.

After adding POE, the thermal conductivity was improved even when preformed Al_2O_3 nanoparticles were used. When compared at a similar Al_2O_3 loading, the thermal conductivity of PP/POE/Al_2O_3-NP (2.8 vol%) was 0.30–0.33 W/m K, i.e. around 11–22% higher than that of PP/Al_2O_3-RGT (2.5 vol%). Considering that the dispersion of Al_2O_3 nanoparticles was superior for PP/Al_2O_3-RGT, different factors must account for this improvement. One

clear reason was the localization of Al_2O_3 nanoparticles in the PP phase, which in turn increased the concentration of the nanoparticles in this phase. Provided that all the Al_2O_3 nanoparticles were localized in the PP phase, the loading to PP was assumed to be 5.5 vol%. Accordingly, PP/Al_2O_3-RGT (5.5 vol%) was prepared and its thermal conductivity, 0.30 W/m K, was found to be much closer to that of PP/POE/Al_2O_3-NP.

The thermal conductivity was further improved when the RGT and the immiscible blend were combined to prepare PP/POE/Al_2O_3-RGT nanocomposites. Among them, PP/POE1/Al_2O_3-RGT achieved the highest thermal conductivity. The uniform dispersion of Al_2O_3 nanoparticles and the small phase domain size guaranteed the successful migration of Al_2O_3 nanoparticles to the interface and formed well-developed thermal conductive networks.

To the end, the effect of the chemical composition of POE is discussed. The thermal conductivity became higher for POE having a greater octene content (i.e. POE1,4), while a more developed network was formed for POE having higher viscosity (i.e. POE1,2). This discrepancy was understood by breaking up the thermal conductivity in the specific heat capacity and the thermal diffusivity. A higher octene content increases the specific heat capacity due to the mobility of side chains [60] (Table 2.1), while higher viscosity enhances

the thermal diffusivity (Fig. 2.15), both of which can positively contribute to the thermal conductivity.

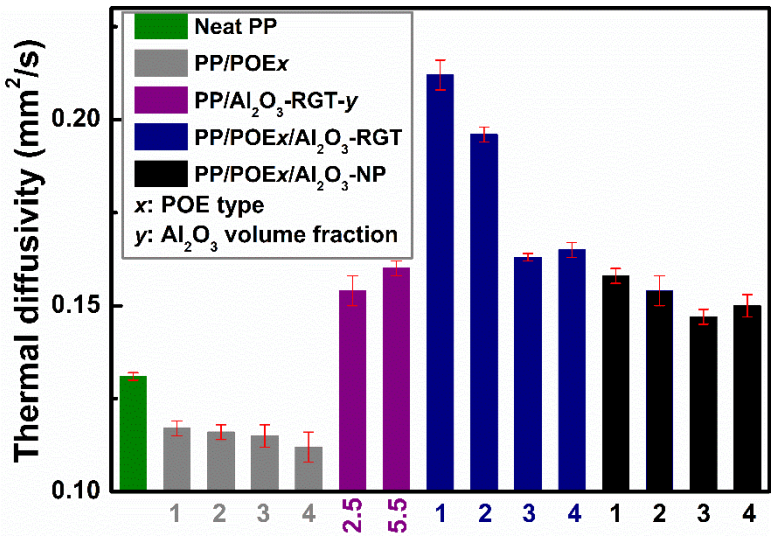

Fig. 2.15. Thermal diffusivity of various samples preapred in this study. It can be seen that PP/POE1,2/Al_2O_3-RGT improved the thermal diffusivity most due to the effective migration of Al_2O_3 nanoparticles to the interface.

2.4. Conclusions

In this chapter, an immiscible polymer blend strategy was employed in combination with the reactor granule technology (RGT) in order to control the selective localization of Al_2O_3 nanoparticles at the interface. Al_2O_3 nanoparticles thermodynamically prefer the localization at the interface between polypropylene (PP) and polyolefin elastomer (POE), but their

successful migration to the interface largely depended on the initial dispersion of the nanoparticles and the phase domain size of the blends. For instance, when preformed nanoparticles were directly melt-mixed, severe agglomeration hindered the migration to the interface, while even with uniform initial dispersion, the coarse phase morphology tended to promote the agglomeration over the migration. The combination of the RGT and POE having high viscosity satisfied the prerequisites of uniform initial dispersion and a small phase size for the short migration distance, thus leading to the selective localization of Al_2O_3 nanoparticles at the interface, creating thermal conductive networks along the co-continuous interface, and eventually giving high thermal conductivity. The results obtained in this chapter firstly demonstrated that the distribution of nanoparticles can be controlled even for the combination of hydrophobic and hydrophilic pairs like PP and Al_2O_3, in which initially uniform dispersion of the nanoparticles in one phase and a small phase domain size are essential to drive successful migration of the nanoparticles. In conclusion, I successfully proposed a facile way to control the localization of filled nanoparticles at the interface in nanocomposites, and key factors thereof. The proposal is believed to be widely applicable for combination of other fillers and immiscible blends, and relevant to practical applications as electrical and thermal conductive materials.

References

[1] Anithambigai P, Shanmugan S, Mutharasu D, Zahner T, Lacey D. Study on thermal performance of high power LED employing aluminum filled epoxy composite as thermal interface material. Microelectr 2014; 45(12): 1726–33.

[2] Baffett J. Electronic systems packaging: future reliability challenges. Microelectronics Reliab. 1998; 38(6-8): 1277–86.

[3] Cui W, Du F, Zhao J, Zhang W, Yang Y, Xie X, et al. Improving thermal conductivity while retaining high electrical resistivity of epoxy composites by incorporating silica-coated multi-walled carbon nanotubes. Carbon 2011; 49(2): 495–500.

[4] Xie T, He Y-L, Hu Z-J. Theoretical study on thermal conductivities of silica aerogel composite insulating material. Int. J. Heat Mass Transfer 2013; 58(1-2): 540–52.

[5] Chen H, Ginzburg VV, Yang J, Yang Y, Liu W, Huang Y, et al. Thermal conductivity of polymer-based composites: Fundamentals and applications. Prog. Polym. Sci. 2016; 59: 41–85.

[6] Zhang X, Zheng S, Zheng X, Liu Z, Yang W, Yang M. Distinct positive temperature coefficient effect of polymer–carbon fiber composites evaluated in terms of polymer absorption on fiber surface. Phys. Chem. Chem. Phys. 2016; 18(11): 8081–7.

[7] Zhang X, Zheng X, Ren D, Liu Z, Yang W, Yang M. Unusual positive temperature coefficient effect of polyolefin/carbon fiber conductive composites. Mater. Let. 2016; 164: 587–90.

[8] Vinod K. Determination of lead using a poly (vinyl chloride)-based crown ether membrane. Analyst 1995; 120(2): 495–8.

[9] Karimi-Maleh H, Tahernejad-Javazmi F, Atar N, Yola MLt, Gupta VK, Ensafi AA. A novel DNA biosensor based on a pencil graphite electrode modified with polypyrrole/functionalized multiwalled carbon nanotubes for determination of 6-mercaptopurine anticancer drug. Ind. Eng. Chem. Res. 2015; 54(14):.3634–9.

[10] Gupta VK, Singh L, Singh R, Upadhyay N, Kaur S, Sethi B. A novel copper (II) selective sensor based on dimethyl 4, 4′(o-phenylene) bis (3-thioallophanate) in PVC matrix. J. Mol. Liq. 2012; 174: 11–6.

[11] Srivastava SK, Gupta VK, Dwivedi MK, Jain S. Caesium PVC–crown (dibenzo-24-crown-8) based membrane sensor. Analytical Proceedings including Analytical Communications: RSC. 1995;.32(1):.21–3.

[12] Vinod K. Neutral carrier and organic resin based membranes as sensors for uranyl ions. Analytical Proceedings including Analytical Communications: RSC 1995; 32(7): 263–6.

[13] Mazov I, Burmistrov I, Ilinykh I, Stepashkin A, Kuznetsov D, Issi JP.

Anisotropic thermal conductivity of polypropylene composites filled with carbon fibers and multiwall carbon nanotubes. Polym. Compos. 2015; 36(11):. 1951–7.

[14] Jo I, Pettes MT, Kim J, Watanabe K, Taniguchi T, Yao Z, et al. Thermal conductivity and phonon transport in suspended few-layer hexagonal boron nitride. Nano. Lett. 2013; 13(2): 550–4.

[15] Yu S, Hing P, Hu X. Thermal conductivity of polystyrene–aluminum nitride composite. Comps. Part. A-Appl S. 2002; 33(2): 289–92.

[16] Li Y, Huang X, Hu Z, Jiang P, Li S, Tanaka T. Large dielectric constant and high thermal conductivity in poly (vinylidene fluoride)/barium titanate/silicon carbide three-phase nanocomposites. ACS. Appl. Mater. Inter. 2011; 3(11): 4396–403.

[17] Timofeeva EV, Gavrilov AN, McCloskey JM, Tolmachev YV, Sprunt S, Lopatina LM, et al. Thermal conductivity and particle agglomeration in alumina nanofluids: experiment and theory. Phys. Rev. 2007; 76(6): 061203.

[18] Kozako M, Okazaki Y, Hikita M, Tanaka T. Preparation and evaluation of epoxy composite insulating materials toward high thermal conductivity. IEEE 2010; 1-4.

[19] Yu J, Huang X, Wang L, Peng P, Wu C, Wu X, et al. Preparation of hyperbranched aromatic polyamide grafted nanoparticles for thermal properties

reinforcement of epoxy composites. Polym. Chem. 2011; 2(6): 1380–8.

[20] Chen C-H, Jian J-Y, Yen F-S. Preparation and characterization of epoxy/γ-aluminum oxide nanocomposites. Comps. Part. A-Appl. S. 2009; 40(4): 463–8.

[21] Fukuyama Y, Senda M, Kawai T, Kuroda S-i, Toyonaga M, Taniike T, et al. The effect of the addition of polypropylene-grafted SiO2 nanoparticle on the thermal conductivity of isotactic polypropylene. J. Therm. Anal. Calorim. 2014; 117(3): 1397–405.

[22] Fang L, Wu C, Qian R, Xie L, Yang K, Jiang P. Nano–micro structure of functionalized boron nitride and aluminum oxide for epoxy composites with enhanced thermal conductivity and breakdown strength. RSC. Adv. 2014; 4(40): 21010–7.

[23] Hu Y, Du G, Chen N. A novel approach for Al_2O_3/epoxy composites with high strength and thermal conductivity. Compos. Sci. Technol. 2016; 124: 36–43.

[24] Maira B, Chammingkwan P, Terano M, Taniike T. Reactor granule technology for fabrication of functionally advantageous polypropylene nanocomposites with oxide nanoparticles. Compos. Sci. Technol. 2017; 144: 151–9.

[25] Maira B, Chammingkwan P, Terano M, Taniike T. New reactor granule technology for highly filled nanocomposites: effective flame retardation of polypropylene/magnesium hydroxide nanocomposites. Macromol. Mater. Eng. 2015; 300(7): 679–83.

[26] Qiagedeer A, Maira B, Strauss R, Zhao Y, Chammingkwan P, Mizutani G, et al. Preparation and characterization of polypropylene/noble metal nanocomposites based on reactor granule technology. Polymer 2017; 127: 251–8.

[27] Maira B, Takeuchi K, Chammingkwan P, Terano M, Taniike T. Thermal conductivity of polypropylene/aluminum oxide nanocomposites prepared based on reactor granule technology. Compos. Sci. Technol. 2018; 165: 259–65.

[28] Dai K, Xu X-B, Li Z-M. Electrically conductive carbon black (CB) filled in situ microfibrillar poly (ethylene terephthalate) (PET)/polyethylene (PE) composite with a selective CB distribution. Polymer 2007; 48(3): 849–59.

[29] Yoon HG, Kwon KW, Nagata K, Takahashi K. Changing the percolation threshold of a carbon black/polymer composite by a coupling treatment of the black. Carbon 2004; 42(8-9): 1877–9.

[30] Le H, Prodanova I, Ilisch S, Radusch H-J. Online electrical conductivity as a measure to characterize the carbon black dispersion in oil containing rubber compounds with a different polarity of rubber. Rubber Chem. Technol. 2004; 77(5): 815–29.

[31] Mao C, Zhu Y, Jiang W. Design of electrical conductive composites: tuning the morphology to improve the electrical properties of graphene filled immiscible polymer blends. ACS. Appl. Mate. Inter. 2012; 4(10): 5281–6.

[32] Scherzer SL, Pavlova E, Esper JD, Starý Z. Phase structure, rheology and electrical conductivity of co-continuous polystyrene/polymethylmethacrylate blends filled with carbon black. Compos. Sci. Technol. 2015; 119: 138–47.

[33] Gao C, Zhang S, Lin Y, Li F, Guan S, Jiang Z. High-performance conductive materials based on the selective location of carbon black in poly (ether ether ketone)/polyimide matrix. Compos. Part. B=Eng. 2015; 79: 124–31.

[34] Zhang S, Deng H, Zhang Q, Fu Q. Formation of conductive networks with both segregated and double-percolated characteristic in conductive polymer composites with balanced properties. ACS. Appl. Mater. Inter. 2014; 6(9): 6835–44.

[35] Zhang X, Zheng S, Zou H, Zheng X, Liu Z, Yang W, et al. Two-step positive temperature coefficient effect with favorable reproducibility achieved by specific “island-bridge” electrical conductive networks in HDPE/PVDF/CNF composite. Compos. Part A-Appl. S. 2017; 94: 21–31.

[36] Al-Saleh MH, Sundararaj U. An innovative method to reduce percolation threshold of carbon black filled immiscible polymer blends. Compos. Part A-Appl. S. 2008; 39(2): 284–93.

[37] Shen L, Wang F, Jia W, Yang H. Thermodynamically induced self-assembled electrically conductive networks in carbon-black-filled ternary polymer blends. Polym. Int. 2012; 61(2): 163–8.

[38] Feng J, Chan Cm, Li J. A method to control the dispersion of carbon black in an immiscible polymer blend. Polym. Eng. Sci. 2003; 43(5): 1058–63.

[39] Gubbels F, Jérôme R, Vanlathem E, Deltour R, Blacher S, Brouers F. Kinetic and thermodynamic control of the selective localization of carbon black at the interface of immiscible polymer blends. Chem. Mater. 1998; 10(5): 1227–35.

[40] Li Z, Kong J, Ju D, Cao Z, Han L, Dong L. Thermal conductivity enhancement of poly (3-hydroxylbutyrate) composites by constructing segregated structure with the aid of poly (ethylene oxide). Compos. Sci. Technol. 2017; 149: 185–91.

[41] Cao J, Zhao X, Zhao J, Zha J, Hu G, Dang Z. Improved thermal conductivity and flame retardancy in polystyrene/poly (vinylidene fluoride) blends by controlling selective localization and surface modification of SiC nanoparticles. ACS. Appl. Mater. Inter. 2013; 5(15): 6915–24.

[42] Cao M, Shu J, Chen P, Xia R, Yang B, Miao J, et al. Orientation of boron nitride nanosheets in CM/EPDM Co-continuous blends and their thermal conductive properties. Polym. Test. 2018; 69: 208–13.

[43] Huang J, Zhu Y, Xu L, Chen J, Jiang W, Nie X. Massive enhancement in the thermal conductivity of polymer composites by trapping graphene at the interface of a polymer blend. Compos. Sci. Technol. 20–5.

[44] Holysz L, Chibowski E. Surface free energy components of. alpha-alumina

from thin-layer wicking. Langmuir 1992; 8(2): 717–21.

[45] Sumita M, Sakata K, Asai S, Miyasaka K, Nakagawa H. Dispersion of fillers and the electrical conductivity of polymer blends filled with carbon black. Polym. Bull. 1991; 25(2): 265–71.

[46] Kaneko K, Yadav N, Takeuchi K, Maira B, Terano M, Taniike T. Versatile strategy for fabrication of polypropylene nanocomposites with inorganic network structures based on catalyzed in-situ sol-gel reaction during melt mixing. Compos. Sci. Technol. 2014; 102: 120–5.

[47] Hashimoto T, Morikawa J. Temperature wave analysis. Netsu Bnssei 2001; 15(2): 113–7.

[48] Yoshida K, Hyuga H, Kondo N, Kita H. Synthesis of precursor for fibrous mullite powder by alkoxide hydrolysis method. Mater. Sci. Eng. B 2010; 173(1–3): 66–71.

[49] Plattier J, Benyahia L, Dorget M, Niepceron F, Tassin J-F. Viscosity-induced filler localisation in immiscible polymer blends. Polymer 2015; 59: 260–9.

[50] Veenstra H, Van Dam J, de Boer AP. On the coarsening of co-continuous morphologies in polymer blends: effect of interfacial tension, viscosity and physical cross-links. Polymer 2000; 41(8): 3037–45.

[51] Utracki LA, Favis B. Polymer alloys and blends: Marcel Dekker: New York; 1989.

[52] Gao F. Advances in polymer nanocomposites: types and applications: Elsevier; 2012.

[53] Burger N, Laachachi A, Ferriol M, Lutz M, Toniazzo V, Ruch D. Review of thermal conductivity in composites: mechanisms, parameters and theory. Prog. Polym. Sci. 2016; 61: 1–28.

[54] Agari Y, Ueda A, Nagai S. Thermal conductivities of composites in several types of dispersion systems. J. Appl. Polym. Sci. 1991; 42(6): 1665–9.

[55] Song YS, Youn JR. Influence of dispersion states of carbon nanotubes on physical properties of epoxy nanocomposites. Carbon 2005; 43(7): 1378–85.

[56] Tessema A, Zhao D, Moll J, Xu S, Yang R, Li C, et al. Effect of filler loading, geometry, dispersion and temperature on thermal conductivity of polymer nanocomposites. Polym. Test. 2017; 57: 101–6.

[57] Agarwal S, Saxena NS, Kumar V. Study on effective thermal conductivity of zinc sulphide/poly (methyl methacrylate) nanocomposites. Appl. Nanosci. 2015; 5(6): 697–702.

[58] Wernik JM, Meguid SA. Recent developments in multifunctional nanocomposites using carbon nanotubes. Appl. Mech. Rev. 2010; 63(5): 050801.

[59] Yorifuji D, Ando S. Enhanced thermal diffusivity by vertical double percolation structures in polyimide blend films containing silver nanoparticles. Macromol.

Chem. Phys. 2010; 211(19): 2118–24.

[60] Eynde SV, Mathot V, Koch M, Reynaers H. Thermal behaviour and morphology of homogeneous ethylene-1-octene copolymers with high comonomer contents. Polymer 2000; 41(13): 4889–900.

Chapter 3

Cooperative Influences of Nanoparticle Localization and Phase Coarsening on Thermal Conductivity of Polypropylene/Polyolefin Elastomer Blends

Chapter 3

Abstract

Polypropylene (PP)/polyolefin elastomer (POE)/aluminum oxide (Al_2O_3) nanocomposites were prepared based on a reactor granule technology (RGT). Cooperation of nanoparticle migration and phase morphology evolution on the formation of thermal conductive networks was systematically studied. The utilization of RGT and POE with high viscosity enabled successful migration of in-situ generated Al_2O_3 nanoparticles at the interface of PP and POE, as combined results of uniform dispersion of Al_2O_3 and a small phase domain size of PP. The localization of the nanoparticles at the interface also contributed to suppression of the phase coarsening during annealing. The nanoparticle migration to the interface and the retarded phase coarsening synergistically contributed to the enhanced thermal conductivity.

Keywords: Thermal conductivity; Nanocomposites; Immiscible blends; Nanoparticle localization; Phase coarsening

3.1. Introduction

With the continuous miniaturization and lightweight of electronic components, thermal conductive polymer composites have been widely studied and used in recent years due to their excellent properties such as low density, good processing ability, and resistance to corrosion [1–7]. Electrical insulating fillers with high thermal

conductivity such as aluminum nitride (AlN) [8], boron nitride [9,10], silicon carbide [11], and aluminum oxide (Al_2O_3) [12] are commonly introduced into polymer matrices to fabricate thermal conductive composites. Many methods have been reported to improve the thermal conductivity of the composites at a reduced loading and it has been found that the thermal conductivity greatly depends on the construction of interconnected thermal conductive networks [13–15]. In particular, the utilization of a co-continuous structure of immiscible blends is regarded as an effective way to construct such networks by the selective localization of fillers in one phase or at the interface. This strategy has been widely applied to reduce the percolation threshold in electrical conductive composites [16–18], and its application to thermal conductive composites started to appear in recent years [19,20].

The distribution of fillers in polymer blends is manipulated by thermodynamic and kinetic factors [21]. Fillers are preferentially distributed in a phase with the surface energy closer to that of fillers [22,23], where surface modification of fillers is one effective way for controlling the localization [24]. When the nanoparticles are initially distributed in the thermodynamically less favorable phase, they tend to migrate to another phase or the interface to reach the equilibrium. For instance, Gong et al. reported the migration of multi-walled carbon nanotubes (MWCNTs) in polyoxyethylene (PEO)/ethylene-α-octene random copolymer composites during

melt compounding [25]. They confirmed that MWCNTs almost completely migrated from the PEO phase to the thermodynamically favorable copolymer phase. The migration is also influenced by kinetic factors such as the filler size, viscosity of the components, mixing procedure, shear strength, and etc. [21]. For instance, graphene nanoplates (GNPs) were kinetically trapped at the interface of polylactic acid/polystyrene (PS) immiscible blends via control of melt-compounding sequences, mixing times and shear rates, although GNPs thermodynamically prefer the PS phase [26]. Shear flow-induced hierarchical self-assembly of fillers is a prominent example of successful manipulation of the distribution and organization of fillers with the aid of kinetic control [27–29]. In Chapter 2, I found that the distribution of Al_2O_3 nanoparticles was not only determined by the thermodynamic and kinetic factors but also greatly influenced by their initial dispersion state [7]. The uniform dispersion of nanoparticles is essential for controlling the migration of nanoparticles, while the formation of aggregates hinders the migration.

Another important parameter for the filler migration is the evolution of phase morphology in immiscible blends. The as-melt-mixed phase morphology is not in an equilibrium state and it evolves to lower interfacial free energy once the external shear is stopped. The most direct consequence of decreasing the interfacial area is the phase coalescence, leading to the increase of the phase domain size [30]. Cooperation between the filler migration and phase morphology evolution has been

reported in several papers. Sun et al. studied the relationship between the phase morphology and electrical conductivity of polypropylene (PP)/PS/carbon black (CB) composites with a co-continuous structure [31]. They found that the electrical conductivity of the composites greatly increased after thermal annealing because the evolution of the co-continuous morphology drove the CB nanoparticles to self-assemble into complete nanoparticle networks. Enhancement of electrical properties by thermal annealing was also reported for a PS/poly(methyl methacrylate) (PMMA)/MWCNTs ternary system [32]. Such enhancement was caused by the coalescence of small phases into co-continuous phases and the enrichment of MWCNTs at the interface of PS/PMMA blends during the thermal annealing. Pan et al. reported an opposite phenomenon that the phase coarsening upon annealing caused the destruction of the conductive pathway of CB nanoparticles [33]. The above-introduced literatures all describe the influence of the phase morphology evolution on the filler migration, while the influence in the opposite direction, i.e. from the filler migration to the phase morphology evolution, is also known. For instance, Li et al. reported that the selective localization of nanoparticles (MWCNTs and SiO_2) at the interface of polymer blends suppressed the coalescence of polymer domain and resulted in a smaller phase domain size [34,35]. Likewise, the filler migration and localization in a co-continuous structure are greatly affected by the evolution of the phase morphology, and this rationalizes a detailed investigation on

the relationship among the filler migration, phase morphology evolution, and formation of thermal conductive networks for designing thermal conductive composites.

In this chapter cooperation of the filler migration and phase morphology evolution was investigated in relation to the formation of thermal conductive networks in PP/POE/Al_2O_3 composites with a co-continuous structure. First, the reactor granule technology (RGT) [7,36–39] was employed to facilitate the uniform dispersion of Al_2O_3 nanoparticles in the PP matrix. Then, POE was blended to fabricate PP/POE/Al_2O_3 nanocomposites with a co-continuous structure. The obtained nanocomposites were treated under quiescent melting annealing. The evolution of the nanoparticle localization, phase coarsening, and thermal conductivity during this process was studied comprehensively. Such study is expected to provide helpful guidance for designing conductive composite materials and engineering the phase morphology of immiscible polymer blends.

3.2. Experimental section

3.2.1. Materials

Polypropylene reactor granule with the weight average molecular weight of 260,000, median size of 637 μm, and pore volume of 0.56 mL/g was synthesized by catalyzed propylene polymerization. Aluminium isopropoxide (Al(O*i*Pr)$_3$, supplied

by Sigma-Aldrich), *n*-octdecyl-3-(3′,5′-di-*t*-butyl-4′-hydroxyphenyl)propionate (AO-50, donated by ADEKA), and bis(1,2,2,6,6-pentamethyl-4-piperidyl) sebacate (LA-77, donated by ADEKA) were used as a precursor, anti-oxidant and catalyst, respectively [40]. Polyolefin elastomer with the octene content of 38 wt% and the melt flow index of 1 g/10 min (measured at 2.16 kg and 190 °C based on ASTM D1238) was supplied by Dow Chemical Co. (Midland, MI, USA). Preformed Al_2O_3 nanoparticles with the average diameter of 15 nm (Alu, Nippon Aerosil) were used to prepare reference samples.

3.2.2. Sample preparation

Nanocomposites were obtained by a masterbatch method, as schematically depicted in Fig. 3-1. First, a PP/Al_2O_3 masterbatch was prepared as follows: 10 g of PP reactor granule was impregnated with a specific amount of Al(O*i*Pr)$_3$ dissolved in 20 mL of toluene at 50 °C under N_2 for 12 h. The amount of the precursor was adjusted so as to obtain different Al_2O_3 loadings in the resultant masterbatch under the assumption of full conversion of the metal alkoxide to the oxide. After the impregnation and solvent removal in vacuo, the impregnated granule was treated at 50 °C and 100% relative humidity for 24 h to promote the hydrolysis and solidification of Al(O*i*Pr)$_3$ in the pores of PP. The obtained granule was melt-mixed at 190 °C and 100 rpm for 10 min (Micro Compounder IM5, Xplore), then a specified amount of POE was added, and blended for another 5 min. The ratio of PP

and POE was kept at 50/50 wt/wt to maintain the co-continuous phase morphology. After mixing, the product was rapidly quenched in cold water to freeze the phase morphology. The obtained samples were denoted as PP/POE/Al_2O_3-RGT-*x*, where *x* represents the volume fraction of Al_2O_3 nanoparticles. Preformed Al_2O_3 nanoparticles were also melt-mixed with PP and then with POE. These reference samples were termed as PP/POE/Al_2O_3-NP-*x*.

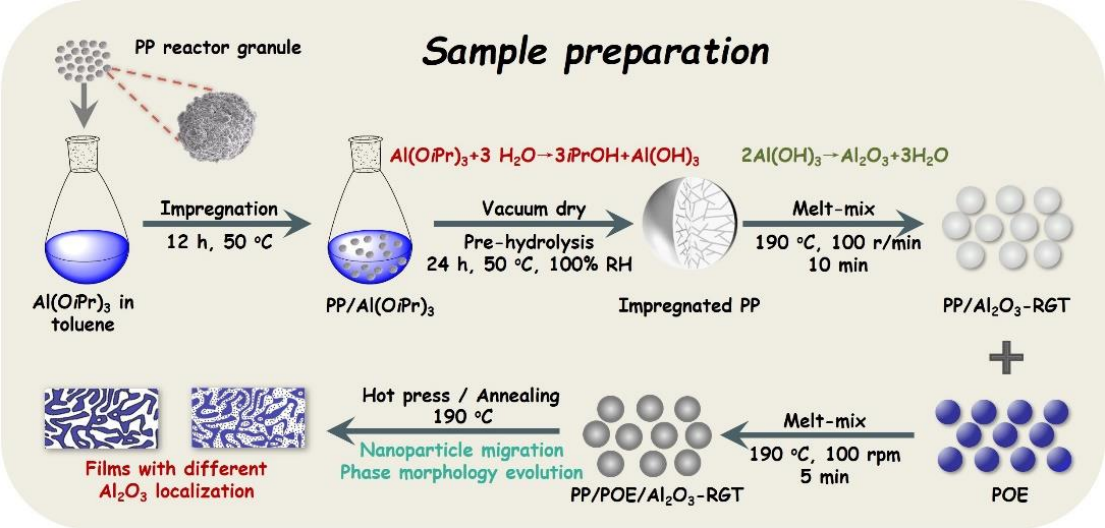

Fig. 3.1. Schematic image of sample preparation.

Nanocomposites were compression-molded into 200 μ-thick films. A melt-mixed sample was preheated at 190 °C for 1 min, then compressed under 10 MPa for 30 s. After releasing the pressure, the sample was kept in the mold and annealed at the same temperature for different durations.

3.2.3. Characterization

To confirm the conversion of the precursor into Al_2O_3, attenuated total reflection infrared spectra (ATR-IR) (FT-IR, 100, Perkin Elmer) were acquired with a resolution of 4 cm^{-1} and 24 scans. The Al_2O_3 loading was determined based on the thermogravimetric analysis (TGA, Thermo plus evo, Rigaku). A specified amount of a sample was loaded into an alumina pan, followed by heating up to 600 ^oC under dry air flow. The residual inorganic content at 600 ^oC was regarded as the Al_2O_3 content.

The dispersion, distribution and migration of Al_2O_3 nanoparticles during the annealing process were studied by transmission electron microscopy (TEM, Hitachi H-7100, 100 kV). TEM specimens with the thickness of 100 nm were prepared by an ultramicrotome (Reichent Ultracut FCS, Reica) equipped with a diamond knife (Diatome). The phase morphology was observed using a scanning electron microscope (SEM, Hitachi S-4100) at 20 kV. A sample was cryo-fractured in liquid N_2, then etched by heptane at 80 ^oC for 24 h to remove POE. The sample was sputtered with Pt/Pd prior to the measurements. The phase domain size was obtained by measuring the widths of rod-like holes and the diameters of circular holes in cross-sectioned SEM images as is often done in the field [31,41–44]. With the aid of Image J software, more than 100 data points were obtained to calculate the average phase domain size for each sample. Elemental mapping was also performed

using an energy dispersive X-ray analyzer (EDX, Hitachi TM 3030Plus).

The thermal diffusivity (α) of nanocomposites was determined by a temperature wave analyzer (ai-Phase mobile 1u/2, Hitachi High-Tech Science). A film sample was placed between the heater and the sensor plates. The phase delay of the temperature wave was acquired at eight frequency points within the range of 0.2–2 Hz. The thermal conductivity (λ) was determined by

$$\lambda = \alpha C_p \rho \quad (3\text{-}1).$$

The specific heat capacity (C_p) was derived from differential scanning calorimetry (DSC, Mettler Toledo DSC-822) in the temperature range of 0–50 °C. The density (ρ) was measured using an electronic density meter (SANSYO DME-220).

3.3. Results and discussion

3.3.1. Distribution of Al_2O_3 nanoparticles

When nanoparticles are introduced into immiscible polymer blends, they are usually distributed in one phase or at the interface rather than homogeneously distributed in the whole polymer blends. In an equilibrium state, the distribution of fillers is dictated by the minimum interfacial energy [45,46]. The wetting coefficient (ω_a) proposed by Sumita et al. [47] is often used to predict the preferential distribution of fillers in immiscible polymer blends,

$$\omega_a = \frac{\gamma_{CA} - \gamma_{CB}}{\gamma_{AB}} \quad (3\text{-}2),$$

where γ_{CA}, γ_{CB} and γ_{AB} are the interfacial energies among polymer A, polymer B, and filler C. The values of ω_a above 1, below –1, and in between mean that the fillers would preferentially be distributed in polymer B, in polymer A and at the interface, respectively. The interfacial energies γ_{ij} can be calculated based on the harmonic mean equation [48],

$$\gamma_{12}=\gamma_1+\gamma_2-4\left(\frac{\gamma_1^d\gamma_2^d}{\gamma_1^d+\gamma_2^d}+\frac{\gamma_1^p\gamma_2^p}{\gamma_1^p+\gamma_2^p}\right) \quad (3\text{-}3),$$

where γ_i, the surface free energy of component i, is divided into the dispersion and polar parts, γ_i^d and γ_i^p. These constants are listed for PP, POE, and Al_2O_3 in Table 3.1 [49,50]. Based on these values and Eq. (3-2), the wetting coefficient was derived as –0.85, i.e. Al_2O_3 nanoparticles were supposed to migrate to the interface, starting from the PP phase.

Table 3.1. Surface free energies of the filler and polymers.

Materials	Total surface energy γ (mJ/m^2)	Dispersion part γ^d (mJ/m^2)	Polar part γ^p (mJ/m^2)
PP[a]	21.71	21.23	0.48
POE[a]	17.51	15.61	1.90
Al_2O_3[b]	114.00	43.70	70.30

[a] According to Ma et al. [49].

[b] According to Holysz et al. [50].

In order to confirm the distribution of Al_2O_3 nanoparticles, the morphology of PP/POE/Al_2O_3 nanocomposites was studied by TEM, SEM, and EDX (Fig. 3.2). When the RGT was employed, Al_2O_3 nanoparticles were selectively distributed and uniformly dispersed in the PP phase of a co-continuous structure (Fig. 3.2a). The formation of Al_2O_3 was also confirmed by TGA and ATR-IR (Table 3.2 and Fig. 3.3). The uniform dispersion of Al_2O_3 nanoparticles (Fig. 3.4a,b) in the PP matrix was attributed to the confinement of the precursor in the pores of reactor granule and its spontaneous conversion to the oxide. After annealing at 190 ^oC for 60 min, most of Al_2O_3 nanoparticles were migrated to the interface (Fig. 3.2b). These results suggested that Al_2O_3 nanoparticles were kinetically retained in the PP phase before annealing, and the annealing facilitated their migration to the interface in accordance with the estimation from the wetting coefficient. When the preformed nanoparticles were used, huge agglomerates were formed and the migration to the interface became much less efficient (Fig. 3.2c,d). Considering that the size of the nanoparticles was not largely different between the two protocols, the particle clusters and agglomerates (Fig. 3.4c,d) significantly hindered the migration.

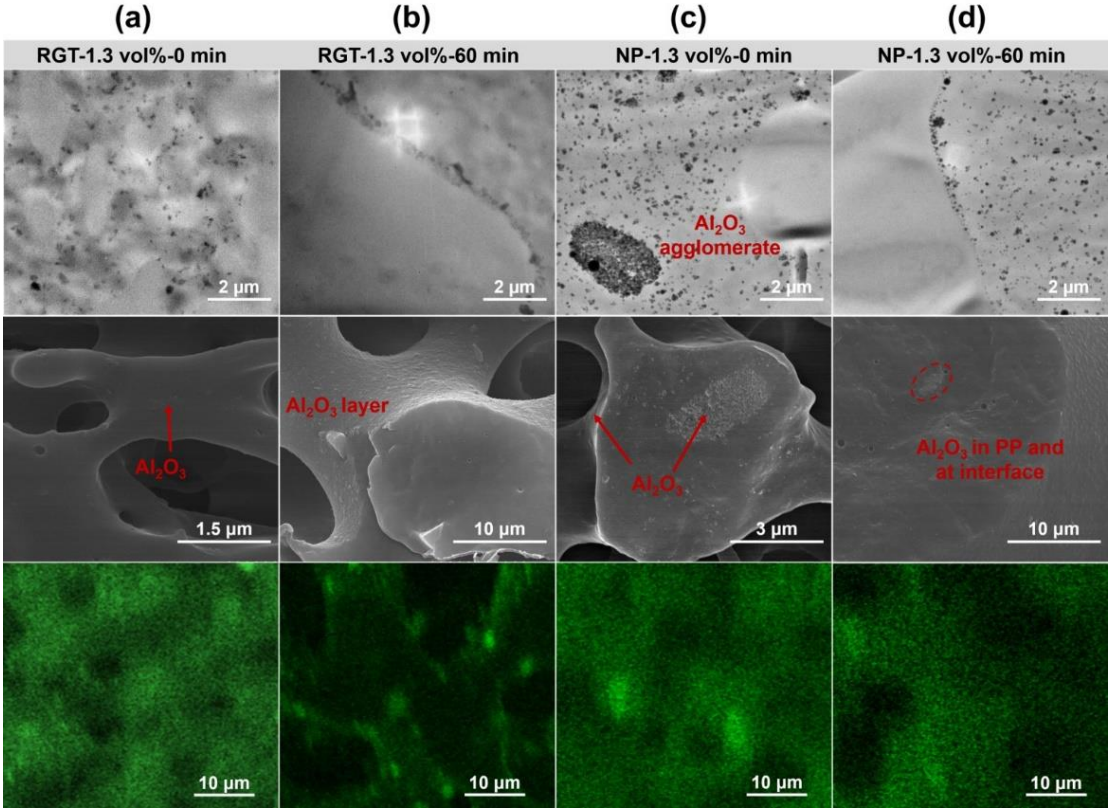

Fig. 3.2. TEM (top), SEM (middle), and EDX mapping for Al (bottom) of PP/POE/Al_2O_3 nanocomposites: RGT-1.3 vol% a) before and b) after annealing at 190 ºC for 60 min, and NP-1.3 vol% c) before and d) after annealing at 190 ºC for 60 min.

Table 3.2. TGA results for PP/Al_2O_3-RGT nanocomposites prepared by RGT.

Sample	Theoretical loading[a] (wt %)	Actual loading[b] (wt %)
PP/Al_2O_3-RGT-1.2 vol%	5	4.7
PP/Al_2O_3-RGT-2.5 vol%	10	9.5
PP/Al_2O_3-RGT-5.5 vol%	20	20.1
PP/Al_2O_3-RGT-9.1 vol%	30	29.6

[a] Theoretical loading was estimated on the assumption of the full conversion to Al_2O_3.

[b] Measured by TGA.

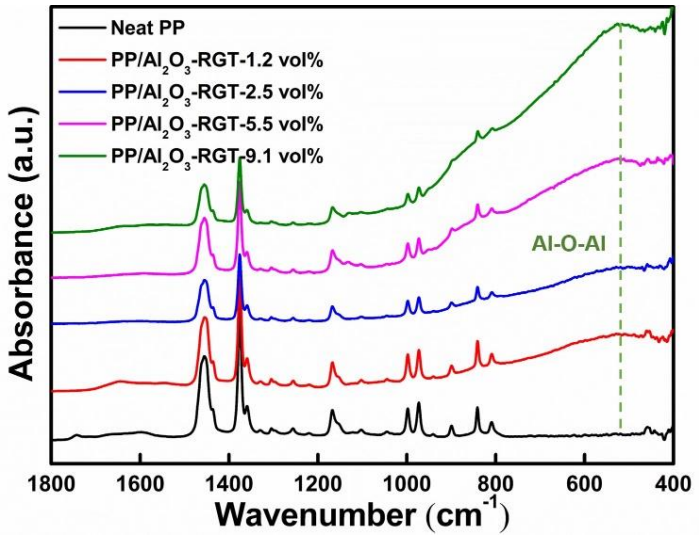

Fig. 3.3. ATR-IR spectra of PP/Al_2O_3-RGT nanocomposites with different Al_2O_3 loadings.

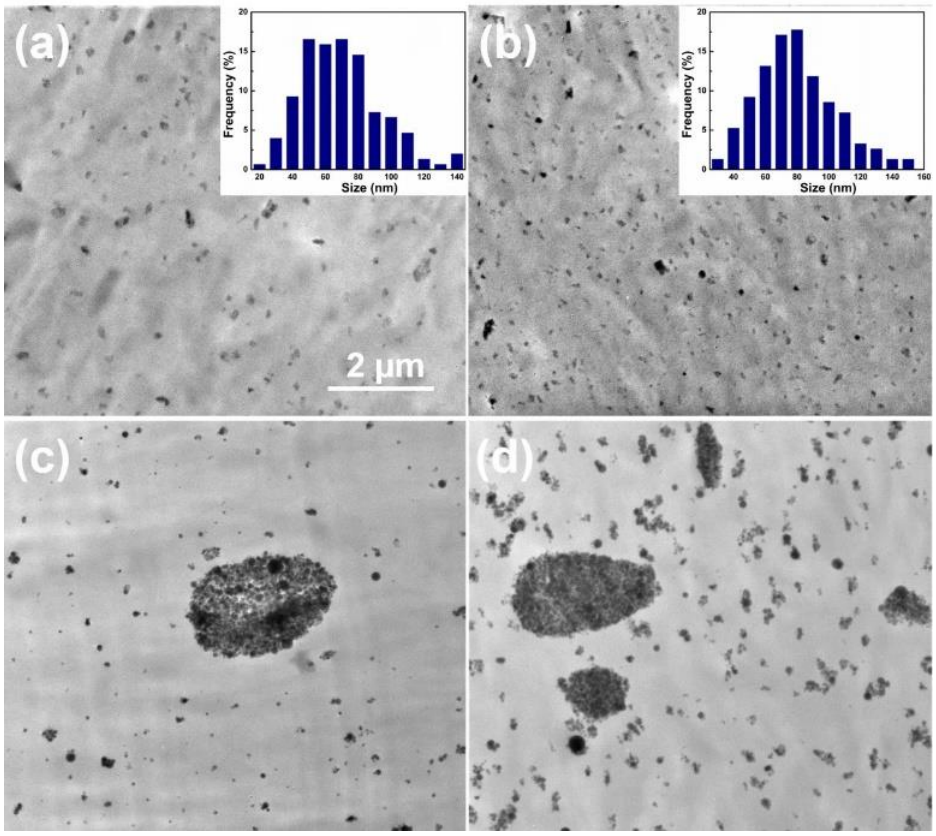

Fig. 3.4. TEM micrographs of PP/Al_2O_3 masterbatch nanocomposites with different Al_2O_3 loadings: a) RGT-2.5 vol%, b) RGT-5.5 vol%, c) NP-2.5 vol%, and d,) NP-5.5 vol%. Note that the scale bar is applied to all the images. The insets show the particles size distribution of Al_2O_3.

3.3.2. Migration of Al_2O_3 nanoparticles and phase morphology evolution

The distribution of Al_2O_3 nanoparticles changed after annealing and the selective localization at the interface was achieved by RGT. In order for deeper understanding, the migration of nanoparticles during the annealing process was tracked. Fig. 3.5

summarizes TEM images of PP/POE/Al_2O_3 nanocomposites that were annealed for different durations. When the RGT was employed, the selective localization of Al_2O_3 nanoparticles was eventually achieved irrespective of the loading. However, the time required for the localization at the interface was found to be shorter at a higher loading. At 0.6 vol%, a part of nanoparticles already reached the interface at 5 min, and successive localization eventually formed an Al_2O_3 layer at 30 min. At 2.8 vol%, many Al_2O_3 nanoparticles were found at the interface even before annealing and a continuous Al_2O_3 layer was formed at 10 min. For the preformed nanoparticles, the migration to the interface happened, but its efficacy was quite poor. At 0.6 vol%, a few nanoparticles arrived at the interface after annealing for 10 min. With the increase of the annealing duration, more nanoparticles arrived at the interface but a continuous Al_2O_3 layer was not eventually formed. Even at an elevated filler loading (2.8 vol%), many of Al_2O_3 nanoparticles stayed in the PP phase after annealing for 60 min. It seems that nanoparticles hardly migrated once they were agglomerated or clustered, and their existence also hindered the migration of other particles, leading to the low efficacy. The same nanoparticle migration process was also observed by SEM images (Fig. 3.6).

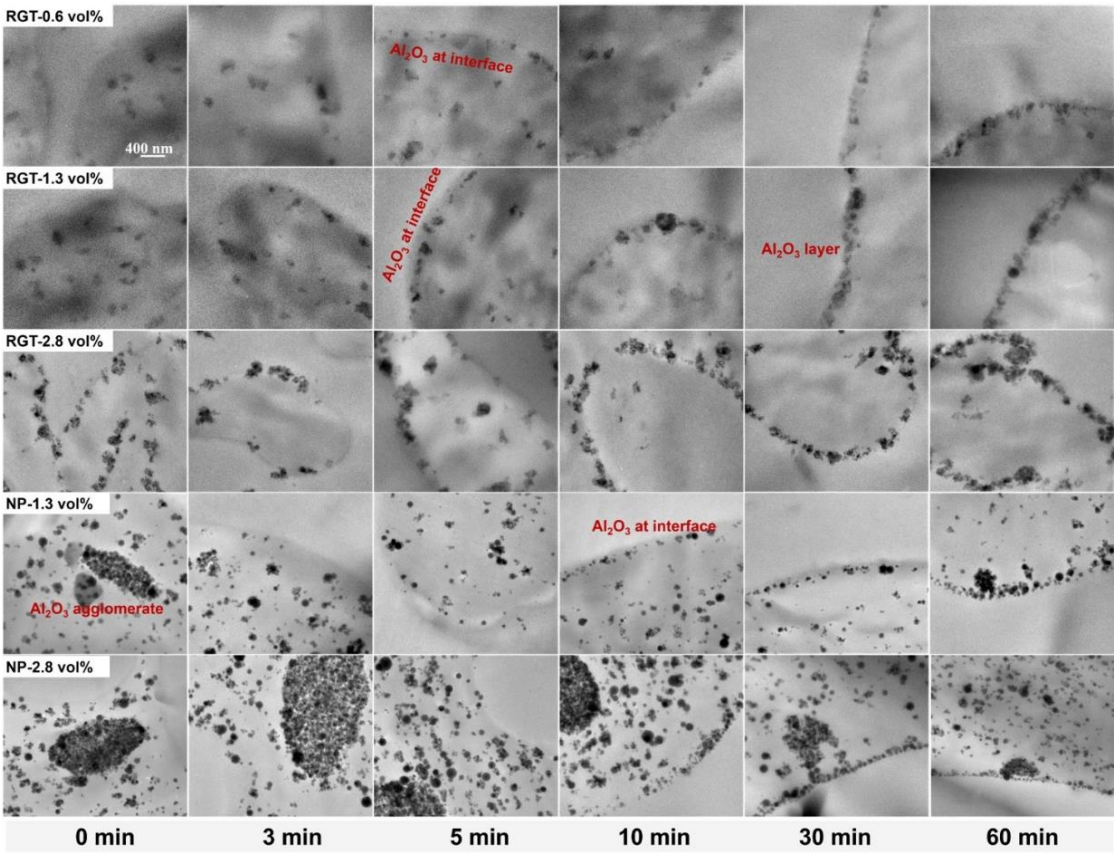

Fig. 3.5. TEM micrographs of PP/POE/Al_2O_3 nanocomposites with different Al_2O_3 loadings. The filler migration was tracked along the annealing at 190 ºC. Note that the scale bar is applied to the whole micrographs.

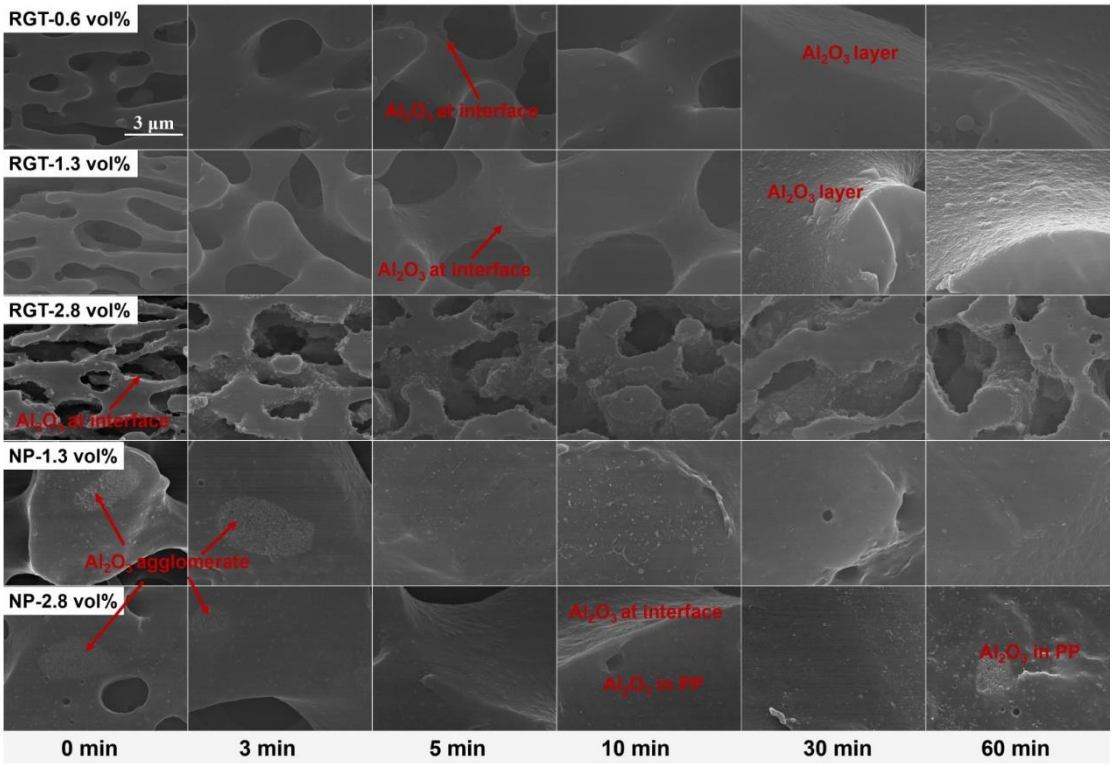

Fig. 3.6. Magnified SEM images of PP/POE/Al_2O_3 nanocomposites tracked along the annealing at 190 °C.

Prerequisites for achieving the selective localization are i) thermodynamic preference of the localization for given combination, ii) uniform dispersion without particle agglomeration that enables the migration of individual nanoparticles, and iii) diffusion of nanoparticles faster than phase coarsening. The first two prerequisites are satisfied in PP/POE/Al_2O_3-RGT nanocomposites, while the last prerequisite depends on the balance between the size of nanoparticles and the viscosity of the matrix. In general, the Brownian motion of a spherical nanoparticle with a radius r in a fluid with the viscosity η at temperature T is described by the

Stokes-Einstein equation [51],

$$D_0 = \frac{k_B T}{6\pi\eta r} \quad (3\text{-}4),$$

where D_0 and k_B correspond to the diffusion coefficient and the Boltzmann constant, respectively. On the one hand, the addition of nanoparticles increases the viscosity of a molten polymer [52], which can be expressed by Mooney's equation [53,54],

$$\eta_c = \eta_r exp\left(\frac{2.5f}{1-af}\right) \quad (3\text{-}5),$$

where η_c is the viscosity of the filled polymer, η_r is the viscosity of the unfilled polymer, f is the volume fraction of fillers, and a is called self-crowding factor that is related to the critical filler fraction for a steep increment in the viscosity. The size of Al_2O_3 nanoparticles was found to be insensitive to the loading (see Fig. 3.4). According to Eq. (3-4) and Eq. (3-5), the increase of the viscosity at a higher loading would slow down the diffusion of nanoparticles. However, the observation in Fig. 3.5 dictated the opposite trend. This contradiction can be understood only when the presence of nanoparticles strongly affects the phase morphology and its evolution.

Accordingly, the evolution of the phase morphology was studied based on SEM micrographs of etched samples (Fig. 3.7). The corresponding phase domain sizes are given in Fig. 3.8. For pure PP/POE blends, the phase domain size increased from 4.1 μm to 36.5 μm after annealing at 190 °C for 20 min. The addition of nanoparticles caused the reduction of the phase domain size before annealing, and suppressed the phase coarsening during the annealing. The extents of the reduction

and suppression were highly dependent on the employed protocol. When preformed nanoparticles were melt-mixed at 0.6 vol%, the initial phase size became 3.5 μm and it was enlarged to 32.6 μm after 30 min. The large phase domain size made it difficult for nanoparticles to reach the interface. This is another reason why the migration of nanoparticles was less effective in PP/POE/Al_2O_3-NP. The utilization of the RGT at the same loading made much greater impacts: 1.1 μm at 0 min and 9.8 μm at 30 min. The phase coarsening rate (k) in an immiscible polymer blend with the interfacial tension σ and viscosity η_c can be expressed by Eq. (5) [44,55],

$$k=c\frac{\sigma}{\eta_c} \quad (3\text{-}6),$$

where c is a dimensionless constant. According to Eq. (3-5) and Eq. (3-6), the deceleration of the phase coarsening was a result of the viscosity increment by the addition of nanoparticles, where the RGT gave larger impacts due to the uniform dispersion. When the loading was increased for the preformed nanoparticles, the phase coarsening became gradually slower, eventually 6.4 μm after 30 min at the loading of 4.7 vol%. In the RGT case, abrupt reduction in the initial phase domain size and significant suppression of the phase coarsening were observed over 2.8 vol% (0.8 to 2.3 μm for 60 min at 2.8 vol% and 0.7 to 1.7 μm for 60 min at 4.7 vol%). Considering that the nanoparticle concentration was proportional to the loading, such abrupt change was plausibly ascribed by the following reasons: The viscosity of the PP phase was increased in a non-linear fashion due to the formation of

physical network structures [40], which in turn decreased the initial phase domain size and slowed down the phase coarsening. Due to a smaller phase domain size and a higher nanoparticle concentration, many Al_2O_3 nanoparticles successfully reached the interface in a very early timing as we have observed in Fig. 3.5, and the formation of a rigid Al_2O_3 layer at the interface plausibly prevented the phase coarsening as like a barrier layer. It is important to say that the localization of nanoparticles and phase morphology evolution strongly affect with each other. Thus, the utilization of RGT at a sufficiently high loading afforded nanocomposites bearing selectively localized and uniformly distributed thermal conductive networks.

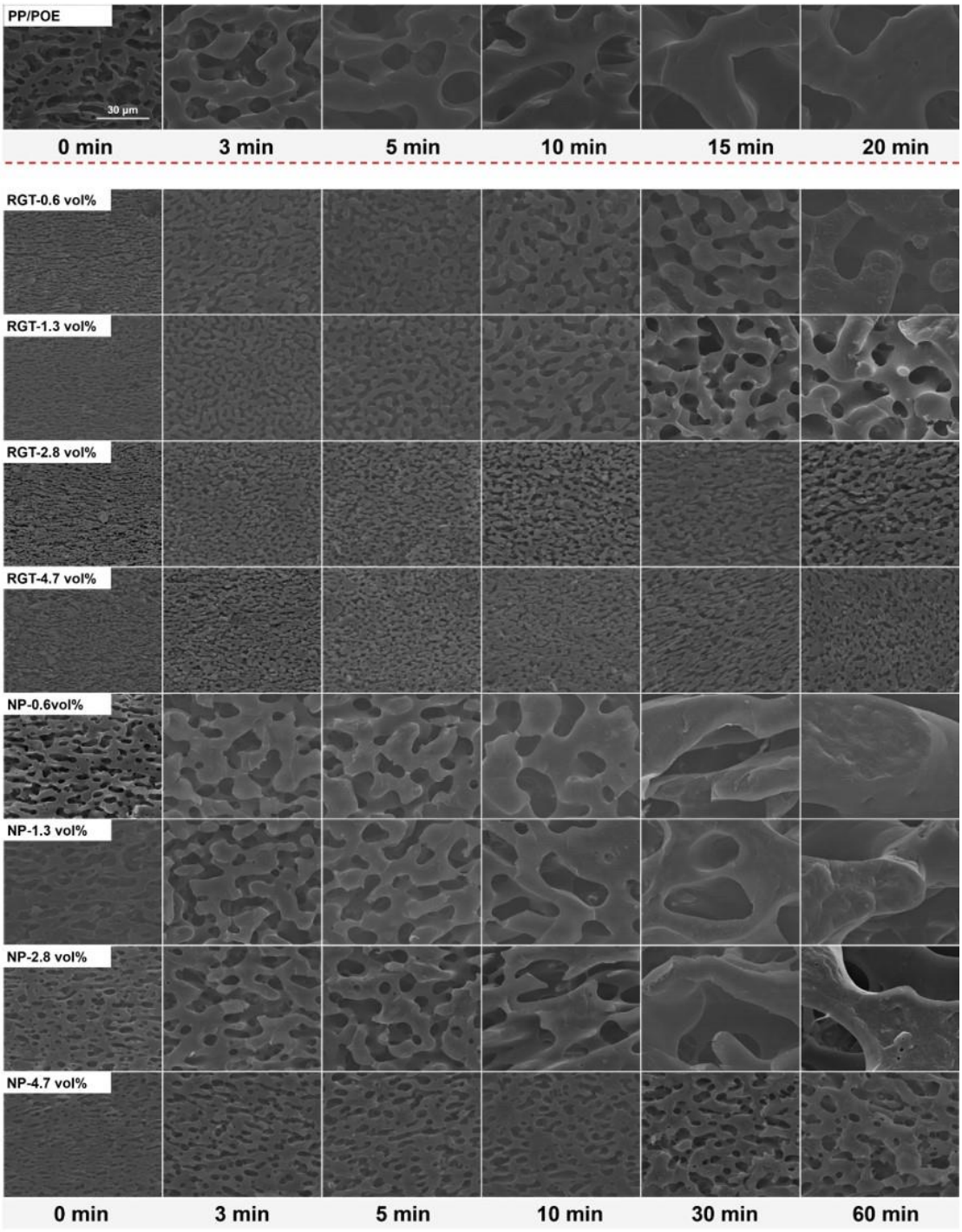

Fig. 3.7. Evolution of the phase morphology of PP/POE/Al_2O_3 nanocomposites tracked along the annealing at 190 ºC. Note that the scale bar is applied to all micrographs.

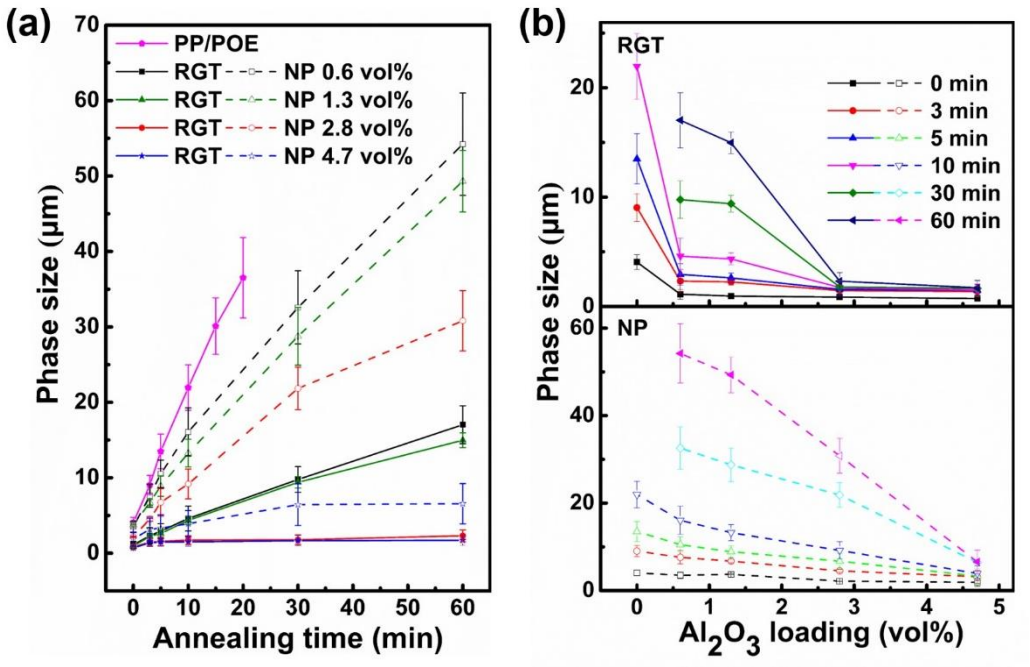

Fig. 3.8. Phase domain size of PP/POE/Al_2O_3 nanocomposites as a function of a) annealing time and b) Al_2O_3 loading.

3.3.3 Thermal conductivity

Cooperative influences of nanoparticle localization and phase morphology evolution on the thermal conductivity of the nanocomposites were studied. Fig. 3.9 summarizes the thermal conductivity of PP/POE/Al_2O_3 nanocomposites prepared by different protocols as a function of annealing time. At a fixed Al_2O_3 loading, PP/POE/Al_2O_3-RGT nanocomposites showed obviously better thermal conductivity than PP/POE/Al_2O_3-NP nanocomposites. Besides, the dependence of the thermal conductivity on the annealing time was largely different between the two series and

among different loadings. In the case of PP/POE/Al_2O_3-RGT at 0.6 and 1.3 vol%, the thermal conductivity increased along annealing time in the first 30 min and decreased slightly with the further increase of the annealing time. When the loading was increased over 2.8 vol%, the thermal conductivity increased with the increase of annealing time and it never decreased by elongated annealing. In the case of PP/POE/Al_2O_3-NP nanocomposites, the thermal conductivity once reached the maximum at 10-30 min and then slowly decreased by the further annealing.

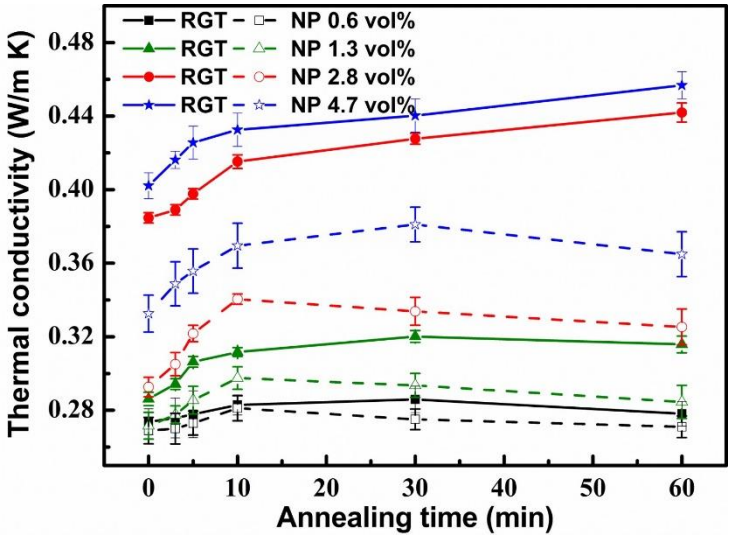

Fig. 3.9. Thermal conductivity of PP/POE/Al_2O_3 nanocomposites annealed at 190 ^oC for different durations.

As stated earlier, the annealing can cause both positive and negative influences on the thermal conductivity. When preformed nanoparticles were employed or when the loading was not sufficiently high for RGT, the phase coarsening cannot be

sufficiently retarded (Fig. 3.8). In the early stage of the annealing, the migration of Al_2O_3 nanoparticles to the interface led to enhancement of the thermal conductivity due to the formation of thermal conductive pathways. The extent of the increment was greater for RGT as most of the nanoparticles were successfully migrated due to the initially uniform dispersion. When the annealing was extended, the negative effect of the phase coarsening was not anymore compensated by further localization. On the other hand, when RGT was employed at a high loading, the phase coarsening was almost completely suppressed. As a result, the thermal conductivity of the nanocomposites monotonously increased by the annealing. Rapid evolution below 10 min corresponded to the time required to form connected networks at the interface, while the slower evolution over 10 min corresponded to the network thickening.

Based on the results and analysis above, the relationship among the evolutions of nanoparticle localization, phase morphology, and thermal conductive networks is illustrated in Fig. 3.10. The uniform dispersion of Al_2O_3 nanoparticles modifies viscoelastic properties of the PP phase and brings about smaller phase domains (Fig. 3.10a). The distance of migration from the initial position to the interface is hence greatly shortened and migration completes in a shorter duration (Fig. 3.10a′). Thus, localized nanoparticles at the interface form thermal conductive networks. These networks also act as a barrier to suppress the phase coarsening. The particle

agglomerates and clusters disturb all the above mechanisms: Smaller viscoelastic modulation, less efficient migration, and less suppressed phase coarsening. The combination of these factors makes the thermal conductivity of resultant nanocomposites much poorer (Fig. 3.10b,b′).

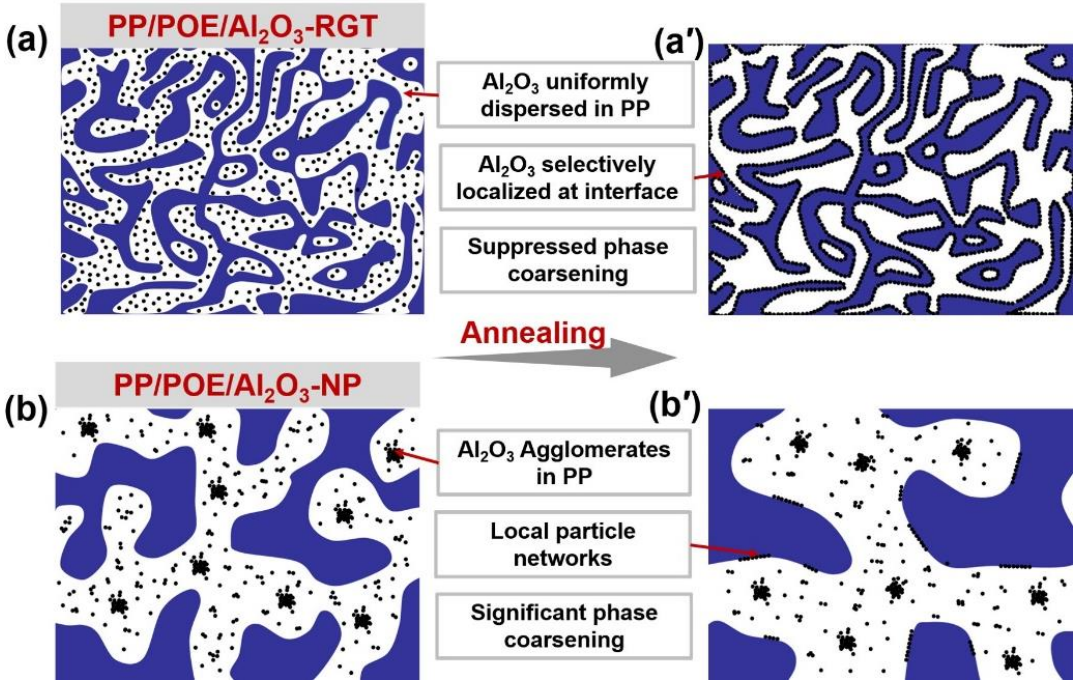

Fig. 3.10. Schematic representation of the network and phase morphology evolution in PP/POE/Al_2O_3 nanocomposites.

3.4. Conclusions

The controlled migration of nanoparticles within a co-continuous structure of

immiscible polymer blends is a key issue to design thermal conductive composite materials. In this chapter, the relationship among nanoparticle migration, phase morphology evolution, and the thermal conductivity were reported based on a PP/POE/Al_2O_3 ternary system. Al_2O_3 nanoparticles spontaneously migrated from the PP phase to the interface, where the uniform dispersion of Al_2O_3 nanoparticles in the PP phase was essential. Important cooperation between nanoparticle localization and phase morphology evolution was evidenced. Nanoparticles that were uniformly dispersed in the PP phase decreased the phase domain size to facilitate successful migration to the interface. Further, the formation of nanoparticle networks decelerated the phase coarsening during annealing. By employing the RGT at a sufficiently high Al_2O_3 loading, uniformly distributed thermal conductive networks were afforded. These findings are believed important not only in designing conductive composite materials but also in engineering the phase morphology of immiscible polymer blends for other applications.

References

[1] Zhang X, Maira B, Hashimoto Y, Wada T, Chammingkwan P, Thakur A, et al. Selective localization of aluminum oxide at interface and its effect on thermal conductivity in polypropylene/polyolefin elastomer blends. Compos. Part B-Eng. 2019; 162: 662–670.

[2] Zhang X, Zheng X, Ren D, Liu Z, Yang W, Yang M. Unusual positive temperature coefficient effect of polyolefin/carbon fiber conductive composites. Mater. Lett. 2016; 164: 587–90.

[3] Zhang X, Zheng S, Zheng X, Liu Z, Yang W, Yang M. Distinct positive temperature coefficient effect of polymer–carbon fiber composites evaluated in terms of polymer absorption on fiber surface. Phys. Chem. Chem. Phys. 2016; 18(11): 8081–7.

[4] Gu J, Lv Z, Wu Y, Guo Y, Tian L, Qiu H, et al. Dielectric thermally conductive boron nitride/polyimide composites with outstanding thermal stabilities via in-situ polymerization-electrospinning-hot press method. Compos. Part A-Appl. S. 2017; 94: 209–16.

[5] Yang X, Tang L, Guo Y, Liang C, Zhang Q, Kou K, et al. Improvement of thermal conductivities for PPS dielectric nanocomposites via incorporating NH_2-POSS functionalized nBN fillers. Compos。 Part A-Appl S. 2017; 101: 237–42.

[6] Li Y, Xu G, Guo Y, Ma T, Zhong X, Zhang Q, et al. Fabrication, proposed model and simulation predictions on thermally conductive hybrid cyanate ester composites with boron nitride fillers. Compos. Part A-Appl. S. 2018; 107: 570–8.

[7] Yang X, Guo Y, Han Y, Li Y, Ma T, Chen M, et al. Significant improvement

of thermal conductivities for BNNS/PVA composite films via electrospinning followed by hot-pressing technology. Compos. Part B-Eng. 2019; 175: 107070.

[8] Dang TML, Kim CY, Zhang Y, Yang JF, Masaki T, Yoon DH. Enhanced thermal conductivity of polymer composites via hybrid fillers of anisotropic aluminum nitride whiskers and isotropic spheres. Compos. Part B-Eng. 2017; 114: 237–46.

[9] Gu J, Meng X, Tang Y, Li Y, Zhuang Q, Kong J. Hexagonal boron nitride/polymethyl-vinyl siloxane rubber dielectric thermally conductive composites with ideal thermal stabilities. Compos. Part A-Appl. S. 2017; 92: 27–32.

[10] Guo Y, Lyu Z, Yang X, Lu Y, Ruan K, Wu Y, et al. Enhanced thermal conductivities and decreased thermal resistances of functionalized boron nitride/polyimide composites. Compos. Part-B Eng. 2019; 164: 732–9.

[11] Li Y, Huang X, Hu Z, Jiang P, Li S, Tanaka T. Large dielectric constant and high thermal conductivity in poly (vinylidene fluoride)/barium titanate/silicon carbide three-phase nanocomposites. ACS Appl. Mater. Inter. 2011; 3(11): 4396–403.

[12] Hu Y, Du G, Chen N. A novel approach for Al_2O_3/epoxy composites with high strength and thermal conductivity. Compos. Sci. Technol. 2016; 124:

36–43.

[13] Kim GH, Lee D, Shanker A, Shao L, Kwon MS, Gidley D, et al. High thermal conductivity in amorphous polymer blends by engineered interchain interactions. Nat. Mater. 2015; 14(3): 295.

[14] Guo L, Xiao C, Wang H, Chen L, Zhang X, Zheng K, et al. Thermally conductive polystyrene/epoxy nanocomposites fabricated by selective localization of hybrid fillers. Colloid Polym. Sci. 2016; 294(5): 901–10.

[15] Huang J, Zhu Y, Xu L, Chen J, Jiang W, Nie X. Massive enhancement in the thermal conductivity of polymer composites by trapping graphene at the interface of a polymer blend. Compos. Sci. Technol. 2016; 129: 160–5.

[16] Zhang X, Zheng S, Zou H, Zheng X, Liu Z, Yang W, et al. Two-step positive temperature coefficient effect with favorable reproducibility achieved by specific “island-bridge” electrical conductive networks in HDPE/PVDF/CNF composite. Comps. Part A-Appl. S. 2017; 94: 21–31.

[17] Huang J, Mao C, Zhu Y, Jiang W, Yang X. Control of carbon nanotubes at the interface of a co-continuous immiscible polymer blend to fabricate conductive composites with ultralow percolation thresholds. Carbon 2014; 73: 267–74.

[18] Nair ST, Vijayan PP, Xavier P, Bose S, George SC, Thomas S. Selective localisation of multi walled carbon nanotubes in polypropylene/natural

rubber blends to reduce the percolation threshold. Compos. Sci. Technol. 2015; 116: 9–17.

[19] Yorifuji D, Ando S. Enhanced thermal conductivity over percolation threshold in polyimide blend films containing ZnO nano-pyramidal particles: advantage of vertical double percolation structure. J. Mater. Chem. 2011; 21(12): 4402–7.

[20] Cao JP, Zhao X, Zhao J, Zha JW, Hu GH, Dang ZM. Improved thermal conductivity and flame retardancy in polystyrene/poly (vinylidene fluoride) blends by controlling selective localization and surface modification of SiC nanoparticles. ACS. Appl. Mater. Inter. 2013; 5(15): 6915–24.

[21] Fenouillot F, Cassagnau P, Majeste JC. Uneven distribution of nanoparticles in immiscible fluids: Morphology development in polymer blends. Polymer 2009; 50(6): 1333–50.

[22] Wu G, Cai X, Lin X, Yui H. Heterogeneous distribution of magnetic nanoparticles in reactive polymer blends. React. Funct. Polym. 2010; 70(10): 732–7.

[23] Chen J, Cui X, Zhu Y, Jiang W, Sui K. Design of superior conductive polymer composite with precisely controlling carbon nanotubes at the interface of a co-continuous polymer blend via a balance of π-π interactions and dipole-dipole interactions. Carbon 2017; 114: 441–8.

[24] Huang J, Li N, Xiao L, Liu H, Wang Y, Chen J, et al. Fabrication of Highly Tough, Strong, and Stiff Carbon Nanotube/Epoxy Conductive Composite with an Ultralow Percolation Threshold via Self-Assembly. J. Mater. Chem. A 2019; 7: 15731–40.

[25] Gong T, Liu MQ, Liu H, Peng SP, Li T, Bao RY, et al. Selective distribution and migration of carbon nanotubes enhanced electrical and mechanical performances in polyolefin elastomers. Polymer 2017; 110: 1–11.

[26] Bai L, Sharma R, Cheng X, Macosko CW. Kinetic control of graphene localization in co-continuous polymer blends via melt compounding. Langmuir 2017; 34(3): 1073–83.

[27] Huang J, Zhu Y, Jiang W, Yin J, Tang Q, Yang X. Parallel carbon nanotube stripes in polymer thin film with remarkable conductive anisotropy. ACS Appl. Mater. Inter. 2014; 6(3): 1754–8.

[28] Huang J, Zhu Y, Jiang W, Tang Q. Parallel carbon nanotube stripes in polymer thin film with tunable microstructures and anisotropic conductive properties. Comps. Part A-Appl. S. 2015; 69: 240–6.

[29] Huang J, Xu J, Sheng Y, Zhu Y, Jiang W, Xu D, et al. fabrication of polymer film with extraordinary conductive anisotropy by forming parallel conductive vorticity-aligned stripes and its formation mechanism. Macromol. Mater. Eng. 2016; 301(6): 743–9.

[30] Fenouillot F, Méchin F, Boisson F, Alcouffe P, Pokropski T, Kallel T, et al. Coarsening of nanodomains by reorganization of polysiloxane segments at high temperature in polyurethane/α, ω-aminopropyl polydimethylsiloxane blends. Eur. Polym. J. 2012; 48(2): 284–95.

[31] Sun XR, Gong T, Pu JH, Bao RY, Xie BH, Yang MB, et al. Effect of phase coarsening under melt annealing on the electrical performance of polymer composites with a double percolation structure. Phys. Chem. Chem. Phys. 2018; 20(1): 137–47.

[32] Zhang H, Chen J, Cui X, Hu Y, Lei L, Zhu Y, et al. Thermal annealing induced enhancement of electrical properties of a co-continuous polymer blend filled with carbon nanotubes. Compos. Sci. Technol. 2018; 167: 522–8.

[33] Pan Y, Liu X, Hao X, Starý Z, Schubert DW. Enhancing the electrical conductivity of carbon black-filled immiscible polymer blends by tuning the morphology. Eur. Polym. J. 2016; 78: 106–15.

[34] Zhao X, Wang H, Fu Z, Li Y. Enhanced interfacial adhesion by reactive carbon nanotubes: new route to high-performance immiscible polymer blend nanocomposites with simultaneously enhanced toughness, tensile strength, and electrical conductivity. ACS Appl. Mater. Inter. 2018; 10(10): 8411–6.

[35] Wang H, Fu Z, Zhao X, Li Y, Li J. Reactive nanoparticles compatibilized

immiscible polymer blends: synthesis of reactive SiO_2 with long poly (methyl methacrylate) chains and the in situ formation of janus SiO_2 nanoparticles anchored exclusively at the interface. ACS Appl. Mater. Inter. 2017; 9(16): 14358–70.

[36] Maira B, Chammingkwan P, Terano M, Taniike T. New reactor granule technology for highly filled nanocomposites: effective flame retardation of polypropylene/magnesium hydroxide nanocomposites. Macromol. Mater. Eng. 2015; 300(7): 679–83.

[37] Maira B, Chammingkwan P, Terano M, Taniike T. Reactor granule technology for fabrication of functionally advantageous polypropylene nanocomposites with oxide nanoparticles. Compos. Sci. Technol. 2017; 144: 151–9.

[38] Qiagedeer A, Maira B, Strauss R, Zhao Y, Chammingkwan P, Mizutani G, et al. Preparation and characterization of polypropylene/noble metal nanocomposites based on reactor granule technology. Polymer 2017; 127: 251–8.

[39] Maira B, Takeuchi K, Chammingkwan P, Terano M, Taniike T. Thermal conductivity of polypropylene/aluminum oxide nanocomposites prepared based on reactor granule technology. Compos. Sci. Technol. 2018; 165: 259–65.

[40] Kaneko K, Yadav N, Takeuchi K, Maira B, Terano M, Taniike T. Versatile strategy for fabrication of polypropylene nanocomposites with inorganic network structures based on catalyzed in-situ sol–gel reaction during melt mixing. Compos. Sci. Technol. 2014; 102: 120–5.

[41] Gong T, Bao RY, Liu ZY, Xie BH, Yang MB, Yang W. The effect of chain mobility on the coarsening process of co-continuous, immiscible polymer blends under quiescent melt annealing. Phys. Chem. Chem. Phys. 2017; 19(20): 12712–9.

[42] Veenstra H, Van Dam J, de Boer AP. Formation and stability of co-continuous blends with a poly (ether-ester) block copolymer around its order–disorder temperature. Polymer 1999; 40(5): 1119–30.

[43] Veenstra H, van Lent BJ, van Dam J, de Boer AP. Co-continuous morphologies in polymer blends with SEBS block copolymers. Polymer 1999; 40(24): 6661–72.

[44] Veenstra H, Van Dam J, de Boer AP. On the coarsening of co-continuous morphologies in polymer blends: effect of interfacial tension, viscosity and physical cross-links. Polymer 2000; 41(8): 3037–45.

[45] Goldel A, Marmur A, Kasaliwal GR, Potschke P, Heinrich G. Shape-dependent localization of carbon nanotubes and carbon black in an immiscible polymer blend during melt mixing. Macromolecules 2011;

44(15): 6094–102.

[46] Goldel A, Kasaliwal G, Potschke P. Selective Localization and Migration of Multiwalled Carbon Nanotubes in Blends of Polycarbonate and Poly (styrene-acrylonitrile). Macromol. Rapid. Commun. 2009; 30(6): 423–9.

[47] Sumita M, Sakata K, Asai S, Miyasaka K, Nakagawa H. Dispersion of fillers and the electrical conductivity of polymer blends filled with carbon black. Polym. Bull. 1991; 25(2): 265–71.

[48] Baudouin AC, Bailly C, Devaux J. Interface localization of carbon nanotubes in blends of two copolymers. Polym. Degrad. Stab. 2010; 95(3): 389–98.

[49] Ma CG, Mai YL, Rong MZ, Ruan WH, Zhang MQ. Phase structure and mechanical properties of ternary polypropylene/elastomer/nano-CaCO3 composites. Compos. Sci. Technol. 2007; 67(14): 2997–3005.

[50] Holysz L, Chibowski E. Surface free energy components of. alpha.-alumina from thin-layer wicking. Langmuir 1992; 8(2): 717–21.

[51] Plattier J, Benyahia L, Dorget M, Niepceron F, Tassin JF. Viscosity-induced filler localisation in immiscible polymer blends. Polymer 2015; 59: 260–9.

[52] Liu XQ, Li R-H, Bao RY, Jiang WR, Yang W, Xie BH, et al. Suppression of phase coarsening in immiscible, co-continuous polymer blends under high temperature quiescent annealing. Soft Matter 2014; 10(20): 3587–96.

[53] Mooney M. The viscosity of a concentrated suspension of spherical particles.

J. Colloid Sci. 1951; 6(2): 162–70.

[54] Schulze KA, Zaman AA, Söderholm KJM. Effect of filler fraction on strength, viscosity and porosity of experimental compomer materials. J. Den. 2003; 31(6): 373–82.

[55] Yoshida K, Hyuga H, Kondo N, Kita H. Synthesis of precursor for fibrous mullite powder by alkoxide hydrolysis method. Mater. Sci. Eng. B, 2010; 173(1–3): 66–71.

Chapter 4

Design of Continuous Segregated Polypropylene/Al_2O_3 Nanocomposites and Impact of Controlled Al_2O_3 Distribution on Thermal Conductivity

Chapter 4

Abstract

Control of nanoparticle distribution in polymer matrices is a key factor for designing highly conductive nanocomposites. Here, polypropylene (PP)/aluminum oxide (Al_2O_3) nanocomposites with a continuous segregated structure were designed. Al_2O_3 nanoparticles were initially distributed in the polyolefin elastomer (POE) phase of PP/POE/Al_2O_3 with a co-continuous structure. Selective extraction of the POE phase provided a porous PP scaffold, whose pore walls were covered by deposited Al_2O_3 nanoparticles. Subsequent compression molding made the porous scaffold tightly compacted to form uniform and dense thermal conductive networks. The thermal conductivity was compared among nanocomposites having three different types of Al_2O_3 distribution. It was found that the continuous segregated distribution was far the most effective for improving the thermal conductivity, where 1.07 W/m K was achieved at an Al_2O_3 loading of 27.5 vol%.

Keywords: Thermal conductivity; Continuous segregated network; Nanocomposite; Aluminum oxide; Polypropylene

4.1. Introduction

In the past decade, thermal conductive polymer composites have attracted great attention due to the continuous integration and miniaturization of microelectronic devices [1–3]. The thermal conductivity of neat polymer is often insufficient, and

thermally conductive and insulating fillers such as boron nitride (BN) [4], aluminum nitride [5], silicon carbide [6], and aluminum oxide (Al_2O_3) [7] are usually introduced to improve the thermal conductivity and simultaneously meet the stringent requirements for electrical insulation. However, conventional methods such as melt mixing, solution mixing, or powder mixing [8] usually lead to random distribution of fillers in the polymer matrix. Therefore, desired thermal conductivity can be obtained only at an unacceptably high filler loading, which causes problems in density, mechanical properties, processability, and fabrication cost [9,10].

It is recognized that the thermal conductivity is determined not only by the choice of fillers, but also interfacial interaction in relation to phonon scattering [11]. The inclusion of fillers of a finite size necessarily generates interfaces. This discontinuity or interfacial mismatch causes phonon scattering [12], i.e. even with the same type and amount of filler, the resultant thermal conductivity of composites largely depends on the design of interfaces. For example, when filler particles are randomly distributed in a polymer matrix, the interfacial connection between the polymer and filler is important. Surface modification of fillers is often adopted to improve the interfacial connection between the polymer and fillers. Shen et al. reported that modification of BN by polydopamine greatly improved the thermal conductivity of polyvinyl alcohol (PVA) to 5.4 W/m K at 10 vol%, which was 63% higher than that of PVA/unmodified BN [13]. Here, it must be noted that surface modification does

not necessarily improve the thermal conductivity. Gulotty et al. studied the effect of the surface modification of single-wall carbon nanotubes on the thermal conductivity of polymer nanocomposites [14]. It was found that the intrinsic thermal conductivity of fillers decreases with the modification, and this negative effect sometimes overcomes the positive effect of improved interfacial connection [15].

A more appropriate way to obtain high thermal conductivity is to form a continuous network through selective distribution of fillers [16–18]. Unlike the propagation of electrons in electric conductive composites, where they can “hop” between fillers through tunneling [19,20], a direct contact between fillers is required for thermal conduction. Many strategies have been proposed to construct continuous thermal conductive networks. In one strategy, a co-continuous morphology of immiscible polymer blends is exploited to control the selective localization of fillers. A volume exclusion effect increases the local concentration of fillers and improves the connectivity of the networks [20–22]. In particular, the selective localization at the interface of a co-continuous structure is one of the most effective ways to form thermal conductive networks at a lower filler loading [23]. However, this strategy relies on a subtle balance of surface energies among polymers and fillers [9]. Moreover, the distribution of fillers is also affected by kinetic factors such as the viscosity, the mixing procedure, and the filler size. In the previous two chapters, I applied a novel reactor granule technology [7,24,25] for the fabrication of thermally

conductive polypropylene (PP)-based nanocomposites. I found that successful migration of nanoparticles to the interface is achieved only when nanoparticles are initially uniformly dispersed, and their migration is faster than the phase coarsening [26,27]. In recent literature, an alternative strategy of forming continuous networks based on a segregated structure is presented for electrically conductive polymer composites [28,29]. Typically, micron-sized polymer particles are physically mixed with fillers in a solid state, then the mixture is hot pressed. This restricts the placement of fillers at the interfaces of particles, thereby forming continuous and dense networks to greatly lower the percolation threshold. A potential concern of this strategy is imperfection of networks, e.g. physical blending may lead to non-uniform coating of polymer particles by fillers, random packing of particles may remain voids even after the hot-pressing, and so on [30–32].

This chapter attempts to enhance the thermal conductivity by constructing a continuous segregated structure in PP/Al_2O_3 nanocomposites. Al_2O_3 nanoparticles were adopted due to their abundance and electrically insulating nature. Moreover, this spherical thermal conductive filler is sensitive to the uniformity and the density of the networks so that it can reflect the efficiency of the proposed strategy. Firstly, Al_2O_3 nanoparticles were selectively distributed in the POE phase of PP/POE blends with a co-continuous structure. After the selective extraction of the POE phase, a porous PP scaffold with continuous channels was formed, where Al_2O_3

nanoparticles were uniformly deposited on the pore walls. The obtained porous scaffold was compression-molded to form a continuous segregated structure. In this unique structure, continuous and dense thermal conductive networks were formed and uniformly distributed in the PP matrix, thus achieving high thermal conductivity at a low loading of Al_2O_3 nanoparticles.

4.2. Experimental section

4.2.1. Materials

Isotactic polypropylene as a matrix (M_w = 2.6×10^5 g/mol, *mmmm* = 98 mol%) was synthesized by propylene polymerization using a $Mg(OEt)_2$-based Ziegler-Natta catalyst. Polyolefin elastomer with a 1-octene content of 38 % and a moony viscosity of 23 MU (ML 1+4 at 121 ºC acquired based on ASTM D1646) was selected. Al_2O_3 nanoparticles with the average diameter of 15 nm were purchased from Nippon Aerosil Co. Ltd.

4.2.2. Sample preparation

The fabrication procedure of a continuous segregated structure is summarized in Fig. 4.1. First, Al_2O_3 nanoparticles were melt-mixed with POE at 190 ºC and 100 rpm for 10 min (Micro compounder IM5, Xplore). Then, PP was added and mixed for another 10 min under the same condition. The mixture was rapidly quenched in

cold water kept at 0 ºC to freeze the phase morphology. The product was compression-molded at 190 °C and 10 MPa for 5 min to obtain films with a co-continuous structure, where Al_2O_3 nanoparticles were aimed to selectively distribute in the POE phase (Fig. 4.1a). The obtained samples are denoted as PP/POE/Al_2O_3. The volume fraction of Al_2O_3 nanoparticles in the nanocomposites was varied from 1.2 to 18.6 vol%, while the weight ratio of PP and POE was kept at 50/50 to maintain the co-continuous phase morphology. The above-prepared PP/POE/Al_2O_3 nanocomposite films were immersed in heptane at 80 ºC for 24 h to extract the POE phase. The POE phase was selectively replaced by heptane to form a PP/solvent/Al_2O_3 ternary system (Fig. 4.1b). Solvent replacement in polymer blends with a co-continuous structure has been reported in a PP/polystyrene/carbon black system [32,33]. By the solvent evaporation, Al_2O_3 nanoparticles were driven to the original PP/POE interface and led to the conformal Al_2O_3 coating (Fig. 4.1c). Thus obtained porous films were vacuum dried at 60 ºC for 24 h, and subjected to the second compression molding at 160 ºC and 10 MPa for 5 min to compact the pores and Al_2O_3 layers tightly. PP was not completely melted at 160 ºC so that the migration of Al_2O_3 nanoparticles into the matrix was restricted [32,34]. Through such a method, PP/Al_2O_3 nanocomposites with a continuous segregated structure (denoted as s-PP/Al_2O_3) were prepared (Fig. 4.1d).

As a reference, PP/Al_2O_3 nanocomposites with random distribution (termed r-

PP/Al_2O_3) were also prepared by melt-mixing PP and Al_2O_3 nanoparticles at 190 ºC and 100 rpm for 10 min. The product was compression-molded into films at 190 °C and 10 MPa for 5 min.

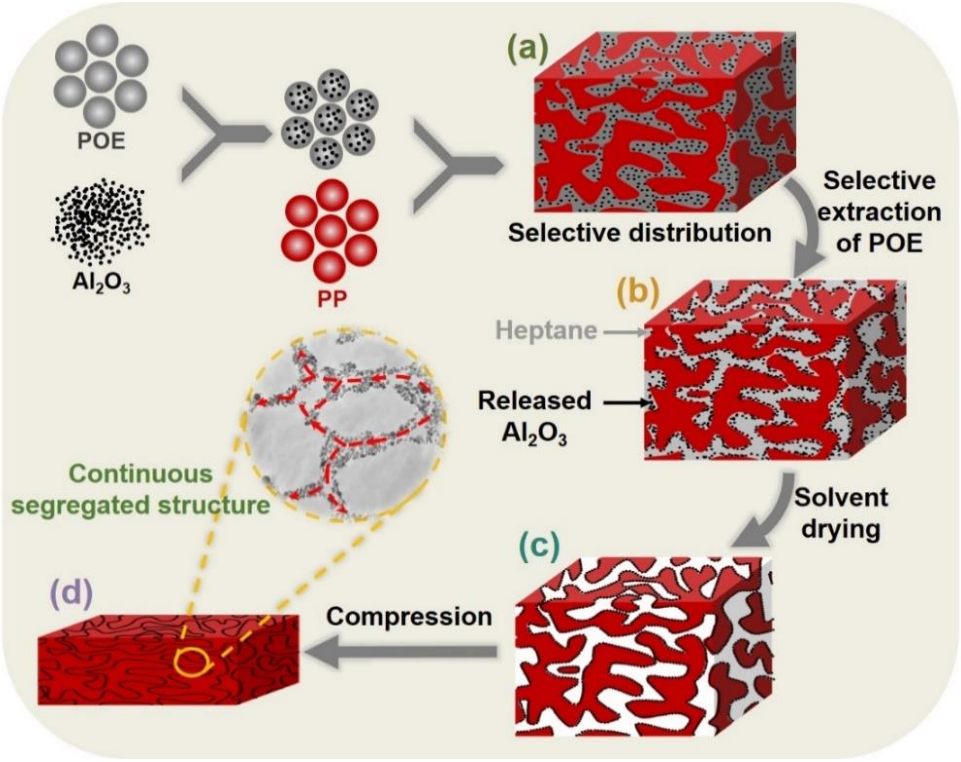

Fig. 4.1. Procedure for the construction of a continuous segregated structure. a) PP/POE/Al_2O_3 nanocomposites with a co-continuous structure, b) PP/heptane/Al_2O_3 ternary system with released Al_2O_3 nanoparticles after the selective extraction of the POE phase; c) continuous porous PP/Al_2O_3 nanocomposites with Al_2O_3 nanoparticles assembled on the pore walls; d) PP/Al_2O_3 nanocomposites with a continuous segregated structure.

4.2.3. Characterization

The morphology of the nanocomposites was observed by a scanning electron microscope (SEM, Hitachi S-4100) with an acceleration voltage of 20 kV. Samples were cryo-fractured in liquid N_2 and the fractured surface was sputter-coated with platinum and palladium prior to the measurement. Elemental mapping was also performed using an energy dispersive X-ray analyzer (EDX, Hitachi 3030Plus). To observe the distribution of Al_2O_3 nanoparticles, a transmission electron microscope (TEM, Hitachi H-7100) was used at an acceleration voltage of 100 kV. TEM specimens with the thickness of 100 nm were prepared by an ultramicrotome (Reichent Ultracut FCS, Reica) equipped with a diamond knife (Diatome).

A weight loss measurement was performed to evaluate the continuity of the POE phase. PP/POE/Al_2O_3 nanocomposite films were immersed in heptane at 80 ºC for 24 h to extract the POE phase. After the extraction, the films were washed and dried at 60 ºC for 24 h. The continuity of the POE phase was evaluated by comparing the weight loss by the extraction with the initial weight of POE using Eq. (4-1).

$$\%continuity = \frac{(weight\ of\ POE)_{initial} - (weight\ of\ POE)_{final}}{(weight\ of\ POE)_{initial}} \quad (4\text{-}1).$$

The Al_2O_3 loading in the porous PP/Al_2O_3 nanocomposites was measured by thermal gravimetric analysis (TGA, Thermo plus evo, Rigaku) to study the remaining amount of Al_2O_3 nanoparticles after the extraction of the POE phase. A sample was heated from 25 to 600 ºC under dry air at a heating rate of 10 ºC/min.

The residual inorganic content at 600 ºC was regarded as the Al_2O_3 content.

The thermal diffusivity (α) of nanocomposites was measured by a temperature wave analyzer (ai-Phase mobile 1u/2, Hitachi High-Tech Science). A sample was sandwiched between the heater and the sensor plates. The phase delay in the temperature wave was measured at eight frequency values within a range of 0.2–2 Hz. The thermal conductivity (λ) was derived from

$$\lambda = \alpha C_p \rho \quad (4\text{-}2).$$

The specific heat capacity (C_p) at room temperature was determined using a differential scanning calorimeter (DSC, Mettler Toledo DSC-822). The density was measured by an electronic density meter (SANSYO DME-220).

Mechanical properties of nanocomposites were measured by a universal testing machine (Instron 3365) with a crosshead speed of 5 mm/min at room temperature. Dumbbell-shaped specimens were cut out from film samples.

4.3. Results and discussion

4.3.1. Construction of continuous segregated structure

When nanoparticles are introduced into immiscible polymer blends, they tend to selectively distribute in one phase or at the interface toward a thermodynamic equilibrium. A prerequisite for the construction of a continuous segregated structure is that Al_2O_3 nanoparticles are initially confined in the POE phase or at the interface,

while the selective distribution at the interface was estimated from the wetting coefficients [35]. Accordingly, Al_2O_3 nanoparticles were firstly melt-mixed with POE prior to the addition of PP in order to prohibit kinetic entrapment in the PP phase. The morphology of the PP/POE/Al_2O_3 nanocomposites was observed by TEM and SEM (Fig. 4.2). As shown in Fig. 4.2a,b, two phases existed in a mutually interpenetrated manner, corresponding to a typical co-continuous structure. The preservation of the co-continuous structure with the addition of Al_2O_3 nanoparticles was verified by evaluating the continuity of the POE phase according to Eq. (4-1) (Fig. 4.3). For all the PP/POE/Al_2O_3 nanocomposites, the continuity of the POE phase was maintained at over 95%, indicating that the morphology of all the samples was regarded co-continuous. Al_2O_3 nanoparticles were distributed in one phase and at the interface, while the other phase contained virtually no nanoparticles. For further confirmation, the POE phase was selectively extracted and the cross-sectional morphology of the etched sample was observed by SEM. As shown in Fig. 4.2c,d, the cross-sectioned surfaces of PP were smooth while Al_2O_3 nanoparticles were exclusively distributed on the surface of the pores remained after etching the POE phase. This fact indicates that Al_2O_3 nanoparticles were barely distributed in the PP phase.

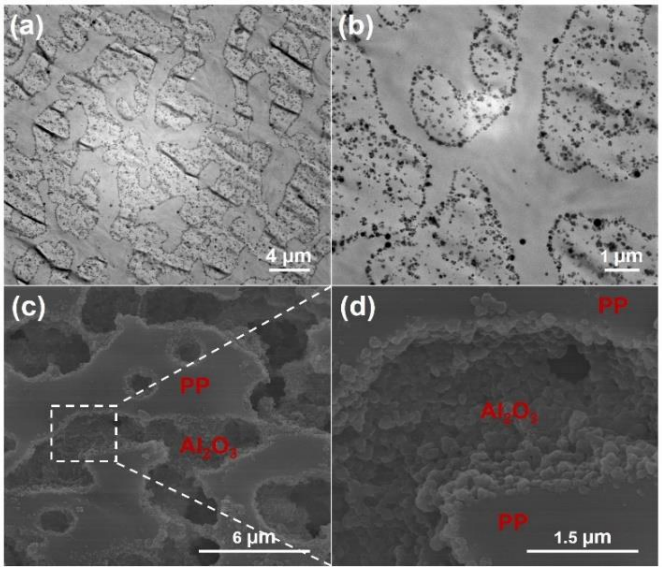

Fig. 4.2. a,b) TEM micrographs of a PP/POE/Al_2O_3 nanocomposite with the Al_2O_3 loading of 5.4 vol% before etching. c,d) SEM micrographs of the same sample after etching the POE phase. The measurements were performed at different magnifications.

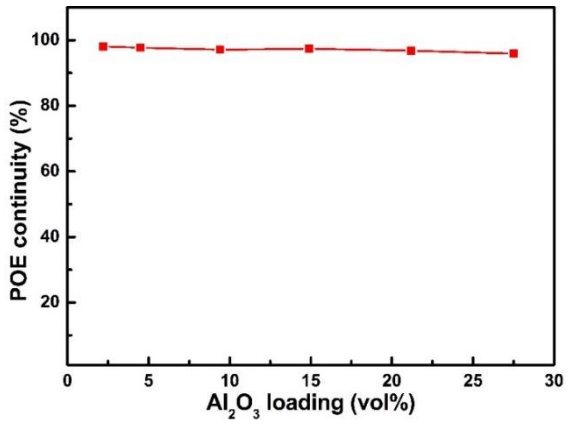

Fig. 4.3. Continuity of the POE phase as a function of Al_2O_3 loading.

The successful coating of pore walls by Al_2O_3 nanoparticles in the continuous

porous structure is a next key step to construct the continuous segregated structure. Fig. 4.4 shows the SEM micrographs of PP/POE/Al_2O_3 nanocomposites after etching the POE phase. All the samples presented a porous structure and many continuous channels interpenetrated with the remaining PP phase. After the extraction of the POE phase and solvent evaporation, the pore surfaces were coated with Al_2O_3 nanoparticles. When the Al_2O_3 loading was low, a part of pore surfaces looked smooth, suggesting incomplete coating (Fig. 4.4a). Along with the increase in the loading, the smooth surfaces disappeared and the coating layer became denser and thicker (Fig. 4.4b–d).

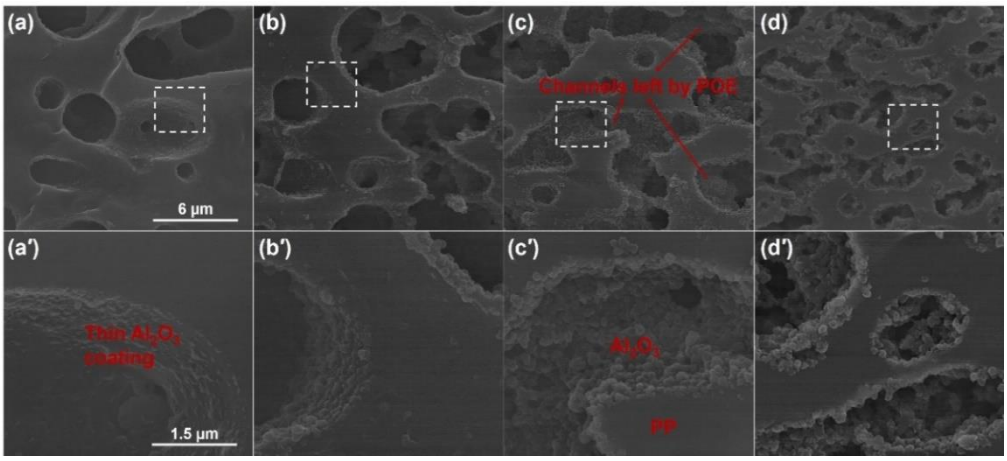

Fig. 4.4. SEM micrographs of PP/POE/Al_2O_3 nanocomposites after the extraction of the POE phase with different Al_2O_3 loadings: a, a′) 1.2 vol%, b,b′) 2.5 vol%, c,c′) 5.4 vol%, and d,d′) 8.9 vol%. The loading refers to the volume fraction of Al_2O_3 nanoparticles in PP/POE/Al_2O_3 nanocomposites before etching the POE phase. Note that the scale bar is applied to individual entire rows.

It was considered that a part of Al_2O_3 nanoparticles could be extracted with heptane. In order to confirm the retention of Al_2O_3 nanoparticles, the Al_2O_3 loading in the remained porous PP scaffold was examined with TGA. The results are shown in Fig. 4.5. The residual weight at 600 ºC was regarded as the weight of retained Al_2O_3 nanoparticles, and it was compared with the theoretical Al_2O_3 content that was derived under the assumption that nanoparticles were fully retained. The results are summarized in Table 4.1. The residual contents of Al_2O_3 nanoparticles were 8.8, 16.8, 30.8, 42.8, 53.5, and 61.9 wt% for nanocomposites with the theoretical contents of 9.5, 18.2, 33.3, 45.8, 57.1 and 66.2 wt%, respectively. The retention percentage was higher than 92% for all the samples, suggesting that the solvent extraction and subsequent evaporation were effective for the deposition of Al_2O_3 nanoparticles. It is noted that the thermal decomposition of porous PP/Al_2O_3 was slower than that of neat PP at lower loadings while faster at higher loadings. This trend is likely attributed to competition between the thermal insulation by pores and acid-catalyzed decomposition of PP.

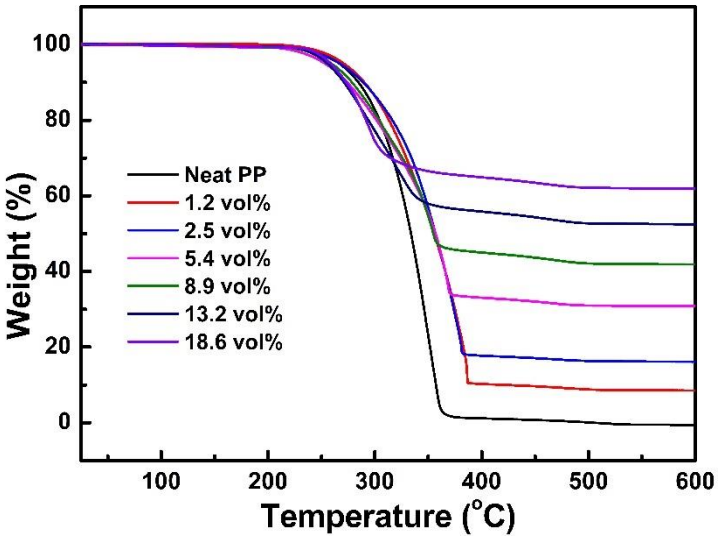

Fig. 4.5. TGA curves for porous PP/Al_2O_3 nanocomposites after etching the POE phase. The loading in the figure refers to the volume fraction of Al_2O_3 nanoparticles in the corresponding PP/POE/Al_2O_3 nanocomposites before etching.

Table 4.1. Retention of Al_2O_3 nanoparticles in the pores.

Sample[a]	Theoretical Al_2O_3 content (wt%)[b]	Residual weight at 600 °C (wt%)	Retention percentage (%)[c]
0 vol%	0	0	n.a.
1.2 vol%	9.5	8.8	92.6
2.5 vol%	18.2	16.8	92.3
5.4 vol%	33.3	30.8	92.5
8.9 vol%	45.8	42.9	93.7
13.2 vol%	57.1	53.5	93.7
18.6 vol%	66.2	61.9	93.5

[a] The sample names correspond to PP/POE/Al_2O_3 nanocomposites with specified Al_2O_3 loadings. Note that the TGA measurements were performed after etching the

POE phase.

[b] The theoretical Al_2O_3 content was calculated under the assumption that Al_2O_3 nanoparticles were perfectly retained in the porous PP scaffold after etching the POE phase.

[c] The retention percentage refers to the ratio of the residual weight at 600 °C with respect to the theoretical Al_2O_3 content.

The tight compaction of porous PP/Al_2O_3 nanocomposites is essential to enhance the interconnection of Al_2O_3 nanoparticles and avoid defects that can cause phonon scattering. Before the compression, the appearance of the porous films was white due to the presence of pores. After the second compression, the pores were tightly compacted and the transparency of the film obviously increased (Fig. 4.6a). The situation was similar for different loadings, while the transparency of the compressed films slightly decreased along with the loading due to the thickening of the Al_2O_3 networks (Fig. 4.7). From SEM micrographs, the obtained s-PP/Al_2O_3 nanocomposites were tightly compressed and voids were hardly observed (Fig. 4.6b-e). The formation of Al_2O_3 networks became more and more evident along with the loading. EDX mapping was also conducted to confirm the formation of Al_2O_3 networks (Fig. 4.8). The Al_2O_3 networks were excluded from the PP phase to form continuous segregated networks.

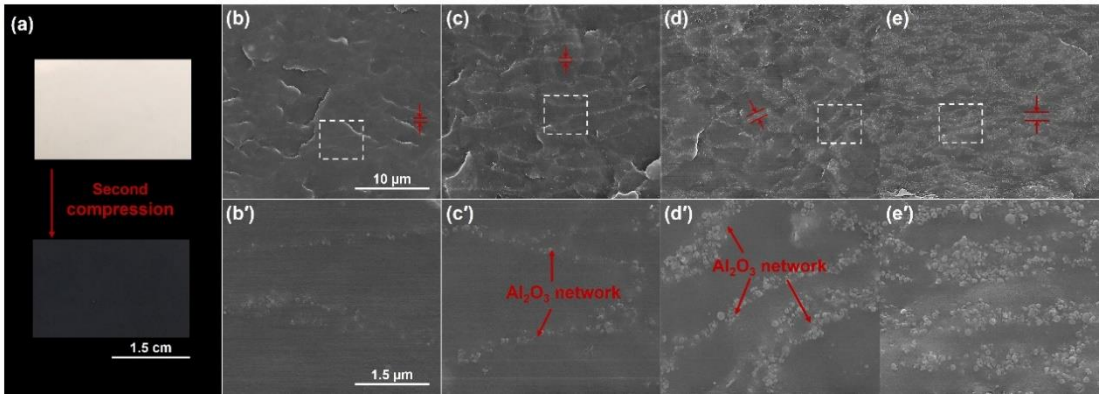

Fig. 4.6. a) Optical images of porous PP/Al_2O_3 nanocomposites and s-PP/Al_2O_3 nanocomposites obtained after the second compression (for 4.5 vol%). b,c,d,e) SEM micrographs of s-PP/Al_2O_3 nanocomposites with different Al_2O_3 loadings: b, b′) 2.2 vol%, c,c′) 4.5 vol%, d,d′) 9.4 vol%, and e,e′) 14.9 vol%. The loading was obtained from the TGA results in Table 4.1. Note that the scale bar is applied to individual entire rows.

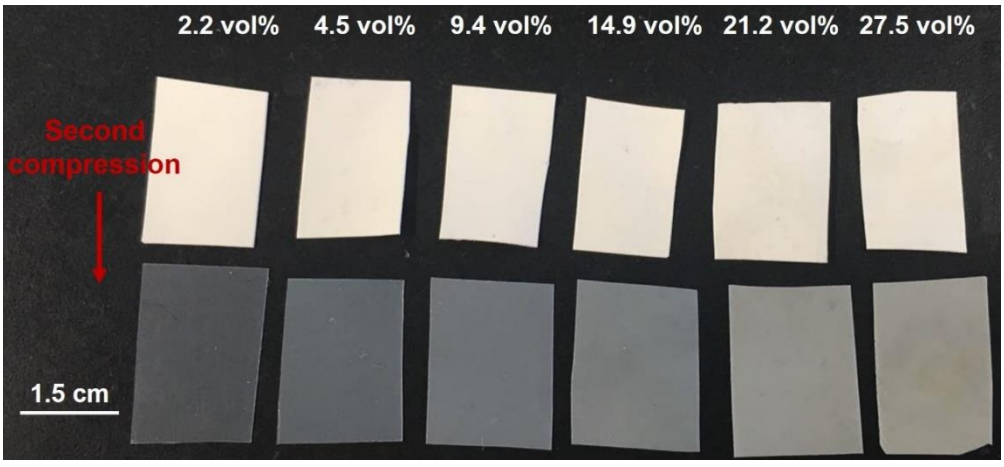

Fig. 4.7. Optical images of porous PP/Al_2O_3 nanocomposites and s-PP/Al_2O_3 nanocomposites obtained after the second compression. Note that the scale bar is applied to all images.

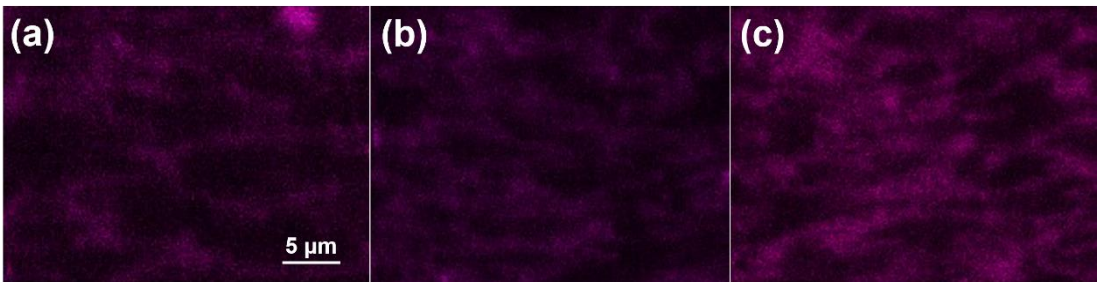

Fig. 4.8. EDX elemental mapping for Al in s-PP/Al_2O_3 nanocomposites with different loadings: a) 2.2 vol%, b) 4.5 vol%, c) 9.4 vol%. Note that the scale bar is applied to all the samples.

The continuous segregated structure was further studied by TEM micrographs (Fig. 4.9). The results were basically consistent with those of SEM and EDX, while a few additional observations were obtained. The second compression molding shortened the spacing between Al_2O_3 nanoparticles. Some of nanoparticles overlapped with each other and this tendency became more evident at a higher loading. On the other hand, the un-overlapped areas were necessarily filled by PP. It was considered that a fraction of PP melted at the temperature of the second compression molding, and it filled interparticle gaps of Al_2O_3 nanoparticles that were not eliminated only by the compression. Indeed, when the compression was made at a lower temperature, a transparent film was hardly obtained. The selection of an appropriate temperature is important not only to fill the interparticle gaps but also to maintain the integrity of the formed networks.

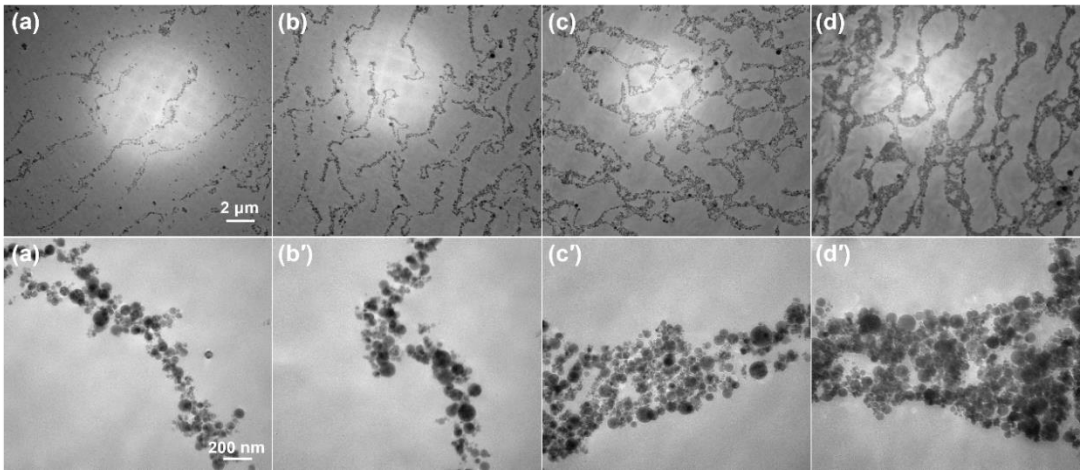

Fig. 4.9. TEM micrographs of s-PP/Al_2O_3 nanocomposites with different loading: a) 2.2 vol%, b) 4.5 vol%, c) 9.4 vol%, and d) 14.9 vol%. a′)–d′) are magnified SEM micrographs. Note that the scale bar is applied to individual entire rows.

4.3.2. Thermal conductivity

Fig. 4.10a depicts the measured thermal conductivity for three types of nanocomposites having different Al_2O_3 distributions: s-PP/Al_2O_3, where Al_2O_3 nanoparticles formed continuous segregated networks (Fig. 4.10b); PP/POE/Al_2O_3, where Al_2O_3 nanoparticles were selectively distributed in the POE phase (Fig. 4.10c); r-PP/Al_2O_3, where Al_2O_3 nanoparticles were randomly distributed (Fig. 4.10d). It must be noted that the random distribution indicates a non-selective distribution, not the random placement of individual nanoparticles. As shown in Fig. 4.10a, the thermal conductivity value and its development along the Al_2O_3 loading significantly depended on the distribution type. The random distribution (r-

PP/Al_2O_3) led to the lowest thermal conductivity at a given loading. In this case, Al_2O_3 nanoparticles were mutually most separated and the phonon transport happened from one particle to the closest particle by crossing the organic pathway with poor thermal conductivity. The presence of many huge agglomerates was also regarded negative in terms of uniform thermal conduction. The selective distribution of Al_2O_3 nanoparticles in the POE phase (and at the interface) greatly improved the thermal conductivity of the nanocomposites (PP/POE/Al_2O_3). This is a natural consequence of the concentration of Al_2O_3 nanoparticles in one phase of a co-continuous structure, which shortens the interparticle distance and raises a possibility to form overlapping nanoparticles. The best thermal conductivity was attained for the continuous segregated distribution (s-PP/Al_2O_3), where the connection between Al_2O_3 nanoparticles was significantly improved as shown in Fig. 4.6. The thermal conductivity reached 1.07 W/m K at a filler loading of 27.5 vol%, while 0.5–0.8 W/m K at 36 vol% was reported for epoxy/Al_2O_3 nanocomposites [36].

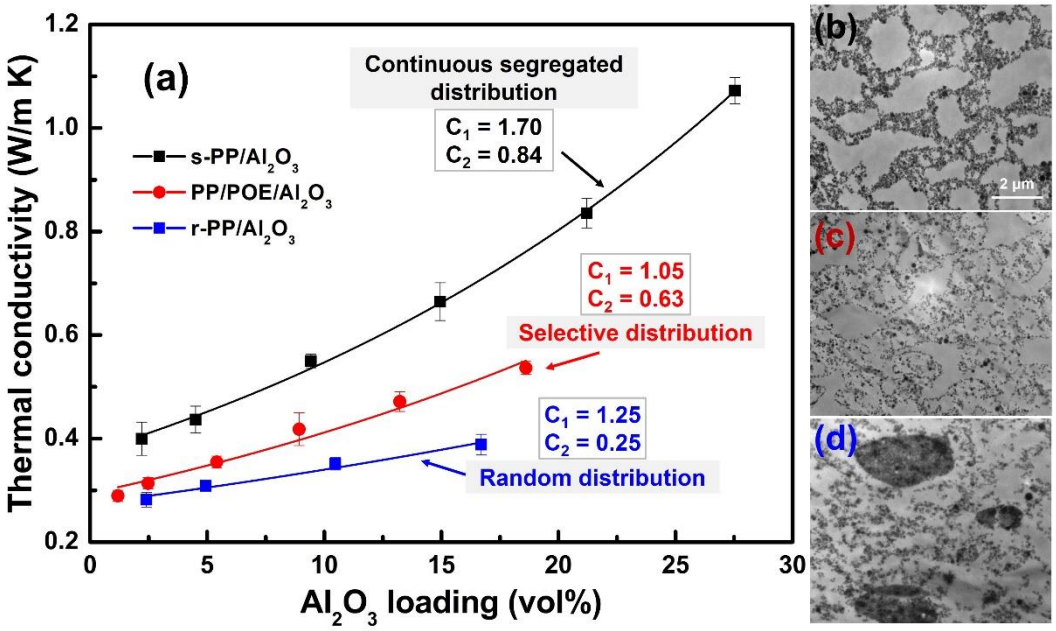

Fig. 4.10. a) Thermal conductivity of nanocomposites with different distributions of Al_2O_3 nanoparticles and fitting of the thermal conductivity based on the Agari's model. TEM micrographs of these nanocomposites are shown in the right side: b) s-PP/Al_2O_3 (9.4 vol%), c) PP/POE/Al_2O_3 (8.9 vol%), and d) r-PP/Al_2O_3 (10.5 vol%). The same scale bar is applied to all the images.

To obtain further insights into the impact of the distribution type on the thermal conductivity of nanocomposites, the experimentally obtained relationships between the thermal conductivity and the Al_2O_3 loading were fit to a theoretical model proposed by Agari et al. [8,37]. This model was derived by generalizing parallel and series conduction with empirical correction factors,

$$log\lambda = V_f C_2 log\lambda_f + (1-V_f) log(C_1 \lambda_p) \quad (4\text{-}3),$$

where λ, λ_p, and λ_f correspond to the thermal conductivity of nanocomposites, polymer, and filler. V_f is the volume fraction of filler. C_1 is a factor related to the effect of filler on the secondary structure of polymer, and the value of $C_1 = 1$ indicated that fillers have no effect on the polymer structure. C_2 is a factor for expressing the ease of the formation of conductive filler networks. The C_2 value is supposed to vary between 0 and 1. When it is closer to 1, it means that conductive networks are more easily formed. Thus, the distribution of nanoparticles affects the thermal conductivity of nanocomposites through the C_2 value. This model is suitable for systems filled with spherical particles at relatively high filler loadings. Fig. 4.10a shows the fitting results for three types of nanocomposites: s-PP/Al_2O_3, PP/POE/Al_2O_3 and r-PP/Al_2O_3. The thermal conductivity of the nanocomposites was well fit to the equation irrespective of the distribution type, while the $C_{1,2}$ values were sensitive to the distribution type. In particular, the C_2 value for r-PP/Al_2O_3 nanocomposites was 0.25, indicating the least effective network formation when randomly distributed. The C_2 value increased dramatically when the distribution was controlled. In particular, the strategy of the continuous segregated structure afforded the highest C_2 value of 0.84. This result clearly revealed the effectiveness of the strategy in constructing thermal conductive networks. The C_1 value for PP/POE/Al_2O_3 nanocomposites was the closest to 1, indicating that almost no effect was caused on matrices in this system. The C_1 value for r-PP/Al_2O_3 nanocomposites

was higher than that of PP/POE/Al_2O_3 nanocomposites. In r-PP/Al_2O_3 nanocomposites, Al_2O_3 nanoparticles were randomly distributed in the whole area rather than selectively distributed at the interface, so that fillers could affect the polymer structure more. For s-PP/Al_2O_3 nanocomposites, the second compression-molding and the barrier effect of filler networks are believed the main reasons that affected the polymer structure.

4.3.3. Mechanical properties

It is known that the introduction of a segregated structure often accompanies significant deterioration of mechanical properties due to the presence of defects and weak interfacial interaction [38]. Accordingly, mechanical properties of s-PP/Al_2O_3 nanocomposites were measured and compared with those of r-PP/Al_2O_3 nanocomposites (Fig. 4.11). In the case of r-PP/Al_2O_3, the particle agglomeration as well as weak interfacial interaction led to significant deterioration in the tensile strength and tensile modulus. Unlike this, the s-PP/Al_2O_3 nanocomposites exhibited enhanced tensile strength and tensile modulus. This enhancement was rather unexpected in a sense that most of previously reported segregated structures caused significant deterioration of mechanical properties. The utilization of a co-continuous template as well as the lack of fatal defects would explain the enhancement.

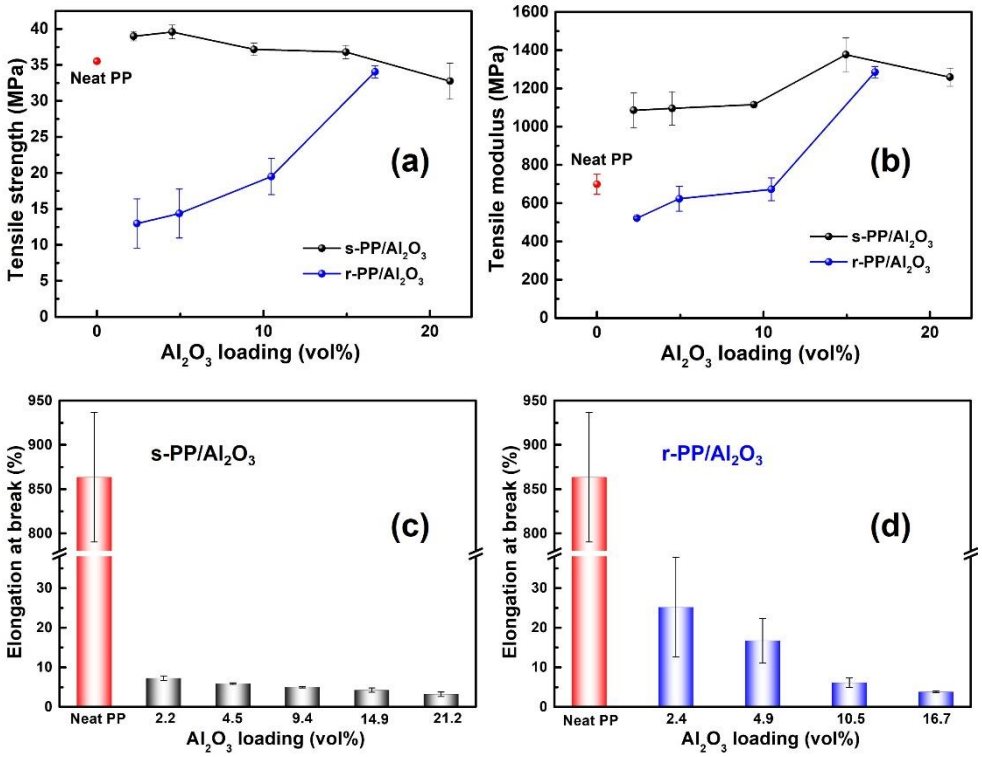

Fig. 4.11. Tensile properties of s-PP/Al_2O_3 and r-PP/Al_2O_3 nanocomposites: a) Tensile strength, b) tensile modulus, and c,d) elongation at break.

4.3.4. Continuous segregated structure based on reactor granule technology

In Chapters 2 and 3, it was found that the phase domain size of PP/POE blends was significantly reduced by employing the reactor granule technology (RGT), which was thought positive in terms of sample uniformity and uniform temperature distribution. Here, I attempted to apply the RGT to design the continuous structure for achieving more uniformly distributed thermal conductive networks.

First, Al_2O_3 nanoparticles were melt-mixed with POE at 190 °C and 100 rpm for

10 min. Then, Al(O*i*Pr)$_3$-impregnated PP granule was added and mixed for another 10 min under the same condition. The impregnated PP was prepared according to the same procedure described in the experiment part of Chapter 2, where the amount of the Al(O*i*Pr)$_3$ precursor was determined so as to obtain the Al_2O_3 loading of 5, 10, and 20 wt% in resultant PP/Al_2O_3 samples. The obtained mixture was compressed into films with the same compression condition for the PP/POE/Al_2O_3 samples, and the films are denoted as PP/POE/Al_2O_3-(RGT+NP). Finally, films with a continuous segregated structure were fabricated according to the same procedure. They are denoted as s-PP/Al_2O_3-(RGT+NP).

The morphology of s-PP/Al_2O_3-(RGT+NP) was studied by TEM micrographs (Fig. 4.12a,b). It can be observed that Al_2O_3 nanoparticles were selectively localized and form a connected network structure throughout the whole composites. The second compression molding shortened the spacing between Al_2O_3 nanoparticles. Some of nanoparticles overlapped with each other and this tendency became more evident at a higher loading (Fig. 4.12a′,b′). Compared to s-PP/Al_2O_3 nanocomposites, the number of thermal conductive paths was obviously improved in s-PP/Al_2O_3-(RGT+NP) (Fig. 4.12c,d).

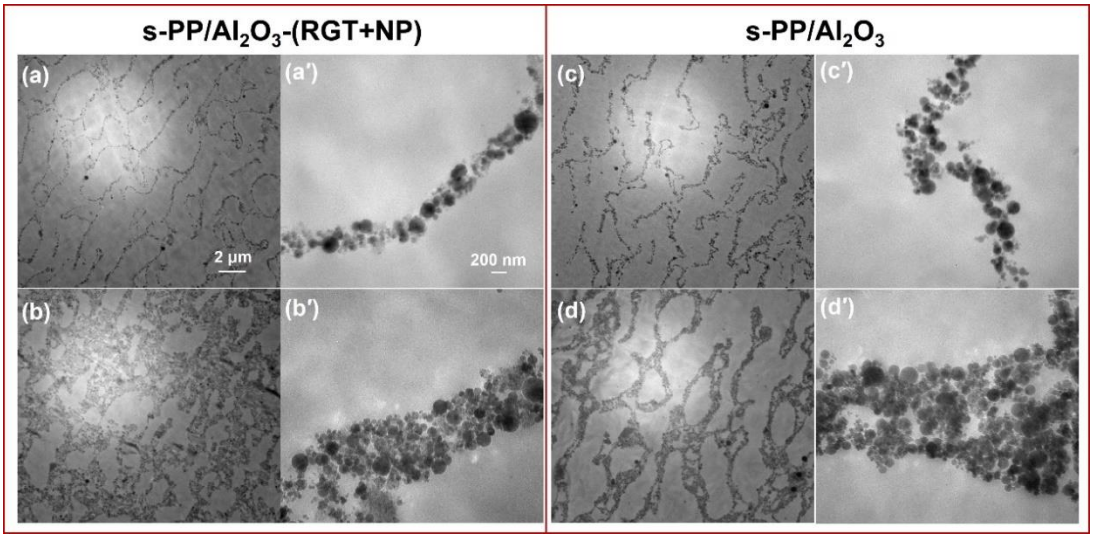

Fig. 4.12. TEM micrographs of s-PP/Al_2O_3-(RGT+NP) nanocomposites with different loadings: a,a′) 4.5 vol%, and b,b′) 15.3 vol%. c,c′) and d,d′) are TEM micrographs of s-PP/Al_2O_3 nanocomposites with the Al_2O_3 loading of 4.5 vol% and 14.9 vol%.

Fig. 4.13 shows the thermal conductivity of s-PP/Al_2O_3-(RGT+NP) and s-PP/Al_2O_3 nanocomposites. It increased with the increase of the Al_2O_3 loading for two kinds of nanocomposites, while s-PP/Al_2O_3-(RGT+NP) nanocomposites presented slightly higher thermal conductivity. This improvement is believed to be originated from the increased number of thermal conductive paths. When the RGT was applied to fabricate PP/POE/Al_2O_3 nanocomposites, the phase domain size was significantly reduced as shown in Fig. 4.14. This small-sized phase domains led to the formation of more thermal conductive paths in s-PP/Al_2O_3-(RGT+NP) (Fig. 4.12a,b). On the other hand, the increased number of thermal conductive paths

resulted in the reduced density of individual paths. Therefore, individual thermal conductive paths were thought to be denser in s-PP/Al_2O_3 nanocomposites.

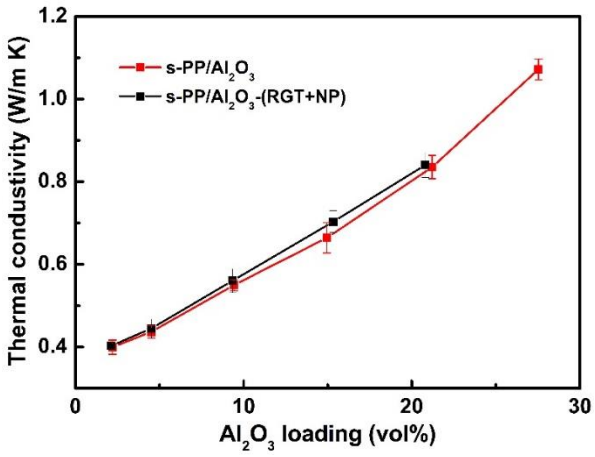

Fig. 4.13. Thermal conductivity of s-PP/Al_2O_3-(RGT+NP) and s-PP/Al_2O_3 nanocomposites.

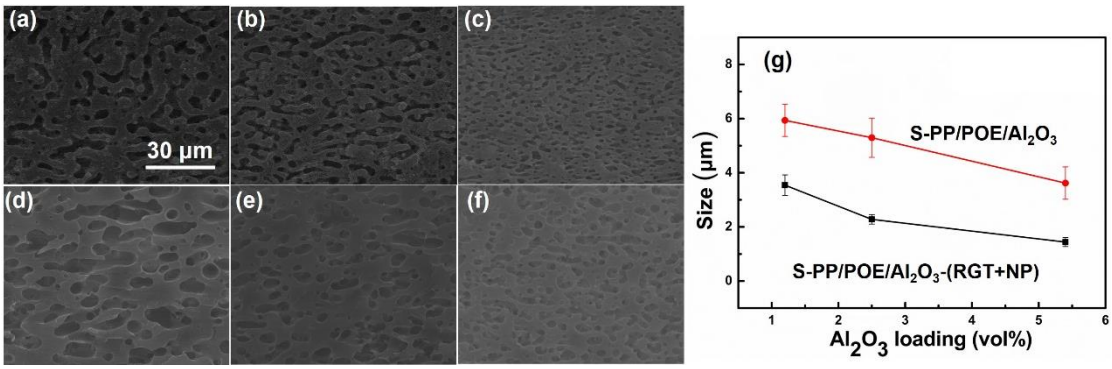

Fig. 4.14. SEM micrographs of a,b,c) PP/POE/Al_2O_3-(RGT+NP) and d,e,f) PP/POE/Al_2O_3 nanocomposites after etching the POE phase. a,d): 1.2 vol%, b,e): 2.5 vol% , c,f) 5.4 vol%). g) is the phase domain size obtained by the analysis of the TEM images.

From the thermal conductivity comparison between s-PP/Al_2O_3-(RGT+NP) and s-PP/Al_2O_3 nanocomposites, it can be known that both the number and density of thermal conductive paths are important for the improvement of thermal conductivity. At a fixed filler loading, the increase in the number of thermal conductive paths necessarily accompanies less dense paths. These two compete in determining the thermal conductivity. Even though great enhancement of thermal conductivity was not achieved by the introduction of RGT to the continuous segregated structure, the obtained results are useful for high thermal conductive nanocomposites design. The RGT provides an opportunity to control the balance between the number and density of thermal conductive paths for desired applications.

4. Conclusions

In this chapter, thermally conductive PP/Al_2O_3 nanocomposites were designed on the basis of a continuous segregated structure. By controlling the mixing order and thermodynamic preference, Al_2O_3 nanoparticles were preferentially distributed in the POE phase of PP/POE blends with a co-continuous morphology. Solvent-aided extraction of the POE phase formed a porous PP scaffold with its pore walls coated by Al_2O_3 nanoparticles. Subsequent compression of the porous scaffold led to the compaction of the porous structure and the densification of the nanoparticle packing, thereby affording PP/Al_2O_3 nanocomposites with continuous segregated networks.

The phase morphology and Al_2O_3 distribution were comprehensively studied by TEM, SEM, and TGA. By comparing the thermal conductivity of nanocomposites having three different types of Al_2O_3 distribution, it was revealed that the continuous segregated distribution gave far the most efficient improvement. Especially, the thermal conductivity of 1.07 W/m K at 27.5 vol% deserves special notice when isotropic nanoparticles are employed. Combination of the RGT with a continuous segregated structure offered an opportunity to control the balance between the number and density of thermal conductive paths. The proposed protocol is directly applicable for designing highly thermal and electric conductive materials, and would be useful for any other applications which require connected networks of fillers.

References

[1] Gu J, Li N, Tian L, Lv Z, Zhang Q. High thermal conductivity graphite nanoplatelet/UHMWPE nanocomposites. RSC Adv. 2015; 5(46): 36334–9.

[2] Min C, Yu D, Cao J, Wang G, Feng L. A graphite nanoplatelet/epoxy composite with high dielectric constant and high thermal conductivity. Carbon 2013; 55: 116–25.

[3] Hu J, Huang Y, Yao Y, Pan G, Sun J, Zeng X, et al. Polymer composite with improved thermal conductivity by constructing a hierarchically ordered three-

dimensional interconnected network of BN. ACS Appl. Mater. Inter. 2017; 9(15): 13544–53.

[4] Yuan C, Duan B, Li L, Xie B, Huang M, Luo X. Thermal conductivity of polymer-based composites with magnetic aligned hexagonal boron nitride platelets. ACS Appl. Mater. Inter. 2015; 7(23): 13000–6.

[5] Dang TML, Kim CY, Zhang Y, Yang JF, Masaki T, Yoon DH. Enhanced thermal conductivity of polymer composites via hybrid fillers of anisotropic aluminum nitride whiskers and isotropic spheres. Compos. Part B-Eng. 2017; 114: 237–46.

[6] Yao Y, Zeng X, Pan G, Sun J, Hu J, Huang Y, et al. Interfacial engineering of silicon carbide nanowire/cellulose microcrystal paper toward high thermal conductivity. ACS Appl. Mater. Inter. 2016; 8(45): 31248–55.

[7] Maira B, Takeuchi K, Chammingkwan P, Terano M, Taniike T. Thermal conductivity of polypropylene/aluminum oxide nanocomposites prepared based on reactor granule technology. Compos. Sci. Technol. 2018; 165: 259–65.

[8] Agari Y, Ueda A, Nagai S. Thermal conductivities of composites in several types of dispersion systems. J. Appl. Polym. Sci. 1991; 42(6): 1665–9.

[9] Wang ZG, Huang YF, Zhang GQ, Wang HQ, Xu JZ, Lei J, et al. Enhanced thermal conductivity of segregated poly (vinylidene fluoride) composites via

forming hybrid conductive network of boron nitride and carbon nanotubes. Ind. Eng. Chem. Res. 2018; 57(31): 10391–7.

[10] Wu K, Lei C, Huang R, Yang W, Chai S, Geng C, et al. Design and preparation of a unique segregated double network with excellent thermal conductive property. ACS Appl. Mater. Inter. 2017; 9(8): 7637–47.

[11] Huang C, Qian X, Yang R. Thermal conductivity of polymers and polymer nanocomposites. Mater. Sci. Eng. R-Rep. 2018; 132: 1–22.

[12] Wang X, Wu P. Preparation of highly thermally conductive polymer composite at low filler content via a self-assembly process between polystyrene microspheres and boron nitride nanosheets. ACS Appl. Mater. Inter. 2017; 9(23): 19934–44.

[13] Shen H, Guo J, Wang H, Zhao N, Xu J. Bioinspired modification of h-BN for high thermal conductive composite films with aligned structure. ACS Appl. Mater. Inter. 2015; 7(10): 5701–8.

[14] Gulotty R, Castellino M, Jagdale P, Tagliaferro A, Balandin AA. Effects of functionalization on thermal properties of single-wall and multi-wall carbon nanotube-polymer nanocomposites. ACS Nano 2013; 7(6): 5114–21.

[15] Burger N, Laachachi A, Ferriol M, Lutz M, Toniazzo V, Ruch D. Review of thermal conductivity in composites: mechanisms, parameters and theory. Prog. Polym. Sci. 2016; 61: 1–28.

[16] Jiang Y, Liu Y, Min P, Sui G. BN@ PPS core-shell structure particles and their 3D segregated architecture composites with high thermal conductivities. Compos. Sci. Technol. 2017; 144: 63–9.

[17] Bai QQ, Wei X, Yang JH, Zhang N, Huang T, Wang Y, et al. Dispersion and network formation of graphene platelets in polystyrene composites and the resultant conductive properties. Compos. Part A-Appl S. 2017; 96: 89–98.

[18] Yang J, Sprengard J, Ju L, Hao A, Saei M, Liang R, et al. Three-dimensional-linked carbon fiber-carbon nanotube hybrid structure for enhancing thermal conductivity of silicon carbonitride matrix composites. Carbon 2016; 108: 38–46.

[19] Zhang X, Zheng S, Zheng X, Liu Z, Yang W, Yang M. Distinct positive temperature coefficient effect of polymer–carbon fiber composites evaluated in terms of polymer absorption on fiber surface. Phys. Chem. Chem. Phys. 2016; 18(11): 8081–7.

[20] Zhang X, Zheng S, Zou H, Zheng X, Liu Z, Yang W, et al. Two-step positive temperature coefficient effect with favorable reproducibility achieved by specific “island-bridge” electrical conductive networks in HDPE/PVDF/CNF composite. Compos. Part A-Appl. S. 2017; 94: 21–31.

[21] Cao J-P, Zhao J, Zhao X, You F, Yu H, Hu G-H, et al. High thermal conductivity and high electrical resistivity of poly (vinylidene

fluoride)/polystyrene blends by controlling the localization of hybrid fillers. Compos. Sci. Technol. 2013; 89: 142–8.

[22] Cao M, Shu J, Chen P, Xia R, Yang B, Miao J, et al. Orientation of boron nitride nanosheets in CM/EPDM Co-continuous blends and their thermal conductive properties. Polym. Test. 2018; 69: 208–13.

[23] Huang J, Zhu Y, Xu L, Chen J, Jiang W, Nie X. Massive enhancement in the thermal conductivity of polymer composites by trapping graphene at the interface of a polymer blend. Compos. Sci. Technol. 2016; 129: 160–5.

[24] Maira B, Chammingkwan P, Terano M, Taniike T. Reactor granule technology for fabrication of functionally advantageous polypropylene nanocomposites with oxide nanoparticles. Compos. Sci. Technol. 2017; 144: 151–9.

[25] Qiagedeer A, Maira B, Strauss R, Zhao Y, Chammingkwan P, Mizutani G, et al. Preparation and characterization of polypropylene/noble metal nanocomposites based on reactor granule technology. Polymer 2017; 127: 251–8.

[26] Zhang X, Maira B, Hashimoto Y, Wada T, Chammingkwan P, Thakur A, et al. Selective localization of aluminum oxide at interface and its effect on thermal conductivity in polypropylene/polyolefin elastomer blends. Compos. Part B-Eng 2019; 162: 662–670.

[27] Zhang X, Wada T, Chammingkwan P, Thakur A, Taniike T. Cooperative

influences of nanoparticle localization and phase coarsening on thermal conductivity of polypropylene/polyolefin elastomer blends. Compos. Part A-Appl. S. 2019; 126: 105602.

[28] Hu H, Zhang G, Xiao L, Wang H, Zhang Q, Zhao Z. Preparation and electrical conductivity of graphene/ultrahigh molecular weight polyethylene composites with a segregated structure. Carbon 2012; 50(12): 4596–9.

[29] Li M, Gao C, Hu H, Zhao Z. Electrical conductivity of thermally reduced graphene oxide/polymer composites with a segregated structure. Carbon 2013; 65: 371–3.

[30] Feng CP, Bai L, Bao RY, Liu ZY, Yang MB, Chen J, et al. Electrically insulating POE/BN elastomeric composites with high through-plane thermal conductivity fabricated by two-roll milling and hot compression. Adv Compos Hybr Mater, 2018;1(1):160–7.

[31] Zhou H, Deng H, Zhang L, Fu Q. Significant enhancement of thermal conductivity in polymer composite via constructing macroscopic segregated filler networks. ACS Appl. Mater. Inter. 2017; 9(34): 29071–81.

[32] Gong T, Peng SP, Bao RY, Yang W, Xie BH, Yang MB. Low percolation threshold and balanced electrical and mechanical performances in polypropylene/carbon black composites with a continuous segregated structure. Compos. Part B-Eng. 2016; 99: 348–57.

[33] Li M, Zhang W, Wang C, Wang H. In situ formation of 2D conductive porous material with ultra low percolation threshold. Mater. Lett. 2012; 82: 109–11.

[34] Chukov D, Stepashkin A, Maksimkin A, Tcherdyntsev V, Kaloshkin S, Kuskov K, et al. Investigation of structure, mechanical and tribological properties of short carbon fiber reinforced UHMWPE-matrix composites. Compos. Part B-Eng. 2015; 76: 79–88.

[35] Sumita M, Sakata K, Asai S, Miyasaka K, Nakagawa H. Dispersion of fillers and the electrical conductivity of polymer blends filled with carbon black. Polym. Bull. 1991; 25(2): 265–71.

[36] Im H, Kim J. Enhancement of the thermal conductivity of aluminum oxide–epoxy terminated poly (dimethyl siloxane) with a metal oxide containing polysiloxane. J. Mater. Sci. 2011; 46(20): 6571–80.

[37] Agari Y, Ueda A, Nagai S. Thermal conductivity of a polymer composite. J. Appl. Polym. Sci. 1993; 49(9): 1625–34.

[38] Potts JR, Shankar O, Du L, Ruoff RS. Processing–morphology–property relationships and composite theory analysis of reduced graphene oxide/natural rubber nanocomposites. Macromolecules 2012; 45(15): 6045–55.

Chapter 5

General Conclusion

Chapter 5

Thermal conductive polymer composites have become a hot research topic along with the rapid miniaturization and high degree of integration of electronic devices. The current research on this topic has mostly assumed the use of specific thermal conductive fillers or methods to improve the thermal conductivity of polymer composites, which are generally only suitable for limited polymer matrices and very expensive. Polyolefin, as one of the most commonly used thermoplastics with balanced properties and price, is very promising to be applied in this field if its thermal conductivity can be improved, especially by adding abundant and cheap thermal conductive fillers. In this thesis, I employed polypropylene and Al_2O_3 nanoparticle as the polymer matrix and thermal conductive filler, respectively, aiming at clarifying key factors such as filler dispersion, filler migration, phase morphology evolution, and their cooperative influences for the formation of thermal conductive networks. The main conclusions are as follows:

In Chapter 2, a reactor granule technology (RGT) was employed to obtain Al_2O_3 nanoparticles uniformly dispersed in the polypropylene (PP) matrix. It was then mixed with polyolefin elastomer (POE) to obtain a co-continuous stricture. It was found that Al_2O_3 nanoparticles thermodynamically prefer the localization at the interface between PP and POE, but their successful migration to the interface largely depended on the initial dispersion of the nanoparticles. The agglomerates hindered the migration of fillers to the interface. The uniform

dispersion of Al_2O_3 nanoparticles achieved by RGT led to the selective localization of Al_2O_3 nanoparticles at the interface, creating thermal conductive networks along the co-continuous structure, and eventually giving high thermal conductivity. This chapter firstly demonstrated that the distribution of nanoparticles can be controlled even for the combination of hydrophobic and hydrophilic pairs like PP and Al_2O_3. In summary, I successfully proposed a facile way to control the localization of filled nanoparticles at the interface in nanocomposites, and key factors thereof in this chapter.

In Chapter 3, I revealed factors that affect the migration of nanoparticles by systematically investigating the nanoparticle migration and phase morphology evolution in the PP/POE/Al_2O_3 ternary system during the annealing process. By analyzing TEM and SEM micrographs of the nanocomposites at different annealing durations, important cooperation between nanoparticle localization and phase morphology evolution was evidenced: The decreased phase domain size facilitated the successful migration to the interface; Further, the formation of nanoparticle networks at the interface decelerated the phase coarsening during annealing. By employing the RGT, the polymer blend presented a much smaller phase domain size and retarded phase coarsening speed. Therefore, uniformly distributed thermal conductive networks were afforded.

Chapter 4 describes results on the development of thermal conductive PP

nanocomposites based on a continuous segregated structure. The design of the continuous segregated structure aimed at constructing continuous filler networks similar to the selective localization at the interface but with denser thermal conductive paths. By solvent-aided extraction of the POE phase in PP/POE/Al_2O_3 nanocomposites with a co-continuous structure and subsequent compression of the porous scaffold, the c PP/Al_2O_3 nanocomposites with continuous segregated networks were constructed. The continuous segregated distribution gave far greater improvement of thermal conductivity (1.07 W/m K at 27.5 vol%) compared with selective distribution and uncontrolled distribution. The combination of this structure with RGT indicated that both the number and density of thermal conductive paths were important for improving the thermal conductivity.

I believe that the research work carried out in this thesis has established a novel and promising rout for the design of thermal conductive composites in a simple and efficient manner. Furthermore, I have clarified some key factors affecting the formation of thermal conductive networks, which are expected to be useful for other thermal conductive composites design.

List of publications and other achievements

Publications

1. **Xi Zhang**, Xiaochao Xia, Hui You, Toru Wada, Patchanee Chammingkwan, Ashutosh Thakur, Toshiaki Taniike, Design of continuous segregated polypropylene/Al_2O_3 nanocomposites and impact of controlled Al_2O_3 distribution on thermal conductivity. Composites Part A: Applied Science and Manufacturing 2020; 131: 105825. (IF = 6.28)

2. **Xi Zhang**, Toru Wada, Patchanee Chammingkwan, Ashutosh Thakur, Toshiaki Taniike, Cooperative influences of nanoparticle localization and phase coarsening on thermal conductivity of polypropylene/polyolefin elastomer blends, Composites Part A: Applied Science and Manufacturing 2019; 126: 105602. (IF = 6.28)

3. **Xi Zhang**, Bulbul Maira, Yuya Hashimoto, Toru Wada, Patchanee Chammingkwan, Ashutosh Thakur, Toshiaki Taniike, Selective localization of aluminum oxide at interface and its effect on thermal conductivity in polypropylene/polyolefin elastomer blends, Composites Part B: Engineering 2019; 162: 662–70. (IF = 6.86)

Conferences

Domestic Conference

1. **Xi Zhang**, Toru Wada, Patchanee Chammingkwan, Toshiaki Taniike, Cooperative Influences of Nanoparticle Localization and Phase Coarsening on Thermal Conductivity of Ternary Nanocomposites, 64th SPSJ Annual Meeting, Fukuoka, Japan, May 27–29, 2020.

International Conferences

1. **Xi Zhang**, Bulbul Maira, Toru Wada, Patchanee Chammingkwan, Toshiaki Taniike, Selective localization of nanoparticles in immiscible polyolefin blends achieved by reactor granule technology. 5th Blue Sky Conference, Naples and Sorrento, Italy, Jun. 24–28, 2019.

2. **Xi Zhang**, Bulbul Maira, Toru Wada, Patchanee Chammingkwan, Toshiaki Taniike, Improved thermal conductivity of PP/POE blends by controlling uniform dispersion and selective distribution of Al_2O_3, the 12th SPSJ International Polymer Conference (IPC2018), Hiroshima, Japan, Dec. 4–7, 2018.